

**APPLICATION OF BIOLOGICALLY ACTIVE
MICELLES IN DRUG DELIVERY ACROSS THE BLOOD
BRAIN BARRIER**

GUO KUN

(Bachelor of Engineering, B.I.T, Beijing)

A THESIS SUBMITTED FOR THE DEGREE OF
DOCTOR OF PHILOSOPHY



**DEPARTMENT OF ANATOMY
YONG LOO LIN SCHOOL OF MEDICINE
NATIONAL UNIVERSITY OF SINGAPORE**

2009

ACKNOWLEDGEMENTS

I wish to express my deepest appreciation and heartfelt thanks to my supervisors: **Assistant Professor He Beiping** and **Associate Professor Lu Jia**, Department of Anatomy, Yong Loo Lin School of Medicine, National University of Singapore, for their invaluable guidance and constant encouragements. They not only introduced me to basic research, but had also been a role model of commitment to research. Their innovative ideas, infinite patience, stimulating discussion and friendly critics have been most invaluable to the accomplishment of this thesis. Without them, this dissertation would never be completed.

I am greatly indebted to **Professor Bay Boon Huat**, Head of Anatomy Department, for his constant encouragements as well as for his full support in providing me with the excellent working facilities and a fascinating academic environment. Also, I am grateful to **Professor Ling Eng Ang**, former HOD who gave me this opportunity to study in NUS, and his support during his term of office.

I must also acknowledge my gratitude to **Assistant Professor Yang Yi-Yan**, Institute of Bioengineering and Nanotechnology, Agency for Science, Technology and Research. Thanks for her and her research team's great cooperation in this research project. Her creative ideas and stimulating discussion impress me most throughout the whole study. Also, I wish to express my special appreciation to **Dr.**

Liu Lihong, Institute of Bioengineering and Nanotechnology, Agency for Science, Technology and Research. Thanks for her kind help. Without her outstanding work, this study would never be carried on.

I also acknowledge my gratitude to **Ms. Yong Eng Siang, Ms. Ng Geok Lan, Ms. Cao Qiong, Ms. Chan Yee Gek** and **Dr. Wu Yajun** for their excellent technical assistance; **Mr. Yick Tuck Yong, Mr. Low Chun Peng** and **Ms. Bay Song Lin** for their constant assistance in computer work; and **Ms. Ang Lye Gek Carlyne, Ms. Teo Li Ching Violet** for their secretarial assistance.

I would like to express my special thanks to **Associate Professor Shabbir M. Moochhala, Dr. Zhao Bin, Mr. Ng Kian Chye, Ms. Tan Mui Hong, Ms. Lai Mui Hoon, Ms. Tan Li Li, Ms. Yeo Su Li, Julie** and **Ms. Lim Geok Yen, Clara**, DEMRI, DSO National Laboratories, for their continuous help, support and advice when I did my project in DSO National Laboratories.

I would like to thank my good friends during my study: **Dr. Li Lv, Dr. Li Zhaohui, Dr. Guo Chunhua, Dr. Li Wenbo, Mr. Xia Wenhao, Ms. Yin Jing, Ms. Wu Chun, Mr. Hu Lingxu, Mr. Feng Luo** and **Mr. Meng Jun**. Their friendships create a pleasant environment for me to complete the 4 year graduate study. I would also like to thank **Mr. Zhu Lie, Ms Jasmin Lim Qian Ru** and **Ms Nicole Liu Su Yun** for their help and support.

I would like to take this opportunity to express my heartfelt thanks to **my parents (Mr. Guo Xuewei and Mdm. Jiang Guangling), parents-in-law (Mr. Xiong Kexun and Mdm. Yang Changjin) and elder sister (Ms. Guo Yi)** for their full and endless support for my study. Also I am greatly indebted to my wife, **Mrs. Xiong Lin** for her full support, understanding and encouragement during this study.

Last but not least, I am thankful to the **National University of Singapore** for the Research Scholarship and **DSO National Laboratories** for the grant that enables me to do this study.

*This thesis is dedicated to
my beloved family*

PUBLICATIONS

International Journals:

1: Guo K, Liu LH, Lu J, Venkatraman SS, Luo D, Ng KC, Ling EA, Moochhala S, Yang YY. Biologically active core/shell nanoparticles self-assembled from cholesterol-terminated PEG-TAT for drug delivery across the blood brain barrier. *Biomaterials* .2008, 29: 1509-1517

2: Liu LH, Venkatraman SS, Yang YY, **Guo K**, Lu J, He BP, Moochhala S, Kan LJ. Polymeric micelles anchored with TAT for delivery of antibiotics across the Blood-Brain Barrier. *Biopolymers*. 2008, 90(5):617-623

3: Guo K, Liu LH, Yang YY, Lu J, He BP. Preparation, Characterization and Application of TAT conjugated Penicillin G potassium for its delivery across the Blood Brain Barrier. (In preparation)

4: Guo K, Zhu L, Lu J, He BP. The study of NG2 expressing cells responses in the LPS focal injected rat brain cortex. (Submitted)

5: Guo K, Liu LH, Yang YY, Lu J, He BP. The *in vivo* and *in vitro* investigation of TAT conjugated PEG-*b*-Cholesterol nanoparticle for drug delivery through the Blood Brain Barrier. (In preparation)

Conference Papers:

1: Liu LH, Lu J, **Guo K**, Zeng YG, Ng KC, Ling EA, Moochhala S, Venkatraman SS, Yang YY. Delivery of ciprofloxacin across the Blood Brain Barrier using cholesterol-PEG-TAT. International Conference on Materials for Advanced Technologies (ICMAT) 2007. 1-6 July 2007, Singapore.

2: Guo K, Wang A, He BP. NG2 cells response to focal injection of lipopolysaccharide (LPS) in the cortex of the rat brain. Proceedings of the SFN 38th Annual Meeting. 2008, 15-19th, November, Washington DC, USA.

3: Guo K, Liu LH, Yang YY, Lu J, He BP. TAT peptide directly conjugated system for Penicillin G delivery through the Blood Brain Barrier. 30th Australian Polymers Symposium (30APS). 30 November-4 December, 2008, Melbourne, Victoria, Australia.

TABLE OF CONTENTS

ACKNOWLEDGEMENTS.....	II
DEDICATIONS.....	V
PUBLICATIONS.....	VI
TABLE OF CONTENTS.....	VII
ABBREVIATIONS.....	XIII
SUMMARY.....	XVIII

CHAPTER 1 INTRODUCTION 1

1. Central nervous system inflammatory diseases.....	5
1.1. Brain infectious diseases.....	5
1.1.1 Viral infections.....	5
1.1.2 Bacterial infections.....	6
1.2 Treatment of CNS infectious diseases.....	7
1.2.1 Anti-inflammatory drugs.....	7
1.2.2 Anti-Pathogen drugs.....	8
1.2.3 Antibiotics selected in this study.....	9
2. The cell biology of the blood brain barrier (BBB).....	10
2.1 Structure of the BBB.....	12
2.1.1 Endothelial cells.....	12
2.1.2 Other cell types.....	13
2.1.2.1 Astrocytes.....	14
2.1.2.2 Pericytes.....	14
2.1.2.3 Neurons.....	15
2.2 The permeability properties of the BBB.....	15
3. Drug delivery into the brain.....	17
3.1 Possible ways of delivering a compound from blood to brain.....	18
3.1.1 Cell migration.....	18
3.1.2 Passive diffusion.....	19
3.1.3 Tight junction modulation.....	19
3.1.4 Active transport.....	20
3.1.4.1 Carrier mediated transcytosis (CMT).....	20
3.1.4.2 Receptor mediated transcytosis (RMT).....	20

3.1.4.3 Absorptive mediated transcytosis (AMT).....	21
3.2 Strategies for drug delivery into the brain	21
3.2.1 Neurosurgically-based strategy.....	21
3.2.2 Pharmacologically-based strategy	22
3.2.2.1 Drug lipophilicity modification	22
3.2.2.2 Other modifications	23
3.2.3 Physiologically-based strategy.....	23
3.2.3.1 Endogenous BBB transporters.....	24
3.2.3.2 Cell-penetrating peptide vectors	25
3.2.3.3 Liposomes and nanoparticles.....	26
4. Nanoparticles in the brain drug delivery.....	27
4.1 Ideal properties of nanoparticles for brain drug delivery.....	28
4.2 Some successfully developed nanoparticles in brain drug delivery	29
4.2.1 PBCA nanoparticles.....	29
4.2.2 PEGylated PLA/PLGA nanoparticles.....	32
4.2.2.1 Nanoparticle preparation.....	32
4.2.2.2 PEGylated nanoparticles conformations.....	33
4.2.2.3 Application of PEGylated nanoparticles in brain drug delivery	34
4.2.3 The advantages and the disadvantages	36
4.3 Possible mechanism of nanoparticle-mediated transport of drugs across the BBB.....	37
5. Drug delivery system designed in this study	38
5.1 PEG (poly (ethylene glycol)) and <i>b</i> -cholesterol	38
5.2 TAT: a cell penetrating peptide	42
6. Pathological model for testing designed nanoparticle drug delivery system...	46
6.1. Major cell types in the brain	46
6.1.1 Neurons	46
6.1.2 Main non-neuronal cells	47
6.1.3 NG2 positive cells.....	49
6.2 Pathological changes of brain cells in brain focal injury model.....	51
6.2.1 Microglia.....	51
6.2.2 Astrocytes	52
6.2.3 Oligodendrocytes	53
6.2.4 Neurons	53
6.2.5 NG2 positive cells responses to brain injury	54
7. Hypothesis.....	54
8. Scope of research	58

8.1 To synthesize and characterize the core-shell structured micelles of PEG- <i>b</i> -cholesterol and TAT-PEG- <i>b</i> -cholesterol:	58
8.2 To study the BBB penetration of PEG- <i>b</i> -Chol and TAT-PEG- <i>b</i> -Chol ...	59
8.3 To study the primary pharmacokinetics of selected antibiotics and FITC encapsulated TAT-PEG- <i>b</i> -Chol <i>in vivo</i>	59
8.4 To synthesize and characterize TAT-Penicillin G	60
8.5 To evaluate PEG- <i>b</i> -Chol and TAT-PEG- <i>b</i> -Chol <i>in vitro</i> and <i>in vivo</i>	60

CHAPTER 2 MATERIALS AND METHODS61

1. Fabrication and characterization	62
1.1 Materials	62
1.2 Synthesis procedures.....	62
1.2.1 PEG- <i>b</i> -Chol.....	62
1.2.2 TAT-PEG- <i>b</i> -Chol	63
1.2.3 Encapsulation of FITC or QDs into PEG- <i>b</i> -Chol and TAT-PEG- <i>b</i> -Chol	64
1.2.4 TAT-Penicillin G	64
1.3 Characterization procedures.....	65
1.3.1 Morphology of blank or drug-loaded nanoparticles	65
1.3.2 ¹ H NMR spectra of nanoparticles	66
1.3.3 MALDI-TOF/MS characterization of Penicillin G and TAT-Penicillin G	66
1.3.4 Particle size and zeta potential analysis	66
1.3.5 <i>In vitro</i> drug release of ciprofloxacin-loaded nanoparticles	67
2. Cell culture.....	67
2.1 Materials	68
2.2 General operating procedures	68
2.2.1 Handling procedure frozen cells	68
2.2.2 Subculture procedure	69
2.2.3 Cell preservation procedure	69
2.3 Procedures of toxicity test.....	70
2.4 Procedures of cellular intake test	71
2.5 Procedures of antibiotic screening.....	71
2.6 Cellular uptake study of Penicillin G and TAT-Penicillin G.....	72
3. Histochemistry and immunohistochemistry studies	73
3.1 Animal and anesthesia procedures.....	73
3.2 Perfusion, tissue sampling and sectioning procedures.....	74
3.2.1 Fixatives.....	74
3.2.2 Preparation of gelatinized slides	74
3.2.3 Perfusion	74

3.2.4 Tissue sampling and sectioning	76
3.3 Procedures of immunofluorescent staining.....	76
3.3.1 Buffers and solutions	76
3.3.2 Antibodies	77
3.3.3 Staining procedure	77
3.3.4 Procedures of DAB staining	79
3.4 Procedures of injection of nanoparticle solution	79
3.5 Pathological brain model setup procedures	80
3.5.1 Materials	80
3.5.2 Procedures of LPS and anti-CD11b antibody cortical injection....	81
3.6 BrdU assay procedures	82
3.6.1 BrdU solution preparation.....	82
3.6.2 BrdU solution intraperitoneal injection	82
3.6.3 Perfusion and sectioning.....	82
3.6.4 DNA denaturation.....	82
4. HPLC analysis	83
4.1 Materials	83
4.2 Procedures of injection and sample preparation	84
4.2.1 Sample collection.....	84
4.2.2 Sample preparation	84
4.3 HPLC analysis method	85
5. Statistical analysis	86

CHAPTER 3 RESULTS

1. Fabrication and characterization of nanoparticle micelles.....	88
1.1 Synthesis of PEG- <i>b</i> -Chol and TAT-PEG- <i>b</i> -Chol	88
1.2 Morphology of nanoparticles micelles.....	89
1.3 Drug loading into nanoparticle micelles	91
1.4 <i>In vitro</i> drug release in PBS	92
2. Investigation of BBB integrity	93
2.1 BBB in developing rat	93
2.2 The BBB penetration of Rhodamine B	94
3. <i>In vivo</i> BBB permeability of nanoparticle micelles	95
3.1 BBB penetration of FITC Encapsulated nanoparticles	95
3.2 BBB penetration of QDs Encapsulated TAT-PEG- <i>b</i> -Chol	97
3.3 Particle size of micelles for its BBB penetration	99
4. Further <i>in vivo</i> investigation of TAT-PEG- <i>b</i> -Chol	101

4.1 Identification of cell types of nanoparticle positive cells in Brain parenchyma	101
4.2 The cellular uptake of TAT-PEG- <i>b</i> -Chol by neurons.....	103
4.3 Primary <i>in vivo</i> kinetics of the BBB penetration of nanoparticles.....	105
5. <i>In vitro</i> characterization of nanoparticle micelles.....	109
5.1 Uptake of nanoparticles in cultured cells.....	109
5.2 The cytotoxicity of nanoparticle micelles.....	110
6. Synthesis and characterization of TAT-Penicillin G	112
6.1 ¹ HNMR spectrum of TAT-Penicillin G potassium.....	112
6.2 Determination of molecular weight of TAT-Penicillin G.....	113
6.3 The cytotoxicity of TAT-Penicillin G potassium	114
7. Application of TAT-Penicillin G	115
7.1 Antibacterial efficacy test of TAT-Penicillin G.....	115
7.2 <i>In vitro</i> uptake of TAT-Penicillin G	117
8. Pharmacokinetics investigation of selected antibiotics.....	119
8.1 HPLC spectra of Penicillin G, Ciprofloxacin and Doxycycline.....	119
8.2 Within and between day assay validation (n=5).....	120
8.3 Inter-Assay precision for the analysis of Penicillin G in rat plasma.....	121
8.4 Pharmacokinetics of selected antibiotics after intravenous injection	123
9. Establishment of brain pathological model.....	124
10. NG2 cell responses in LPS treated pathological brain.....	125
10.1 NG2 cell responses	125
10.2 The activated NG2 cells do not produce some cytokines.....	127
10.3 Expression of BrdU in NG2 cells after LPS administration	128
11. NG2 cell responses after blockage of microglial complement receptor type 3 in LPS treated brain	129
11.1 The change of NG2 positive cells' expression	129
11.2 Morphology of NG2 cells after anti-CD11b antibody+LPS treatment	131
11.3 The cells near the needle track.....	132
12. Distribution of TAT-PEG- <i>b</i> -Chol nanoparticles in LPS triggered pathological brain.	134
12.1 The permeability of TAT-PEG- <i>b</i> -Chol.....	134
12.2 The distribution of TAT-PEG- <i>b</i> -Chol	135
CHAPTER 4 DISCUSSION	137

1. PEG- <i>b</i> -Chol and TAT-PEG- <i>b</i> -Chol system.....	138
1.1. Critical micelle concentration value of nanoparticle micelles.....	138
1.2. Particle size control in the nanoparticles fabrication	139
1.3 The length of PEG chain and TAT-PEG- <i>b</i> -Chol BBB penetration.....	140
1.4 Ciprofloxacin and ciprofloxacin lactate.....	143
1.5 Consideration in injecting and sampling methods for application of nanoparticles in BBB penetration	144
1.6 The cellular uptake of TAT-PEG- <i>b</i> -Chol in brain parenchyma	146
1.7 Dynamic transport of TAT-PEG- <i>b</i> -Chol <i>in vivo</i>	147
1.8 Drug transport with TAT-PEG- <i>b</i> -Chol in pathological brain.....	148
1.9 HPLC analytical and detective method for nanoparticle system.....	150
1.10 Application of nanoparticle micelles for gene targets delivery	150
2. TAT-Penicillin G potassium system	152
2.1 Encapsulation of hydrophobic and hydrophilic antibiotics	152
2.2 Conjugation of TAT to Penicillin G potassium	153
2.3 Cytotoxicity of TAT-Penicillin G.....	154
2.4 Antibiotics screening of TAT-Penicillin G.....	156
2.5 <i>In vitro</i> uptake of TAT-Penicillin G	158
2.6 The <i>in vivo</i> labeling of TAT-Penicillin G	159
3. Application of TAT conjugated drug delivery system.....	160
4. LPS focal injected rat pathological brain model.....	161
4.1 The responses of NG2 expressing cells	161
4.2 The relationship between NG2 positive cells and microglia	162
CHAPTER 5 CONCLUSIONS AND FUTURE STUDIES.....	164
1. Conclusions.....	165
2. Future studies	167
CHAPTER 6 REFERENCES	170

ABBREVIATIONS

ABC	avidin-biotinylated horseradish peroxidase complex
AJ	adherent junction
AMT	absorptive mediated transcytosis
BBB	blood brain barrier
BCEC	brain capillary endothelial cells
BCSFB	blood cerebrospinal fluid barrier
BrdU	5-Bromo-2'-deoxyuridine
CCA	common carotid artery
CED	convection-enhanced diffusion
CMC	critical micelle concentration
CMT	carrier mediated transcytosis
CNS	central nervous system
CO₂	carbon dioxide
COX-2	cyclooxygenase-2
CPP	cell-penetrating peptide
CSF	cerebral spinal fluid
CSPG	chondroitin sulphate proteoglycan
CV	coefficients of variation
DA	dopamine
DAB	3, 3'-diaminobenzidine tetrahydrochloride
DCM	Dichloromethane

DI	de-ionized
DNA	deoxyribonucleic acid
DMEM	Dulbecco's Modified Eagle's Medium
DMF	Dimethylformamide
DMSO	Dimethyl sulfoxide
EC	endothelial cell
EDC	1-ethyl-3-[3-dimethylaminopropyl] carbodiimide hydrochloride
FBS	fetal bovine serum
FITC	Fluorescein5-isothiocyanate
FK-506	Tacrolimus or Fujimycin
GFAP	glial fibrillary acidic protein
IFN-γ	interferon gamma
HIV	human immunodeficiency virus
HPLC	High performance Liquid Chromatography
IC	Intra-cerebral
ICV	Intracerebroventricular
IFN-γ	Interferon gamma
IL-1β	interleukin-1 beta
IL-2	interleukin-2
IL-4	interleukin-4
IL-6	interleukin-6
IR	infrared

iNOS	inducible Nitric Oxide Synthase
JEV	Japanese encephalitis virus
LDL	low density lipoprotein
L-DOPA	3,4-dihydroxy-L-phenylalanine
LPS	lipopolysaccharide
LSCM	Laser-Scanning Confocal Microscopy
MALDI-TOF	matrix-assisted laser desorption ionization of time-of-flight
MAO	monoamine oxidase
MIC	minimum inhibition concentration
mPEG	methoxypoly (ethylene glycol)
MES	2-(N-morpholino) ethanesulfonic acid
MPS	monuclear phagocyte system
MPTP	1-methyl 4-phenyl 1,2,3,6-tetrahydropyridine
MS	mass spectrometry
MS	multiple sclerosis
NMR	nuclear magnetic resonance spectroscopy
O-2A	oligodendrocyte-type-2 astrocyte
OD	optical density
OPC	oligodendrocyte precursor cells
PDGFαR	platelet-derived growth factor α receptor
PB	phosphate buffer
PBCA	poly(butyl)cyanoacrylate

PBS	phosphate buffered saline
PD	Parkinson's disease
PDGF	platelet-derived growth factor
PEG	polyethylene glycol
PF	paraformaldehyde
PHDCA	poly (hexadecylcyanoacrylate)
PLA	polylactide
PLGA	poly(lac-tide-co-glycolide)
QDs	Quantum Dots
RES	reticuloendothelial system
RMT	receptor mediated transcytosis
SD	Sprague-Dawley
SD	standard deviation
SEM	scanning electrical microscope
S-NHS	N-hydroxy-sulfosuccinimide
SSPE	subacute sclerosing panencephalitis
TAT	transactivating-transduction
TBS	Tris buffer saline
TEA	Triethylamine
TEM	transmission electron microscopy
TGF-β	transforming growth factor-beta
TJ	tight junction

TNF- α tumor necrosis factor alpha

UV ultraviolet

VIS visible

SUMMARY

The most challenging task in treatment of various diseases or injuries in the central nervous system (CNS) is to overcome the barrier preventing the drugs moving into the brain parenchyma. The blood brain barrier (BBB) lies between the blood flow and the brain parenchyma. The BBB prohibits most foreign molecules entering from the blood to brain, including CNS drugs. The limited penetration of drugs through the BBB into the brain parenchyma is the rule, not the exception

In the treatment of brain infection or inflammatory diseases, antibiotics such as ciprofloxacin, penicillin or doxycycline are commonly used, especially for those diseases caused by bacteria. However, high mortality and morbidity among those infected diseases are still inevitable because of the difficulty in delivering antibiotics across the BBB. Therefore, exploring strategies for delivering drugs across the BBB is of great importance in the therapy of CNS diseases.

Up to now, three main strategies have been developed to penetrate the BBB: neurosurgically-based strategy to physically introduce a drug in the brain by temporally opening the BBB; pharmacologically-based strategy to increase permeability of drugs to the BBB through the modification of molecular features of drugs; and physiologically-based strategy to enhance permeability of drugs through the BBB by physiological carrier. The physiologically-based strategy is a safe way to deliver a drug with high drug transport efficiency. The present study is intended to

develop a novel biologically active drug carrier in the physiologically-based strategy. Here, antibiotic molecules will be coupled to a vector by chemical or physical force. The efficacy of the novel drug delivery system to cross the BBB through receptor mediated transcytosis (RMT) or absorptive mediated transcytosis (AMT) will be tested.

In the first part of this thesis, a new core shell nanoparticles system for the ciprofloxacin delivery was devised. Firstly, the hydrophilic poly (ethylene glycol) (PEG) chain was connected to hydrophobic *b*-cholesterol molecules by EDC/NHS chemistry in organic solvent. The amphiphilic polymeric micelles of PEG-*b*-cholesterol can self-assemble a core shell structure in aqueous solution. Then, transactivator of transcription (TAT) peptide ---a cell penetrating peptide which can recognize some receptors of cell membrane---was conjugated to the surface of PEG-*b*-cholesterol to form the final nanoparticle micelle drug carrier designed--- TAT-PEG-*b*-Chol. Lastly, FITC, Quantum dots (QDs) and ciprofloxacin molecules were efficiently loaded into the core shell of the nanoparticles by a membrane dialysis method respectively. The morphology of blank and drug-loaded micelles was characterized using dynamic light scattering and transmission electron microscopy (TEM). These particles were spherical in nature, having an average size lower than 200 nm. Meanwhile, sustained *in vitro* drug release of ciprofloxacin from micelles was achieved in PBS solution.

The *in vitro* uptake of nanoparticles was tested by cultured human brain endothelial cells and astrocytes. Many more particles with TAT peptide were taken up by these cells than those without TAT. Most importantly, the *in vivo* bio-distribution investigation demonstrated that only TAT-PEG-*b*-Chol could penetrate the BBB and carry drug molecules to the brain parenchyma. Further study had indicated that the nanoparticles of TAT-PEG-*b*-Chol were mainly taken up by neurons after they reached the brain parenchyma. They only distributed in the cytoplasm of neuron but not nuclei. The primary pharmacokinetics study of TAT-PEG-*b*-Chol showed that they could reach the brain parenchyma shortly within 15 minutes after they entered the blood stream. In a word, the nanoparticle of TAT-PEG-*b*-Chol may be a promising drug carrier to deliver antibiotics across the BBB in the future clinical therapy of brain infectious diseases.

Successfully delivery of hydrophilic Penicillin G potassium was the main goal of the second part of this thesis. Here, this antibiotic was directly conjugated to TAT peptide *via* EDC/NHS chemistry since the drug cannot be well encapsulated into the core shell of TAT-PEG-*b*-Chol micelles. The drug-carrier system was characterized by NMR and MALDI-TOF/MS. The *in vitro* absorption test and antibiotics screening experiments proved that conjugation of TAT to Penicillin G potassium not only increase the penetration of this antibiotic to cell membrane but also enhance their antibacterial efficacy to infectious microorganisms to achieve better therapeutical results. Results of its cytotoxicity test indicated that TAT-Penicillin G was safe to be a drug carrier in the treatment of certain brain infectious diseases. Direct conjugation of

TAT penetrating peptide may become a feasible way to deliver hydrophilic Penicillin G through the BBB.

In the last part, a pathological rat brain model was successfully mimicked by focal cerebral injection of lipopolysaccharide (LPS). In this model, the responses of NG2 cells in response to the injury were studied. In the LPS injection surrounding areas, NG2 cells were activated and undergone dramatic morphological changes. NG2 expression was significantly upregulated. Using anti-CD11b antibody to block microglial complement receptor type 3 (CR3) in the injury site resulted in a down-regulation of NG2 cell reaction contrast to those accepted LPS administration only. It suggests that NG2 cells may respond to the pathological stimulation as a component downstream to microglia in pathological brain. In future, the novel drug delivery system and the roles of various types of neurons and non-neuronal cells on drug delivery, release, and effects will be further studied in this model.

In conclusion, nanoparticle of TAT-PEG-*b*-Chol is a good nano-carrier to deliver drug molecules cross the BBB. In pathological brain, sustained drug release could be expected in targeted site. With the aid of TAT cell penetrating peptide, Penicillin G-TAT system also was able to penetrate the BBB. They may be a promising drug carrier in future clinical application.

CHAPTER 1
INTRODUCTION

The most challenging task in treatment of various diseases or injuries in the central nervous system (CNS) is to overcome the barrier preventing the drugs moving from blood circulation into the brain parenchyma. The limited penetration of drugs through the blood brain barrier (BBB) is the rule, not the exception (Pardridge, 2007). Essentially, almost 100% of large-molecule pharmaceuticals, including peptides, recombinant proteins, monoclonal antibodies and RNA interference (RNAi)-based drugs, do not cross the BBB. More than 98% of small molecules cannot cross the BBB either (Greig, 1989). Ghose have analyzed drugs in the comprehensive medicinal chemistry (CMC) database and reported that among more than 7000 drugs, only 5% of these drugs may have treatment effects on the CNS diseases, but those drug were limited to treatment of just three conditions: depression, schizophrenia and insomnia (Ghose et al., 1999). Similarly, Lipinski has also pointed out that although 12% of all drugs are active in the CNS, only 8% of them are active in the brain for the treatment of diseases or disorders (Lipinski, 2000).

The BBB lies between the blood flow and the brain parenchyma and formed with three layers. The first layer of the BBB is mainly consists of a monolayer of polarized endothelial cells connected by complex tight junctions (Brightman, 1977). The basement membrane forms the second layer. Other cells, such as astrocytes, neurons or pericytes which dynamically regulate BBB's function are the third layer (Janzer and Raff, 1987). The specific property of BBB (tight junction) was formed by endothelial cells inside the blood vessels. It was just the tight junction which enables BBB to prohibit most foreign molecules from entering the brain including CNS drugs.

In physiological condition, the BBB provide stability and prevention for the CNS. But under pathological condition, the BBB may block the drugs entering the brain and therefore void drug effects. For example, many infectious diseases such as encephalitis may lead to CNS infection or inflammation, causing hearing loss, learning disability, or even endanger the patient life. However, in the therapy of CNS infectious and inflammatory diseases, the drug effects may have been hampered by the existence of the BBB simply because we may fail to deliver the drug components into the brain parenchyma. Thus, exploring strategies for delivering drug across the BBB is of great importance in the CNS diseases therapy.

Up to now, three main strategies have been developed for drug molecules penetrating the BBB. The neurosurgically-based strategy intends to temporarily open tight junctions between endothelial cells and thus allowing drug molecules to enter the BBB directly. The pharmacologically-based strategy is designed to work through modification of drug molecules, such as improving their lipophilicity and reducing their molecule weights in order to create new properties to facilitate drug transport crossing the BBB. However, certain problems are encountered for these two strategies, while the neurosurgically-based strategy may face the problem of infection and the pharmacologically-based strategy can probably change the therapeutic effects of drug components. Recently, a third strategy emerged. It is a physiologically-based strategy. This strategy uses chemical bond to couple or physical force to encapsulate the drug molecules to a vector or carrier. The vector or carrier may help drug molecules cross the BBB through receptor mediated transcytosis or absorptive mediated transcytosis.

In this strategy, different kinds of vector/carrier systems, such as monoclonal antibody and cationic protein, have been investigated (Bickel et al., 1993; Pardridge et al., 1995; Tamai et al., 1997). Among them, the nanoparticle carrier system (Kreuter, 2001) may be an outstanding system in the drug transport as many physical properties of the nanoparticles can benefit drug transport efficiency across the BBB.

In this study, a new core-shell nanoparticle micelle system was firstly devised to deliver an antibiotic to cross the BBB. This nanoparticle micelle system is made from amphiphilic copolymers by self-assembly in aqueous solution. Then, a cell penetrating peptide from human immunodeficiency virus (HIV) protein, trans-activating transcriptor (TAT) peptide was conjugated to the surface of the amphiphilic copolymer. TAT can recognize some receptors of cell plasma membrane to induce the transcytosis to bring the drug-nanoparticles system across the BBB (Brooks et al., 2005; Lewin et al., 2000; Torchilin et al., 2001). FITC, Quantum Dots and hydrophobic antibiotics molecules were successfully encapsulated into this core shell structured nanoparticle. They had achieved good penetration through the BBB *in vivo* and *in vitro*. In addition, hydrophilic antibiotics molecules were directly coupled to TAT peptide to form drug-vector system. The delivery of coupled antibiotics was primarily investigated. In summary, physiologically-based strategy was used to encapsulate or couple drug molecules to a delivery vector. The successful delivery of those antibiotics molecules across the BBB suggesting that the TAT-conjugated drug delivery system may be a promising carrier for the drug delivery targeting the brain.

1. Central nervous system inflammatory diseases

Inflammation is the reaction of a tissue and its microcirculation to a pathogenic insult. It is characterized by the generation of inflammatory mediators and movement of fluid and leukocyte from the blood into tissues (Raphael et al., 2004). CNS inflammatory diseases are those inflammation reactions involved diseases that are happened in brain or spinal cord. They can be triggered by immunological challenges (bacterial or viral infections), neuronal injury, and other epigenetic factors including chronic inflammatory syndromes and environmental toxins (Aloisi, 1999; Block and Hong, 2005; Hirsch et al., 2005; Kreutzberg, 1996; Minghetti, 2005; Minghetti et al., 2005; Mrak and Griffin, 2005; Streit, 2000).

1.1. Brain infectious diseases

Brain infectious disease is a severe CNS disease. Generally, the infection that predominantly affects the meninges surrounding the brain and the spinal cord is called meningitis. The infection of the brain tissue is called encephalitis. If both brain and meninges are affected, the term meningo-encephalitis is then used (Raphael et al., 2004). Virus and bacteria are two main sources to infect the brain and induce the infectious diseases.

1.1.1 Viral infections

Encephalitis is an inflammation of the brain, usually caused by a direct viral infection or a hypersensitivity reaction to foreign proteins (such as prion). It is well known that Japanese encephalitis virus (JEV) can cause the viral infection of

encephalitis (Shoji et al., 1993). Therefore, JEV has been experimentally used to create a preclinical model of post-encephalitic parkinsonism in rats (Ogata et al., 1997). In addition, other viruses such as HSV or HIV can also cause inflammation in the CNS.

1.1.2 Bacterial infections

Meningitis is mostly caused by bacterial infection. *Neisseria meningitidis* and *Haemophil influenzae* are the most important causes of this gram-negative bacterial meningitis. However, part of gram-negative bacteria or its secretion products can also induce brain inflammation. Lipopolysaccharide (LPS), the major component of the outer membrane of the gram-negative bacterial cell wall, is just a potent stimulus of brain inflammatory diseases (Rietschel and Brade, 1992). The LPS can stimulate the secretion of many products by microglial cells including cytokines (TNF- α , IL-1 β , and IL-6), chemokines, and prostaglandins (Ajmone-Cat et al., 2003; Chao et al., 1992; Nagai et al., 2001). *Streptococcus pneumoniae* is another most common and most serious cause of bacterial meningitis, with a mortality rate of 30% and neurologic sequelae in 30% to 50% of survivors (Durand et al., 1993; Pfister et al., 1993). In addition, brain abscesses, CNS tuberculosis and Lyme disease also are serious brain inflammatory diseases caused by bacterial infections (Curto et al., 2004; Leonard and Des Prez, 1990; Mathisen and Johnson, 1997; Rock et al., 2004; Townsend and Scheld, 1998).

1.2 Treatment of CNS infectious diseases

1.2.1 Anti-inflammatory drugs

Use of anti-inflammatory agents is one of potential therapies for CNS inflammatory diseases. A number of animal studies have indicated that there were upregulated expressions of certain inflammatory cytokines such as TNF- α , IL-1 β , IL-2, IL-4 and IL-6 by activated microglial cells in inflammation area (Hunot et al., 1999; Mogi et al., 1994; Mogi et al., 1996). Therefore, a strategy has been developed to inhibit the glial reaction or target inflammatory cytokines. For example, IL-1 β levels have been reported to increase rapidly after nigral administration of LPS in mice, so the neuroprotection can be achieved with nigral administration of an anti-IL-1 β neutralizing antibody (Arai et al., 2004; Arai et al., 2006).

There are many anti-inflammatory drugs that have been used in current therapies, including monoamine oxidase B (MAO) inhibitor drug pargyline (Kohutnicka et al., 1998) and selegiline (Deprenyl) (Klegeris and McGeer, 2000). In addition, the immuno-suppressants cyclosporine A and FK-506 and the nonselective COX-2 inhibitor sodium salicylate have all shown neuroprotective activity in CNS inflammatory diseases (Liu and Hong, 2003; Wersinger and Sidhu, 2002).

In recent years, it has been reported that selective inducible Nitric Oxide Synthase (iNOS) inhibitors S-methylisothiourrea and LN (G)-nitroarginine had neuroprotective effects on dopamine neurons in rats treated with LPS (Arimoto and Bing, 2003; Hemmer et al., 2001; Iravani et al., 2002; Le et al., 2001). It is therefore suggested that free radical scavengers or iNOS inhibitors may have potential

therapeutic effects in CNS inflammatory diseases.

1.2.2 Anti-Pathogen drugs

The choice of treatment for brain infection generally depends on its cause (Liu et al., 2008b). For the encephalitis caused by virus, the best treatment way is to find compound inhibits the replication of the virus. For instance, inosiplex and interferon- α were reported to be effective for the CNS disease of subacute sclerosing panencephalitis (SSPE), which is a progressive and fatal CNS disorder that results from a persistent SSPE virus infection (Hosoya, 2007).

However, for the therapy of CNS inflammatory diseases caused by bacteria or fungi, antibiotics (Dashti et al., 2008; Grayo et al., 2008; Kanellakopoulou et al., 2008; Kramer and Bleck, 2008; McPherson et al., 2008) and steroids (Dvorak et al., 2004; Fitch and van de Beek, 2008; Jubelt, 2006; van de Beek and de Gans, 2006; van de Beek, 2007; Weisfelt et al., 2007) may be good choices. Antibiotics are drugs derived wholly or partially from certain microorganisms and are used to treat bacterial or fungal infections. Antibiotics can either kill microorganisms or stop them from reproducing, allowing the body's natural defense system to eliminate them. They have been administrated for several decades, and are capable of sterilizing the cerebral spinal fluid (CSF) in a relatively rapid and reliable way.

Antibiotics that are effective in the laboratory may not necessarily work in an infected brain or spinal cord. However, the effectiveness of the treatment depends on how well the drug will be absorbed into the bloodstream, how much of the drug can

reaches the sites of infection in the body, and how quickly the body can eliminate the drug. During the clinical application, the biggest obstacle in the antibiotic therapy of CNS infectious diseases lies in the successfully delivery of effective antibiotics from the bloodstream to the brain parenchyma or spinal cord (Pardridge, 1997; Rubin and Staddon, 1999), due to the existence of the blood brain barrier (BBB) or the blood cerebral spinal fluid barrier (BCSFB).

1.2.3 Antibiotics selected in this study

Ciprofloxacin is a broad-spectrum synthetic antibiotic, belonging to an antibiotics group called fluoroquinolones. Its mode of action depends upon blocking bacterial DNA replication by binding itself to an enzyme called DNA gyrase, a type II topoisomerase, and topoisomerase , which is an enzyme necessary to separate replicated DNA (Drlica and Zhao, 1997), thereby inhibiting the unwinding of bacterial chromosomal DNA during and after the replication (Ball, 1986). Ciprofloxacin is used in the chemotherapy of various infectious diseases, including CNS infectious diseases, because of their broad and strong antibacterial activity, especially against Gram-negative bacteria (de Lange et al., 2000; Ivanov and Budanov, 2006; Moellering, 1996). Unlike Ciprofloxacin, Penicillin is a group of antibiotics derived from *Penicillium* fungi. They are Beta-lactam antibiotics used in the treatment of bacterial infections caused by susceptible, usually Gram-positive, organisms. Penicillin works by inhibiting the formation of peptidoglycan cross-links in the bacterial cell wall. The β -lactam moiety (functional group) of penicillin binds to the

enzyme (DD-transpeptidase) that links the peptidoglycan molecules in bacteria, which weakens the cell wall of the bacterium. In addition, the build-up of peptidoglycan precursors triggers the activation of bacterial cell wall hydrolases and autolysins, which further digest the bacteria's existing peptidoglycan. Penicillin G has been widely used in the treatment of CNS infectious diseases, especially brain bacterial meningitis, in recent decades (Reed, 1986; Tunkel et al., 1990; Vital Durand et al., 2002).

Ciprofloxacin and Penicillin are two typical broad-spectrum antibiotics commonly used. Ciprofloxacin is mainly against Gram-negative bacteria and Penicillin is usually against Gram-positive bacteria. In addition, Ciprofloxacin is hydrophobic but Penicillin is hydrophilic. Without any vectors, these two type antibiotics both have poor penetration rates through the BBB. As the BBB represents an obstacle for the delivery of these antibiotics from the blood to the brain, therefore, these two FDA approved antibiotics have been chosen in this study for the investigation of drug delivery through the BBB with designed nanoparticles micelles.

2. The cell biology of the blood brain barrier (BBB)

The existence of the BBB has been recognized for more than 100 years. In 1885, a German microbiologist, Ehrlich, first demonstrated the BBB. He showed the evidence for the existence of this barrier between the blood and brain parenchyma. He injected vital dyes intravenously and found that, in contrast to other tissues, the brain parenchyma was not stained (Ehrlich, 1885). His successor Goldman injected the dyes

into the CSF and observed the staining of the brain parenchyma but not of the peripheral organs (Goldman, 1913). Since these discoveries, extensive studies have been done on the physiology and pharmacology of the BBB (Abbott, 2005; Begley and Brightman, 2003; Hawkins and Davis, 2005).

The brain is perhaps one of the least accessible organs for the delivery of functional pharmacological compounds. There are two physiological barriers that separate the brain from its blood supply and control the entry and exit of endogenous and exogenous compounds. One is the BBB and the other is the BCSFB. The BBB is mainly consists of a monolayer of polarized endothelial cells connected by complex tight junctions (Brightman, 1977). The function of BBB is dynamically regulated by various cells, including astrocytes, neurons and pericytes (Janzer and Raff, 1987). The endothelial cells are separated from these other cells by a basal lamina, whose components such as type IV collagen, laminin, fibronectin and heparan sulfate may be involved in drug transport (Vorbodt, 1989).

The BCSFB is located at the choroid plexuses. They are mainly formed by epithelial cells held together at their apices by tight junctions. There is a stroma containing the blood vessels beneath the epithelial cells. Thus, the fenestrated blood vessels of the choroid plexus allow large molecules to pass, but the tight junctions at the epithelial cell surfaces restrict their passage into the CSF (Spector and Johanson, 1989). Because the surface area of the human BBB is estimated to be 5000 times greater than that of the BCSFB, the BBB is considered to be the main region controlling the uptake of drugs into the brain parenchyma and the target for drug

delivery to the brain (Pardridge, 1995).

2.1 Structure of the BBB

2.1.1 Endothelial cells

The BBB is mainly formed by brain capillary endothelial cells (BCEC) (Rubin and Staddon, 1999), as Figure 1.1 shown. The tight junctions (TJ) between the endothelial cells are an important structural element of the BBB. They prevent paracellular transport of foreign compounds from the blood to the brain (Brightman and Reese, 1969; Reese and Karnovsky, 1967; Rubin and Staddon, 1999). The tight junction consists of tight junctional strands between adjacent brain capillary endothelial cells at multiple appositional sites by freeze fracture electron microscopy (Weerasuriya, 1987).

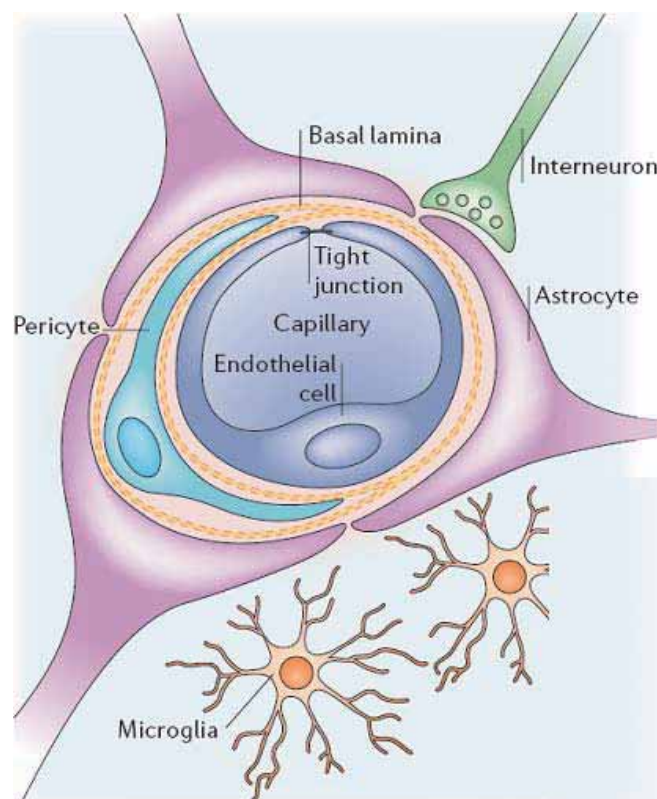


Figure 1.1: The structure of the BBB. The BBB is mainly formed by endothelial cells, astrocytes, pericytes and interneuron. (Abbott, 2002)

BCEC generally are situated at the interface between the blood and the brain. They perform many essential biological functions such as barrier, transport of micronutrients and macronutrients, receptor-mediated signaling, leukocyte trafficking, and osmoregulation (Persidsky et al., 2006). However, their most important function is the barrier function that prevents the free entry of compounds from the blood to the brain (Doolittle et al., 2005). BCEC have greater number and volume of mitochondria as compared with endothelium of other organs. The increased content of mitochondria enhances the energy potential and is thought to be required for active transport of nutrients to the brain. It is estimated that cerebral capillaries have five to six times more mitochondria per capillary section than rat skeletal muscle capillaries (Oldendorf et al., 1977).

2.1.2 Other cell types

Other cell types, such as pericytes, astrocytes, and interneurons, also play an important role in the structure and function of the BBB (Gaillard et al., 2000; Janzer and Raff, 1987; Lai and Kuo, 2005). Among them, astrocytes form a network fully surrounding the capillaries with their foot processes. The tight junction is just induced and maintained by the endfeet of these astrocyte cells surrounding the BCEC (Rubin and Staddon, 1999). Pericytes share the continuous capillary basement membrane with the BCEC (Lai and Kuo, 2005). Their phagocytotic activity forms an additional BBB property. Furthermore, pericytes also regulate endothelial homeostasis, thereby

negatively regulating brain endothelial fibrinolysis (Kim et al., 2006)). Axons from neurons also connect closely against the endothelial cells and contain vasoactive neurotransmitters and peptides (Gaillard et al., 2000; Janzer and Raff, 1987).

2.1.2.1 Astrocytes

Astrocytes are glial cells that envelop >99% of the BBB endothelium (Hawkins and Davis, 2005). In addition to the support function of astrocytes to endothelial cells, these two cell types can influence each other's structure. Their interactions not only induce and modulate the development of the BBB and unique BCEC phenotype, but also greatly enhance endothelial cell TJ and reduce gap junctional area (Tao-Cheng and Brightman, 1988). Besides that, this interaction can increase the number of astrocytes membrane particle assemblies and astrocyte density (Abbott, 2002; Tao-Cheng et al., 1987; Tao-Cheng and Brightman, 1988). Astrocytes are greatly essential for proper neuronal function, suggesting that astrocyte–BCEC interactions are essential for a functional neurovascular unit (Abbott et al., 2006). Therefore, it is plausible that astrocytes may modulate the BBB phenotype without being directly involved in changing the physical BBB properties.

2.1.2.2 Pericytes

It has been reported that the association of pericytes to blood vessels may regulate endothelial cell proliferation, survival, migration, differentiation, and vascular branching (Lai and Kuo, 2005). Pericytes are flat, undifferentiated, contractile connective tissue cells that develop around capillary walls (Figure 1.1). Microvascular pericytes lack the α -actin isoform, suggesting that these cells may not

be involved in capillary contraction (Lai and Kuo, 2005). Part of pericytes of the BBB may belong to macrophage lineage and they possess the capacity to phagocytose exogenous proteins and present antigen (Williams et al., 2001). It was found that the lack of pericytes resulted in endothelial hyperplasia and abnormal vascular morphogenesis in the brain. There is evidence that pericytes are able to mimic astrocyte ability to induce BBB “tightness”(Persidsky et al., 2006). These evidences support the hypothesis that pericytes play an important role in maintaining the structural integrity of the BBB.

2.1.2.3 Neurons

High level of neuronal activity requires tight junction regulation of the microcirculation. Also, a close relationship between regional brain activity and blood flow was demonstrated by neuroimaging (Paemeleire, 2002). In addition, there are evidences that neurons induce expression of enzymes unique for BCEC, such as reversible expression of sm alpha-actin protein and sm alpha-actin mRNA induced by neuron in cloned cerebral endothelial cells (Tontsch and Bauer, 1991). Therefore, these significant evidences suggest that neurons also can regulate functions of the BBB.

2.2 The permeability properties of the BBB

The BBB significantly impedes free entry of all molecules from blood to brain, except those compounds are lipophilic and/or with small molecular weight. Generally, the drug molecules with a molecular weight higher than 500 Da and lower

lipophilicity cannot penetrate the BBB (de Boer and Gaillard, 2007). These impermeable macromolecules may include peptide, protein or other drug molecules. However, there are a number of small and large hydrophilic molecules that can enter the brain by active transport (Rowland et al., 1992). This active transport is a mediated process of moving particles across BBB cell membrane against a concentration gradient using chemical energy. For the transport of some essential nutrients, such as glucose and certain amino acids (or related molecules, including L-DOPA), specific active membrane transporting proteins are present in relatively high concentrations in brain endothelial cells. There also seems to be receptor mediated transport which is capable of transferring macromolecules into the brain. The best known of these is the transferrin receptor (Pardridge, 1997) . Therefore, the impermeability or permeability of the BBB is selective.

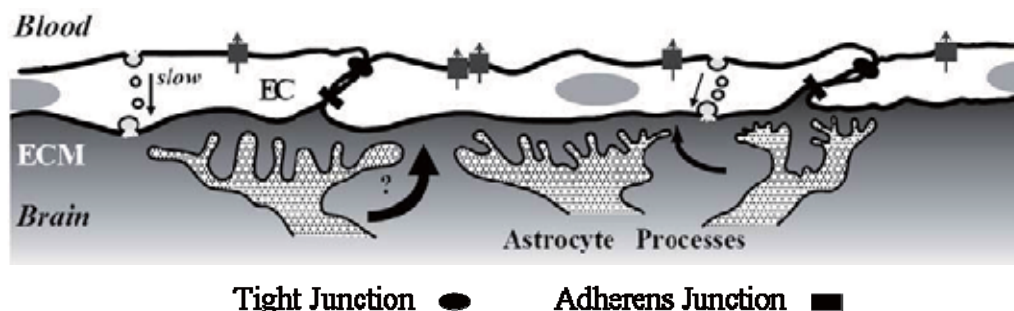


Figure 1.2: Essential features of the blood brain barrier. The BCEC are coupled by adherent junction and tight junctions, the latter limiting the paracellular flux. (Rubin and Staddon, 1999)

The permeability properties of the BBB greatly affect the therapy of the CNS inflammatory diseases. The BBB is by far the biggest obstacle to CNS drug delivery since the BBB excludes proteins, complex carbohydrates, and other "foreign" molecules such as toxins and drugs to enter the brain parenchyma. It results in many

potential therapeutic agents such as antibiotics cannot reach the CNS (Ghose et al., 1999; Lipinski, 2000; Pardridge, 2007). For selected antibiotics in this study, they also have the difficulty to pass through the BBB. Although Ciprofloxacin tend to distribute rapidly into peripheral tissues and fluids, and reach concentrations often higher than found in serum or plasma (Sorgel et al., 1989), However, distribution of the unbound drugs into the cerebrospinal fluid (CSF) and brain extracellular fluid was shown to be poor (Ooie et al., 1996a; Ooie et al., 1996b; Ooie et al., 1996c). For Penicillin G, after they enter the blood stream (100%), only 2.6-4.9% (rabbit) or 7.8% (human) of Penicillin G entered the CSF because of existence of BBB and BCSFB (Lutsar et al., 1998; Richards et al., 1981). Therefore, it is of great importance to explore effective strategies to overcome the obstacle and deliver the antibiotic drugs to brain.

3. Drug delivery into the brain

Since the BBB represents an insurmountable obstacle for a large number of drugs, including antibiotics, antineoplastic agents, and a variety of CNS-active drugs, especially neuropeptides (Kreuter, 2001), for the therapy of brain infectious diseases, the biggest challenge is how to introduce a drug to penetrate this barrier. According the Comprehensive Medicinal Chemistry database, among more than 7000 drugs, only 5% of these drugs may have treatment effects on the CNS diseases, but they are limited to treatment of just three conditions: depression, schizophrenia and insomnia (Ghose et al., 1999). Another study reports that 12% of all drugs are active in the CNS, but of which only 8% are active in the brain for diseases or disorders (Lipinski, 2000).

Therefore, it is necessary to develop effective strategies to successfully deliver drug molecules through the BBB.

3.1 Possible ways of delivering a compound from blood to brain

The existing possible ways to deliver a compound from the blood to the brain are shown in Figure 1.3.

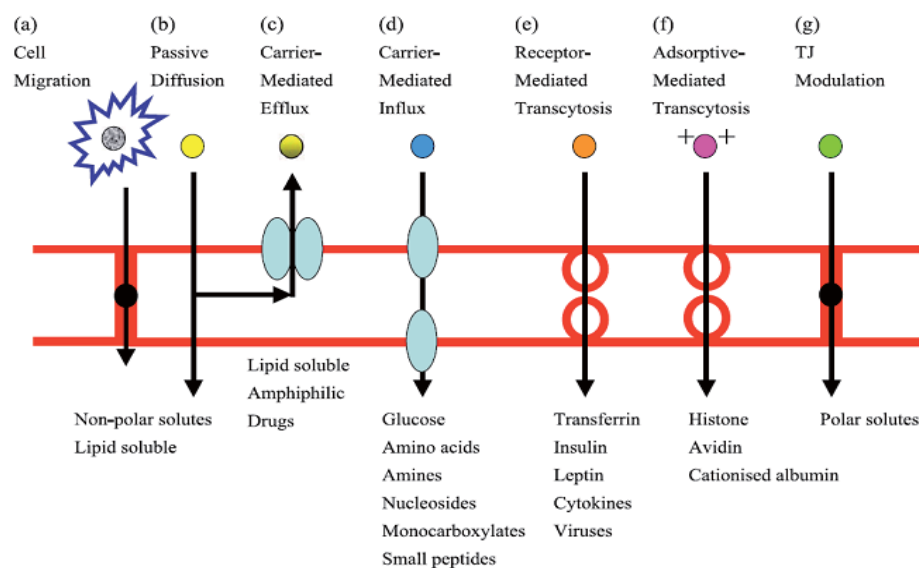


Figure 1.3: Potential routes for transport through the BBB: cell migration (a), passive diffusion (b), active transport (c, d, e and f) and tight junction modulation (g) (Begley, 2004)

3.1.1 Cell migration

It is reported that the leukocyte cells of immune system can migrate through tight junction of the BBB under the inflammatory conditions (Begley, 2004; Coisne et al., 2007; Edens and Parkos, 2000; Shumei Man, 2007). The entry of leukocyte cells into brain tissues is governed by the presence of chemokines and adhesion molecules at post-capillary venules (Butcher and Picker, 1996; Schenkel et al., 2004; Shumei Man, 2007; Springer, 1994; Weninger and von Andrian, 2003). Based on the concept of cell

migration, the endothelial cells of the BBB actively participate in the inflammatory leukocyte migration into the brain by sequential molecular interactions with circulating leukocytes. Therefore, if a compound (including possible drugs) can be successfully taken into the body of leukocyte cells, it can enter the brain through this pathway using drug loaded leukocytes as drug carriers.

3.1.2 Passive diffusion

Passive diffusion is a direct and energy free transport way of substance from the blood to brain from high concentration side to low concentration side. It only depends on lipophilicity and molecular weight of the compound being delivered (Pardridge, 1995). In general, Lipinski's rule-of-five and the Abraham's equation can be used to predict the passive transport of a drug molecule across the BBB (Abraham and Weathersby, 1994; Lipinski et al., 2001). For hydrophilic compounds, their transport via the paracellular route is limited. However, lipophilic drugs smaller than 400–600 Da may freely enter the brain via this transcellular route.

3.1.3 Tight junction modulation

The connection of tight junction is adjusted by stretch and shrinkage of endothelial cells and some inflammatory mediators (Abbott and Revest, 1991). The result of tight junction modulation would change the permeability of the BBB. Recent evidence suggests that many mediators may increase the trans-endothelial permeability by raising intracellular free calcium or causing a contractile event that

pulls apart the tight junctions (Coisne et al., 2007; Huber et al., 2001; Staddon and Rubin, 1996). It suggests that the tight junction modulation can “relaxes” the junctions and wholly or partially opens the paracellular aqueous diffusional pathway and let the compounds in (Begley and Brightman, 2003).

3.1.4 Active transport

Active transport system is the most important transport pathway in the drug delivery from the blood to the brain. It can be divided into absorptive-, carrier-, or receptor mediated transcytosis.

3.1.4.1 Carrier mediated transcytosis (CMT)

Carrier-mediated transcytosis is generally used for the delivery of nutrients, such as glucose, amino acids, and purine bases to the brain (Abbott and Romero, 1996; Ikumi Tamai, 2000). Up to now, at least eight different nutrient transport systems have been identified, with each transporting a group of nutrients of the same structure. CMT is substrate selective and the transport rate is dependent on the degree of occupation of the carrier (Smith, 1993). Therefore, only drugs that closely mimic the endogenous carrier substrates will be taken up and transported into the brain.

3.1.4.2 Receptor mediated transcytosis (RMT)

In contrast to CMT, some larger molecules, such as peptides, proteins, and genes specifically enter the brain via receptor-mediated transcytosis. Classical examples of receptors involved in receptor-mediated transcytosis are the insulin receptor (Duffy and Pardridge, 1987); the transferrin receptor (Moos and Morgan, 2000; Pardridge et

al., 1987); and the transporters for low-density lipoprotein (Dehouck et al., 1997), leptin (Bjorbaek et al., 1998), and insulin-like growth factors (Duffy et al., 1988).

3.1.4.3 Absorptive mediated transcytosis (AMT)

Absorptive-mediated transcytosis is initiated by the binding of poly-cationic substances (such as most cell-penetrating peptides) to negative charges on the surface of cell plasma membrane (Vorbrodts, 1989). The substance for delivery was charged. This is the biggest difference contrast to those substance transported by RMT. This process of AMT does not involve any specific plasma membrane receptors. Endocytosis occurs upon the binding of the cationic compound to the plasma membrane. Some nanoparticle drug delivery systems with a cell-penetrating peptide may use this way to penetrate the BBB and bring drug molecules to the brain (Santra et al., 2005; Torchilin et al., 2001).

3.2 Strategies for drug delivery into the brain

Clinically, several strategies for drug delivery into the brain have been developed according possible routes of transport through the BBB

3.2.1 Neurosurgically-based strategy

The BBB disruption is a neurosurgically-based strategy (Bobo et al., 1994; Kroll et al., 1996). A number of means such as intra-carotid arterial infusion of hyperosmotic solutions, administration of noxious agents including vasoactive compounds, or local ultrasonic irradiation of the brain can transiently disrupt the BBB (Emerich et al., 1998; Neuwelt and Rapoport, 1984). The temporary opened tight

junction of the BBB will allow the drug molecules to enter the brain parenchyma. Although these invasive methods are traditional and have achieved some success, the risks of infection and neuropathological changes due to disruption of the BBB emphasize the need to develop new noninvasive delivery strategies.

3.2.2 Pharmacologically-based strategy

The pharmacologically-based strategy is a noninvasive approach. Recent studies have found that factors such as lipophilicity and molecular weight may modulate the passive transport of a drug across the BBB. Therefore, this strategy will focus on drug molecule modification by reducing polar groups or adding methyl groups to create new drug properties (such as lipophilicity) to allow drug crossing the BBB easily (Greig, 1989).

3.2.2.1 Drug lipophilicity modification

Lipophilicity modification can convert water-soluble drugs into lipid-soluble drugs or attach lipid carriers to water-soluble drugs to facilitate the drugs to cross the BBB. However, it is not easy for the reformulation of a water-soluble drug with lipidization modifications. Therefore, currently no drug has been successfully converted from non-brain-penetrating into a brain penetrating molecule that could cross the BBB in pharmaceutical market.

Lipid carriers that have been used include dihydropyridine, adamantane and fatty acylcarriers, such as N-docohexaenoyl (Bodor, 1994; Shashoua and Hesse, 1996; Tsuzuki et al., 1994). However, the increased lipid solubility obtained by attaching a

lipid carrier to a drug may not simply increase its passage across the BBB; it may also increase its penetration into other cells and tissues in the body.

3.2.2.2 Other modifications

As the BBB generally allowed molecules <400 Da crossing the BBB and reach brain, drug molecule can be modified by reducing the relative number of group without affecting the functional group to get a lower molecule weight. It will promote the penetration of the drug through the BBB. In addition to the molecular weight modification, drugs can also be modified to take advantage of native BBB nutrient transport systems. For example, the BBB large neutral amino-acid carrier has been used to deliver L-DOPA in Parkinson's disease (Wade and Katzman, 1975).

However, in most cases, the modification of the drug molecules may change the therapeutic properties of the drug, resulting in the dysfunction of drug. Therefore, a better drug delivery strategy is required to transport a drug with preservation of the functional molecular structure into the brain.

3.2.3 Physiologically-based strategy

This strategy takes advantages of the physiological transport of endogenous substances from blood to brain. It uses physical force to encapsulate or chemical bonds to couple the drug molecules to a vector and deliver them across the BBB through RMT or AMT (Pardridge, 1999; Tamai et al., 1997). These vectors can be monoclonal antibody, liposome, cationic protein and nanoparticle system. Vectors can be recognized by the receptors located in the endothelial cell membrane and absorbed

into the cell by transcytosis. Besides, vectors may form the endosomes at cell plasma membrane to induce transcytosis. This strategy is also noninvasive to the BBB and has good safety profiles and high efficacy drug transport.

3.2.3.1 Endogenous BBB transporters

This approach is based on knowledge of endogenous BBB transporters. It aims to reformulate drugs to be substrates for various endogenous transporters at the BBB so that these molecules can cross the BBB via endogenous transport systems. The principle of this strategy can be also applied to large peptides and proteins that may use either RMT or CMT to carry the peptide or protein across the cerebral endothelium (Bickel et al., 1994).

An example of the drug transport by endogenous BBB transporters is the use of monoclonal antibodies (OX26) to the transferrin receptor that abundantly expressed in the luminal membrane of the BBB. The OX26 antibody may be used as a vector for CNS delivery and can be linked to a drug or biologically active peptide or protein which normally can not cross the BBB. The binding of the OX26 antibody to the transferrin receptor appears to induce endocytosis and the entire construct will then penetrate the BBB (Bickel et al., 1994).

Drugs that enter the brain via endogenous transporters includes valproic acid, L-DOPA, mepyramine, oxazolamine COR3224 et al (Begley, 2004). They use different transports (such as Medium-chain fatty acid carrier, large neutral amino acid carrier or Nucleoside carrier) to cross the BBB by RMT or CMT.

3.2.3.2 Cell-penetrating peptide vectors

Several cell-penetrating peptides which can quickly enter cells have been developed recently (Wadia and Dowdy, 2002; Zhao and Weissleder, 2004). At present, it is still not completely clear what the mechanism by which these peptides can cross the cell membrane is. Some researchers believed that the peptides by virtue of their structure penetrated directly through the cell membrane (Derossi et al., 1996; Vives et al., 1997). They may thus be able to penetrate the cell membrane without causing any damage. They may use a similar manner to a signal peptide entering the endoplasmic reticulum and carrying with it a nascent protein during the normal process of protein synthesis and post-translational modification.

One of these cell-penetrating peptides, transactivating-transduction (TAT), has been a research hotpot in recent years. It acts in the process of replication of the HIV virus by penetrating the nuclear membrane and acting as an activator of transcription (Torchilin et al., 2001; Wadia and Dowdy, 2002). The TAT peptide has been shown to carry heterologous proteins into several cell types (Fawell et al., 1994) and across the BBB (Schwarze et al., 1999). Other two cell-penetrating peptides, penetratin and SynB1 were also investigated. When they were linked to doxorubicin in a rat in situ brain perfusion model, the increased CNS levels of doxorubicin by 3 to 8 times compared with doxorubicin alone was found (Rousselle et al., 2000).

Therefore, this physiologically-based strategy may require drug molecules to be linked to the cell-penetrating peptide vector by chemical or physical force (Liu et al., 2008a). With the aid of the vector, the drug can penetrate the BBB and be delivered to the brain parenchyma.

3.2.3.3 Liposomes and nanoparticles

Liposomes and nanoparticles have large and complex constructs which can be made from a variety of chemical constituents. Relatively large amounts of drug or agent can be incorporated into these structures. Liposomes and nanoparticles may provide the possibility for significant drug delivery to the CNS. The surface of the liposome or nanoparticle can be modified and be attached with some biological ligands so that the construct can be targeted to the CNS via specific BBB mechanisms.

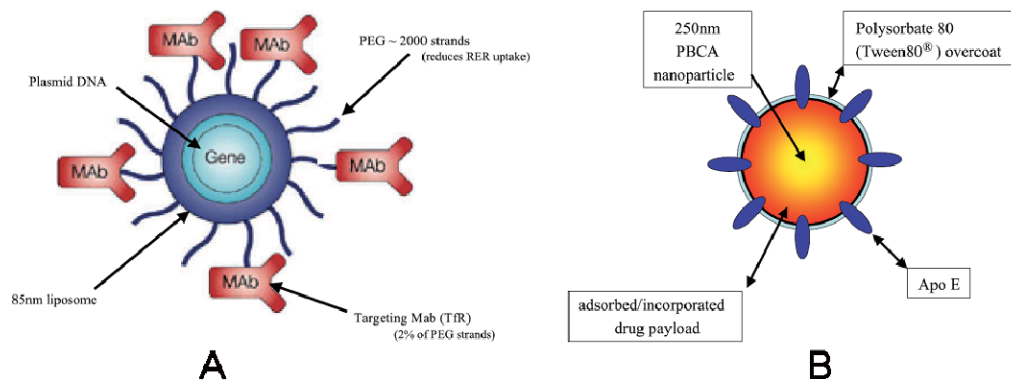


Figure 1.4: An immunoliposome (A) and a PBCA nanoparticle (B). A: A plasmid DNA containing a gene is packaged into the center of an 85 nm diameter liposome. The surface of the liposome is coated with ~2000 strands of PEG, which reduces uptake by the RER. B: A drug can be incorporated into the 250 nm diameter nanoparticle during polymerization or absorbed onto the surface of the preformed particle. The particle is then coated with polysorbate 80 (Tween 80), which further binds Apo-E in the bloodstream. (Begley, 2004)

PEGylated immunoliposomes or nanoparticles have been employed to deliver many kinds of CNS drugs. Also, they are applied to target and transfect h-galactosidase (LacZ reporter gene) or luciferase into the brain (Pardridge, 2002; Shi et al., 2001). The gene is encapsulated into the center of the liposome and its surface

is then coated with polyethylene glycol (PEG) to prolong the circulation time by reducing uptake by the reticulo-endothelial system (RES). Using this approach, both hgalactosidase and luciferase have been targeted to the brain and the relevant enzyme is expressed (Shi et al., 2001).

Poly(butyl)cyanoacrylate (PBCA) nanoparticle is another nanoparticle that has also been used to deliver drugs to the CNS with a good degree of success (Alyautdin et al., 1997; Alyautdin et al., 1998; Steiniger et al., 2004). Drugs such as Loperamide (Alyautdin et al., 1997), Tubocurarine (Alyautdin et al., 1998), Doxorubicin (Steiniger et al., 2004) have been successfully delivered to the CNS using PBCA nanoparticles

TAT cell-penetrating peptide may be conjugated to the surface of both liposomes (Torchilin et al., 2001) and nanoparticles (Lewin et al., 2000). It appears to greatly penetration ability through the BBB, although nanoparticles and liposomes are relatively complex and large structures. This may be applied in the drug delivery targeted the brain.

4. Nanoparticles in the brain drug delivery

Nanoparticles are solid colloidal matrix-like polymeric particles made of natural or artificial polymers (Soppimath et al., 2001) or lipids (Wissing et al., 2004). Their particle sizes range from about 10 nm to 1000 nm (Kreuter, 1994). Generally administered by the intravenous route similar like liposomes, they have been developed as therapeutic or imaging agents for targeted brain delivery. Their main advantages over liposomes are the simple preparation procedures, a high physical

stability, and the possible sustained drug release and these advantages may be suitable for treatment of chronic diseases (Olivier, 2005).

One potential application of nanoparticles is the drug delivery to the brain. It accompanied with the local sustained release of the new large therapeutic molecules, such as peptides, proteins, genes or anticancer drugs, to treat CNS diseases. However, due to their size ranging between 10 and 1000 nm (generally 50–300 nm), they are unable to diffuse through the BBB to reach the brain parenchyma. The RMT or AMT might be the route for the particle to cross the BBB and deliver the drug to the targeted site.

4.1 Ideal properties of nanoparticles for brain drug delivery

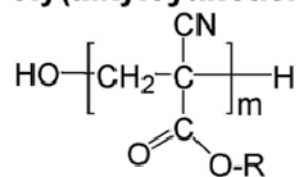
Based on general formulation considerations and specific BBB features, the ideal properties of nanoparticles for brain drug delivery must meet the requirements as follows: 1) Nontoxic, biodegradable, and biocompatible; 2) Particle diameter <200 nm; 3) Physical stability in blood (no aggregation); 4) Avoidance of the mononuclear phagocyte system (MPS, no opsonization), prolonged blood circulation time; 5) BBB-targeted and brain delivery (receptor-mediated transcytosis across brain capillary endothelial cells); 6) Scalable and cost-effective manufacturing process; 7) Amenable to small molecules, peptides, proteins, or nucleic acids; 8) Minimal nanoparticle excipient-induced drug alteration (chemical degradation/alteration, protein denaturation); and 9) Possible modulation of drug release profiles (Olivier, 2005).

4.2 Some successfully developed nanoparticles in brain drug delivery

Since the first papers in 1995, nanoparticles made of poly(butyl) cyanoacrylate (PBCA) that coated with the nonionic surfactant polysorbate 80 have been intensely investigated. This nanoparticle permits the delivery of drugs to the brain (Kreuter et al., 1995). Also, in the mid 1990s, long-circulating PEGylated PLA or PLGA nanoparticles have opened great opportunities for targeted drug delivery to brain (Gref et al., 1995). The nanoparticle made of polylactide homopolymers (PLA) or poly(lac-tide-co-glycolide) heteropolymers (PLGA) may be a promising drug delivery carrier to deliver drugs across the BBB.

4.2.1 PBCA nanoparticles

Nanoparticles made by poly(alkylcyanoacrylate) polymers were described in 1977 at the first time (Couvreur et al., 1977). They are generally prepared from (iso) butyl-cyanoacrylate or (iso)hexyl-cyanoacrylate monomers (Figure 1.5) by emulsion anionic polymerization in an acidic aqueous solution of a colloidal stabilizer such as dextran 70, polysorbates, and poloxamers. These particles typically have diameters of 250nm. Inclusion of a drug can be made during the polymerization process or by adsorption into preformed nanoparticles. The particles are then coated with polysorbate 80 (Ramge et al., 2000), a compound that might induce the transcytosis in the surface of the endothelial cells, to form the nanoparticle drug delivery system.

Poly(alkylcyanoacrylate)

R = methyl, ethyl, (iso)butyl, (iso)hexyl

Figure 1.5: Structure of poly(alkylcyanoacrylate).

The use of PBCA nanoparticles to deliver a drug to the CNS has achieved a good degree of success (Alyautdin et al., 1997; Alyautdin et al., 1998; Gulyaev et al., 1999; Kreuter, 2001; Steiniger et al., 2004). It was reported that intravenous administration of polysorbate 80-coated PBCA nanoparticles encapsulated with doxorubicin (Gulyaev et al., 1999; Steiniger et al., 2004), loperamide (Alyautdin et al., 1997), tubocurarine (Alyautdin et al., 1998) or hexapeptide dalargin (Kreuter et al., 1995) could facilitate the delivery of the compounds to the brain, where they could have their pharmacological effects. As for the mechanism, it was hypothesized that polysorbate-coated nanoparticles were transported across the BBB via endocytosis by the brain capillary endothelial cells (Kreuter, 2001). This endocytosis may be triggered by a serum protein, apolipoprotein E. It was reported that the absorption on polysorbate 80-coated nanoparticles occurred 5 minutes after incubation in citrate-stabilized plasma at 37°C. Despite a number of arguments listed by Kreuter (Kreuter, 2001), Olivier hypothesized a possible mechanism involved in a nanoparticle-induced nonspecific BBB permeabilization (Olivier et al., 1999), which has been supported by some important observations (Olivier, 2005). It suggested that the polysorbate 80 can cause BBB disturbance and dramatically increase BBB permeability. However, the exact mechanism of the transport through this

nanoparticle system is still not clear.

Although the study of the PBCA nanoparticle carrier has achieved great success in delivering some drugs to the CNS, certain limitations may preclude, or at least limit, their potential in clinical applications. First, the interaction between encapsulated drugs and the nanoparticles may lack stability (Olivier et al., 1999), or, the drug-encapsulated nanoparticles may disperse in blood stream by a combined effect of serum protein competition and polymer degradation (Olivier et al., 1996). Second, the rapid degradation rate of nanoparticles *in vivo* greatly limits their application. Because of the lacking of stable properties, the PBCA nanoparticles intravenously administered will be rapidly cleared from the blood stream by the mononuclear phagocyte system (MPS) and mainly accumulate in liver and spleen (Douglas et al., 1987; Grislain et al., 1983; Waser et al., 1987). The degradation of nanoparticles may also affect the loss of compounds entrapped (Lobenberg et al., 1998; Simeonova et al., 1988; Verdun et al., 1990). At last, the toxicity of nanoparticles can not be neglected. It has been known for a long time that polysorbate 80 can cause BBB disturbance (Azmin et al., 1985) and dramatically increase BBB permeability. This is a potential threat to the safe application of drugs in the CNS. The polysorbate 80-coated PBCA nanoparticles can induce a dramatic decrease in mice locomotor activity *in vivo*. In summary, novel designed nanoparticles, which are nontoxic and have prolonged blood circulation time and lower mononuclear phagocyte system uptake, should be developed to serve as a drug carrier system for brain drug delivery.

4.2.2 PEGylated PLA/PLGA nanoparticles

PEGylated nanoparticles are a newly developed drug delivery system for intravenous drug administration. The PEG coating on the particle surface can provide protection against interference from the blood components, resulting in a prolonged time in blood circulation by reducing the particle capture by the reticulo-endothelial system (RES) cells (Mosqueira et al., 2001). The degradable core of nanoparticle was formed by a variety of polymers, such as polylactide (PLA) or poly(lac-tide-co-glycolide) (PLGA). Various drugs could be encapsulated into the core and released continuously (Gref et al., 1995). PEGylated nanoparticles could be good candidates to encapsulate drugs and transport them through the BBB and reach the brain parenchyma.

4.2.2.1 Nanoparticle preparation

Nanoparticles made of mPEG-PLA/PLGA copolymers are mainly prepared by the technique of emulsion/solvent evaporation or the precipitation/solvent diffusion (Soppimath et al., 2001). Briefly, for the technique using emulsion/solvent evaporation, copolymers are dissolved in an organic solvent immiscible to water and emulsified in an aqueous phase generally containing an emulsifying agent. Then the solvent is evaporated off under normal or low pressure to form nanoparticles. In the method employing solvent diffusion, polymers are dissolved in an organic solvent miscible to water and dispersed in an aqueous phase generally containing a colloid stabilizer. The almost instantaneous diffusion of the organic solvent into the aqueous phase results in the precipitation of the copolymers as nanoparticles. Finally, the

solvent is evaporated off as above or extracted by dialysis against water (Lee et al., 2004). Generally, only compounds that can dissolve in the organic solvent can be incorporated by the second method.

Because of their difference in water solubility, the hydrophobic PLA/PLGA and hydrophilic PEG of the mPEG-PLA/PLGA copolymer tend to phase-separate in aqueous solvent. Therefore, in the process of the organic solvent evaporation or diffusion, the PEG chains migrate to the aqueous phase, whereas the hydrophobic PLA/PLGA moieties aggregate as the nanoparticle core.

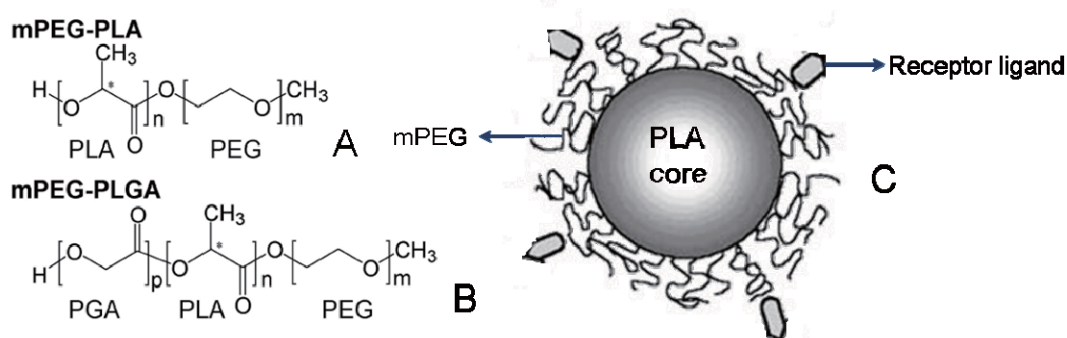


Figure 1.6: Structure of methoxypoly (ethylene glycol)-polylactide [or poly (lactic acid)] (mPEG-PLA)(A), methoxypoly (ethylene glycol)-poly (lactide-co-glycolide) [or poly-(lactic-co-glycolic acid)] (mPEG-PLGA) (B) and the core shell structure of nanoparticles (C).

4.2.2.2 PEGylated nanoparticles conformations

mPEG-PLA/PLGA nanoparticles are constituted of a PLA/PLGA hydrophobic core inside and surrounded by a hydrophilic PEG corona outside. PEG conformation at the surface of PLA-PEG nanoparticle is important for the function of the PEG layer (Chognot et al., 2003; Gref R et al., 1998; Riley T et al., 1999; Riley T et al., 2001; Stolnik et al., 2001). The thickness of PEG layer depends on the PEG molecular

weight and surface density. Depending on their surface density, PEG chains may have brush-like (high density) or mushroom-like (low density) conformations (Gref R et al., 1998; Stolnik et al., 2001). PEG surfaces in brush-like and intermediate configurations may be able to reduce phagocytosis and complement activation, whereas PEG surfaces in mushroom-like configuration could be potent complement activators and favored phagocytosis (Gbadamosi et al., 2002; Gref R et al., 2000; Moghimi and Szebeni, 2003; Vittaz et al., 1996). Due to the variation in the PLA or PEG molecular weights, the conformation of PEG chains at the PEG-PLA nanoparticle surface is a complex issue to be addressed. At nanoparticle surface, the area available per PEG chain at the outer boundary of the shell is dependent on PEG to PLA molecular weight ratio that governs the PLA packing density and the surface curvature (linked to the nanoparticle size) of the assembly (Chognot et al., 2003; Heald et al., 2003; Riley T et al., 1999).

4.2.2.3 Application of PEGylated nanoparticles in brain drug delivery

Various kinds of conventional drugs can be encapsulated into the PEGylated PLA/PLGA nanoparticles. Examples are savoxepine (Allemann et al., 1993), doxorubicin (Yoo and Park, 2001) and irinotecan (Onishi et al., 2003). Because PLA and PLGA are hydrophobic molecules, lipophilic or hydrophobic drugs are easier to encapsulate in PLA/mPEGPLA nanoparticles than hydrosoluble ones.

Besides conventional drugs, peptides, polypeptides, and protein drugs also can be formulated as PEGylated nanoparticles. Except for the formulation issues inherent to peptide chemical instability or chemical reaction between peptides and polymer

degradation products (Lucke et al., 2002), the formulation of peptide-encapsulated nanoparticles is similar to conventional drugs (Elamanchili et al., 2004; Hiroaki et al., 1994; Kawashima et al., 1998). But for the protein drug, it is of great importance for their stability, integrity and activity during the process of encapsulation. It requires that each nanoparticle encapsulation of protein is unique and requires specific adaptation and evaluation. This goal can be achieved by various means such as altering preparation processes (Zambaux et al., 1999) and changing polymer (Gasper et al., 1998; Tobio et al., 1998), which may provide sustained release of active protein over several weeks *in vitro* (Gasper et al., 1998; Tobio et al., 1998).

PEGylated nanoparticles have also been used to targeted transfection of h-galactosidase (LacZ reporter gene) and luciferase into the brain (Pardridge, 2002; Shi et al., 2001). This kind of plasmid DNA encapsulated nanoparticles are generally prepared using the solvent evaporation technique (Perez et al., 2001; Prabha et al., 2002) to incorporate drugs into the center of the nanoparticles.

Great successes have achieved in the field of brain targeting with colloidal drug carriers with PEGylated immunoliposomes that access the brain from blood via RMT and deliver small drug molecules or plasmid into the brain parenchyma, without damaging the BBB (Huwyler et al., 1996; Shi and Pardridge, 2000; Shi et al., 2001; Zhang et al., 2003). This requires the presence of receptor-specific biological targeting ligands at the tip of 1-2% of the PEG2000 strands, such as TAT peptide. Up to now, several functionalized copolymers have been recently synthesized: the biotinylated (Salem et al., 2001), the amine-reactive (Tessmar et al., 2002) and the

thiol-reactive copolymers (Olivier et al., 2002; Tessmar et al., 2003) that permit protein chemical conjugation in nondenaturing conditions. Biotinylated PEG-PLA nanoparticles may link biotinylated antibodies through an avidin spacer (Gref et al., 2003), or avidinantibody conjugates (Kang et al., 1995). Amine-reactive PEG-PLA can directly react with amino groups of the lysine residues of antibodies in mild conditions. With the biological ligands, the PEGylated nanoparticles could be promising brain drug carrier for the delivery across the BBB.

4.2.3 The advantages and the disadvantages

Most of PEGylated nanoparticles are biodegradable and have a good CNS biocompatibility. They can provide sustained drug release *in vitro* and *in vivo*. The core shell structure formed by PEG and hydrophobic molecules can encapsulate various drug molecules. Therefore, this PEGylated nanoparticle can be carrier for drug delivery to the brain. After penetrating the BBB with the aid of different biological ligands, these targeted specific nanoparticles can be delivered to the specific area of the brain.

In addition, PEGylated nanoparticles may be possibly used for encapsulation of various contrast agents. This encapsulation of contrast-enhancing agents have been developed to resolve and contrast tissues for diagnostic imaging (Unger et al., 1989).

Another advantage of PEGylated nanoparticles is the possibility of attaching antibodies or a fragment of them to the surface of the particles. In order to achieve site specific drug delivery, it is not necessary to destabilize these antibodies and fragments

because of the stability of PEGylated nanoparticles (Gref et al., 1995).

Although the mPEG-PLA/ PLGA nanoparticle provides great opportunities for drug delivery through the BBB, it still faces the problem of toxicity. The PLA parts of nanoparticles are toxic with 40% death at a 220 mg/kg dose and 100% at a 440 mg/kg dose along with marked clinical signs such as dyspnea, reduced locomotor activity or alteration of hematological and biochemical parameters and lung hemorrhage (Plard and Didier, 1999). As compounds with both hydrophobic and hydrophilic groups can form the core shell structure by self assembly, in this project, a new core shell PEGylated nanoparticle can be designed using nontoxic *b*-Cholesterol to substitute toxic PLA/PLGA.

4.3 Possible mechanism of nanoparticle-mediated transport of drugs across the BBB

The mechanism by which the nanoparticles facilitate drug entry into the brain is not fully elucidated. In principle, six different possibilities exist that could enhance transport of drugs across the BBB by means of nanoparticles (Kreuter and Alyautdin, 2000):

- 1) Preferential adsorption of nanoparticles to the walls of the brain blood vessel without transport of particles across the endothelium;
- 2) Fluidization of the endothelium by the surface activity of the surfactant polysorbate-80;
- 3) Opening of the tight junctions of the brain endothelium;
- 4) Endocytosis by the brain endothelial cells;
- 5) Transcytosis through the brain endothelial cells;
- 6) Blockage of the

P-glycoprotein by polysorbate 80.

5. Drug delivery system designed in this study

As described before, PEGylated polymer micelles formed by a hydrophilic shell and a hydrophobic core are promising carriers for incorporation of hydrophobic drugs to improve the bioavailability of the drugs and prolong their blood circulation. In this project, in order to take advantage and overcome disadvantage of PEGylated nanoparticles, a novel nanoparticle carrier system with PEG and *b*-cholesterol has designed in the current study. A cell penetrating peptide, TAT, was further conjugated to the surface of the nanoparticle to facilitate the cell transcytosis. The drug molecules will be encapsulated into the core of the PEGylated polymer micelles.

5.1 PEG (poly (ethylene glycol)) and *b*-cholesterol

In early 1980s, Illum and Davis found that after coating of the nanoparticles with PEG-containing surfactants, the blood circulation time for the compound could be prolonged and their uptake by the RES organs was reduced significantly (Illum and Davis, 1983). A highly flexible and hydrated PEG chain attached to the nanoparticle surface is assumed to have an effective protein-resistant property due to its steric repulsion effect. Polysorbate 80 coated PBCA nanoparticles were first investigated *in vivo* to enhance the brain transport of the hexapeptide dalargin (Schroder and Sabel, 1996). The results showed that after intravenous injection, polysorbate 80 coating enabled the highest induction of analgesia in mice. Likewise, other drugs that

normally do not penetrate the BBB, such as tubocurarine, loperamide and doxorubicin showed higher concentrations in the brain when associated with polysorbate 80-coated nanoparticles (Blasi et al., 2007). The protein ApoE or B adsorption on the nanoparticles, followed by low density lipoprotein (LDL) receptor mediated endocytosis and transcytosis, is believed to facilitate the uptake of the nanoparticles by the brain (Figure 1.7).

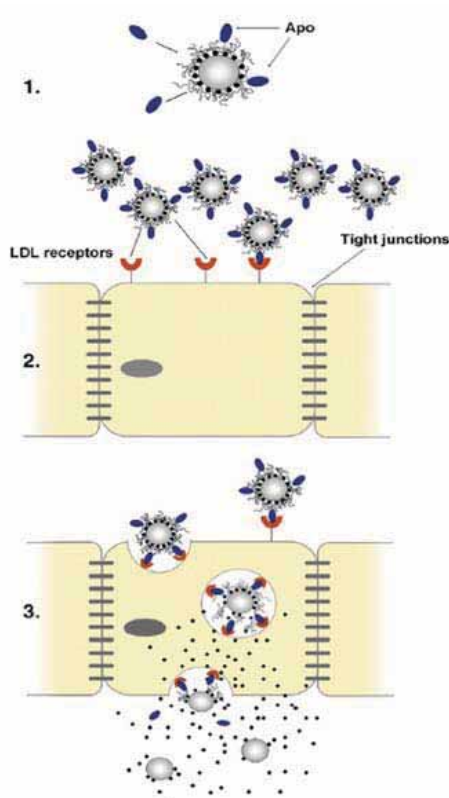


Figure 1.7: A proposed mechanism of brain uptake of polysorbate 80-coated nanoparticles. 1. Apo adsorption on nanoparticle surface. 2. Nanoparticle binding to the LDL receptors of the BBB. 3. Drug release after endocytosis and transcytosis. (Blasi et al., 2007)

In addition to PEG-surfactant coating, micelles self-assembled from amphiphilic PEGylated polymers provide better choice due to chemical binding of PEG. The PEG chains were first bound to poly (lactic acid) nanoparticles by Gref (Gref et al., 1994) and (Bazile et al., 1995). Later on PEG was chemically linked to poly(hexadecyl

cyanoacrylate nanoparticles (PHDCA) (Peracchia et al., 1997; Peracchia et al., 1999). The preparation of the PEG-PHDCA copolymer was achieved by the synthesis of a cyanoacrylate monomer substituted with PEG and its co-polymerization with hexadecylcyanoacrylate in a 1:4 ratio. Both types of nanoparticles, the PEGylated poly (lactic acid) and poly (hexadecylcyanoacrylate) (PHDCA) nanoparticles, significantly prolonged the blood circulation time and reduced the liver uptake. Calvo et al. investigated the distribution of PEG-PHDCA nanoparticles in EAE rats (Calvo et al., 2001). Analysis by confocal microscopy evidenced that fluorescent PEG-PHDCA nanoparticles were present in the endothelial cells of the brain and spinal cord surface and in the ependymal cells of the choroid plexus. It was hypothesized that PEG-PHDCA nanoparticles reached the brain by two mechanisms: passive diffusion due to the increase of the BBB permeability and transport by nanoparticles-containing macrophages, which infiltrated these inflammatory tissues. The PEGylated PHDCA nanoparticles accumulated in the brain was at a 4-8 fold higher concentration than non-PEGylated PHDCA nanoparticles after intravenous injection into rats (Brigger et al., 2002).

Therefore, the covalent attachment of PEG chains is a promising step forward. Other PEG-containing copolymers showing potential ability for drug delivery to the brain are depicted in Figure 1.8.

In addition to provide spatial stabilization, the presence of PEG on the surface of the micelles also allows the preparation of bioactive polymeric micelles. The bioactive ligands can be attached on the surface of micelles for drug delivery to the targeted brain. Two reasons for the design of ligands coating for drug carriers: 1, Ligands (antibody, protein, peptide, sugar moieties, folate or carbohydrate) attached to the carrier surface may increase the rate of its elimination in the blood and uptake in the liver and spleen; 2, Longevity of the specific ligand-bearing nanocarrier may allow for its successful accumulation in targets.

Covalent linkage of biological ligands to the nanoparticles is typically made by a simple coupling reaction between amine-functionalized nanoparticles and succinimidyl ester derivatives.

The successful strategy of delivering substances that are unable to cross the BBB is the use of transport vectors, which activate natural transport routes. The endogenous CMT for nutrients and AMT /RMT for peptides are portals of entry to the brain for circulating drugs.

The BBB expresses several transport systems for nutrients (Tsuji and Tamai, 1999), but the utilization of these transport systems for targeting the drugs into the brain is mainly limited to peptide drugs, which must have a molecular structure mimicking the endogenous nutrients. The prototypical example is levodopa, a lipid-insoluble precursor of dopamine that has been used for the treatment of Parkinson's disease because it contains the carboxyl and α -amino groups that allow it to compete for transport across the BBB by the large neutral amino acid carrier (Wade

and Katzman, 1975). In addition, since nutrient carriers stay in the membrane of the cells, the size of the drugs must be close to that of the endogenous ligand if they will be taken up and transferred into the brain

In the past decade, a number of cell-penetrating peptides (CPPs) have emerged, facilitating the intracellular delivery of polar biomolecules *in vitro* and *in vivo*. While these individual peptides differ in length and sequence, they share a few common features, which include theoretical hydrophobicity and helical moment, the ability to interact with lipidic membranes, and to adopt a distinct secondary structure upon association with lipids (Deshayes et al., 2005). These CPPs theoretically would be expected to be less able to affect the physicochemical properties of the active molecule. In any case, the ability of these short peptides to cross plasma membranes even when associated with hydrophilic cargoes, makes them a worthwhile technology for further study and development.

Table 1 summarizes the majority of cell penetrating peptides with their principal features. Primary attention is dedicated to TAT peptide.

Table 1: Principal features of the cell penetrating peptides

Name	Sequence	Charge	Cell lytic activity
MAP	KLALKLALKALKAALKLA	+5	YES
pAntp ₄₃₋₆₈	RQIKIWFQNRMMKWKK	+8	NO
Transportan	GWTLNSAGYLLGKINLKALAALAKKIL	+4	YES
SBP	MGLGLHLLVLAALQGAWSQPKKKRKV	+6	–
FBP	GALFLGWLGAAGSTMGAWSQPKKKRKV	+6	–
TAT ₄₈₋₆₀	GRKKRRQRRRPPQ	+8	NO
SynB1	RGGRLSYSRRRFSTSTGR	+6	NO

SynB3	RRLSYSRRRF	+6	NO
-------	------------	----	----

TAT protein is a HIV-transcription activating factor with a full length of 101 amino acids. Figure 1.10 shows the chemical structure of TAT (47-57) peptide, a NH₂-terminal 11 amino acid cell penetrating peptide used in this study. TAT protein consists of five domains; the probably best-studied region of TAT is located in domain 4, which contains a highly basic region (with two lysines and six arginines in nine residues) involved in nuclear and nucleolar localization (Brigati et al., 2003). While all CCPs listed above have been used for small cargoes such as peptide and oligonucleotides, TAT has been used more often for delivery of larger molecules such as proteins, one example is β -galactosidase (MW=540 kDa) (Loftus et al., 2006).

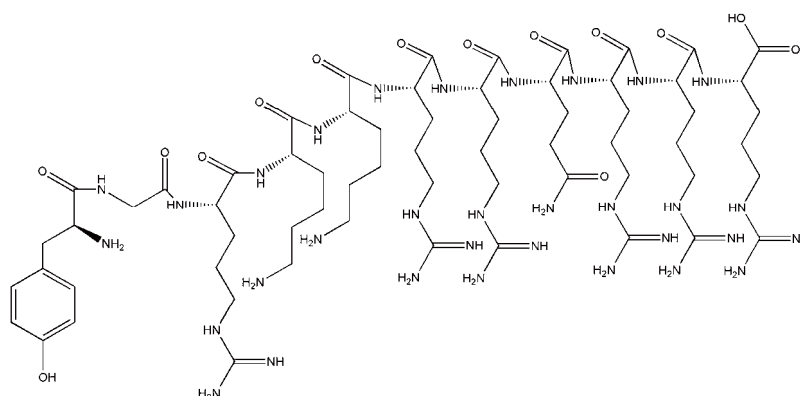


Figure 1.10: Structure of TAT (47-57) peptide

Schwarze firstly synthesized the full-length fusion proteins that contained a NH₂-terminal 11-amino acid protein transduction domain from HIV transactivator of transcription (TAT) protein (Schwarze et al., 1999). Transduction of the proteins evaluated was non-cell-specific, and was seen to occur even across the BBB. Further proof of this mode of peptide delivery was attained by Cao who fused the antiapoptotic protein Bcl-xL to TAT and injected the construct intraperitoneally into

mice that were affected by stroke (Cao et al., 2002). The Bcl-xL protein is expressed in adult neurons of the CNS and is believed to have an important role in the prevention of neuronal apoptosis that normally would occur during brain development, or results from varying stimuli leading to pathology, including cerebral ischemia. Protein transduction with this entity occurred in a rapid, concentration-dependent fashion, with entry into cells thought to occur via the lipid bilayer component of the cellular membrane. A study by Kilic using the same model showed that brain tissue was progressively transduced with TAT proteins within 3–4 hours after intravenous delivery (Kilic et al., 2002). TAT-Bcl-xL treatment reduced infarct volume and neurological deficits after long ischemic insults lasting 90 minutes, when applied both before and after ischemia. Dietz demonstrated that the same TAT-Bcl-xL construct, when injected into the eye, prevented 24% of mouse retinal ganglion cells from undergoing retrograde neuronal apoptosis caused by optic nerve lesion (Dietz et al., 2002). Thus, at least for neurological disorders, application of TAT fusion proteins may greatly facilitate protective therapy strategies.

Studies have also shown that even relatively large particles could be delivered into various cells by the TAT vector. A biocompatible 45 nm particle with an iron core, a dextrane coating, and covalently linked TAT peptides are efficiently taken up by human hematopoietic CD34⁺ cells (Zhao et al., 2002). Even liposomes having a diameter of 200 nm have been reported of cytoplasmatic uptake (Fretz et al., 2005; Torchilin et al., 2001).

Taking the TAT-mediated nanoparticles delivery approach a leap further, one of the most exciting demonstrations of the effectiveness of TAT-shuttled nanocarriers across the BBB was accomplished by TAT-conjugated CdS:Mn/ZnS quantum dots (Santra et al., 2005). Histological data clearly showed that TAT-QDs penetrated endothelial cells and reached the brain parenchyma. TAT-mediated intracellular delivery of large molecules and nanoparticles was proved to proceed via the energy-dependent macropinocytosis with subsequent enhanced escape from endosome into the cell cytoplasm (Wadia et al., 2004). TAT promises a powerful delivery of giant cargo, and is the focus of the current project.

6. Pathological model for testing designed nanoparticle drug delivery system

The designed drug delivery system will be evaluated *in vitro* and *in vivo*. For the *in vitro* evaluation, the cytotoxicity and cellular intake of designed nanoparticles will be studied in different brain cell types. Regarding the *in vivo* study, in addition to the investigation in normal brain, a pathological brain model which mimics the brain under pathological condition will be adopted for the testing.

6.1. Major cell types in the brain

6.1.1 Neurons

Neurons are responsive cells in the CNS that process and transmit information by electrochemical signaling. They are the core components of the brain, the vertebrate spinal cord, the invertebrate ventral nerve cord, and the peripheral nerves. A number of different types of neurons exist: sensory neurons respond to touch, sound, light and

numerous other stimuli affecting cells of the sensory organs that then send signals to the spinal cord and brain. Motor neurons receive signals from the brain and spinal cord and cause muscle contractions and affect glands. Inter-neurons connect neurons to other neurons within the brain and spinal cord. Neurons respond to stimuli, and communicate the presence of stimuli to the central nervous system, which processes that information and sends responses to other parts of the body for action (Wikipedia, 2008).

6.1.2 Main non-neuronal cells

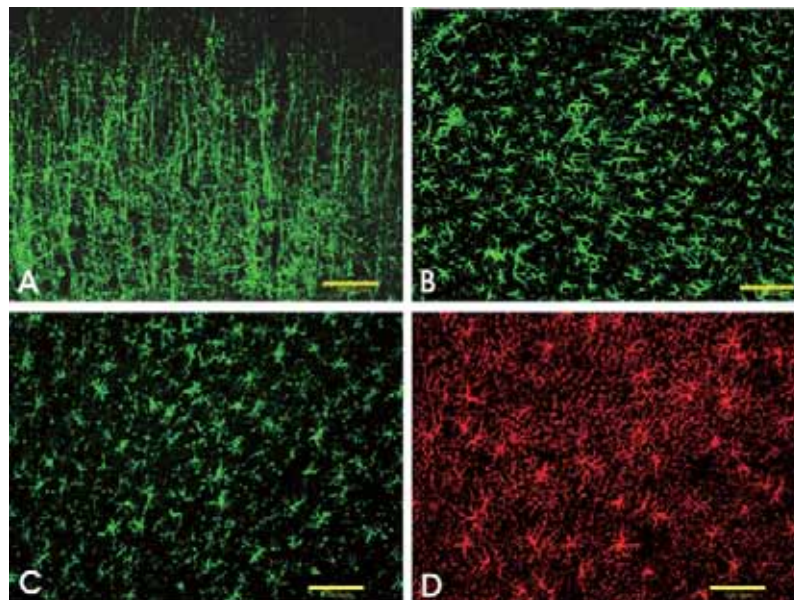


Figure 1.11: Major cell types in the brain. A. oligodendrocytes; B. astrocytes; C. Microglia; D. NG2 cells.

Although non-neuronal cells (or neuroglia, which occupy about 90% of total brain cells) are believed to possess important roles in the nervous system, these glial cells are less studied. Non-neuronal cells in the adult can be divided into two groups depending on their distribution: distributed throughout brain parenchyma, or restricted to a specific region. Four types of glial cells were conventionally thought to support

the brain, namely astrocytes, oligodendrocytes, microglia, and ependymal cells. Among them, astrocytes, oligodendrocytes, and microglia are ubiquitously spread over the brain parenchyma. Ependyma is a thin epithelial membrane lining containing ependymocytes. Ependymocytes, the main cells in the brain ventricular system, produce and circulate of cerebrospinal fluid (CSF).

Some other special non-neuronal cell types can be found only in specific brain regions or during development, for instance, tanycytes on the floor of the third ventricle, Müller cells in the retina, pituicytes in the posterior pituitary, and Bergmann glia or radial glial cells in the developing CNS.

Astrocytes:

Not only are astrocytes distributed evenly in the brain parenchyma, they are also important cells in the glial-limiting membrane of ventricular and pial surfaces and the BBB. Several functions include providing nutrition to neurons and other non-neuronal cells, maintaining extracellular ion balance during neuronal activity, recycling neurotransmitter substances, and healing upon CNS injury to form dense glial scar tissue.

Oligodendrocytes:

Oligodendrocytes ensheath neuronal processes to form either myelinated or unmyelinated axons in the white matter, satellite cells for ion exchange with neurons in gray matter. Myelination enables the saltatory conduction via nodes of Ranvier and leads to faster interaction transmission of impulses.

Microglia:

Microglia is the most important immune cells in the CNS because most other inflammatory cells are largely excluded from normal CNS. Microglia resembles tissue macrophages of the CNS and exhibit many features of monocytes: signaling cascades involving chemokines and cytokines and their receptor systems, similar to those in the immune system. Under normal physiological conditions, microglial cells are quiescent. Upon activation, they begin to proliferate, migrate toward the impaired region, and change morphology from ramified resting status into hypertrophic and finally amoeboid phagocytic forms. Microglial cells are believed to play a critical role in host defense against microorganisms and malignant cells and in the processes of neurodegeneration.

6.1.3 NG2 positive cells

NG2, a chondroitin sulphate proteoglycan (CSPG), is expressed by a special type of mature glial cell in the adult CNS. These were identified at first as ‘protoplasmic’ astrocytes on the basis of their morphology in adult CNS in 1987 by Levine and Card (Levine and Card, 1987). The NG2 positive cells have ultrastructural features in common with oligodendrocytes (Dawson et al., 2000). In 1987, Stallcup and colleagues (Levine and Stallcup, 1987; Stallcup and Beasley, 1987) demonstrated that in glial cultures derived from developing CNS, antibodies to NG2 label oligodendrocyte-type-2 astrocyte (O-2A) cells, which give rise to oligodendrocytes and type-2 astrocytes *in vitro* (Raff et al., 1983). Therefore, NG2 expressing glia are considered to be either O-2A cells, or oligodendrocyte precursor cell (OPC) that generate oligodendrocytes in the developing brain and then persist in the mature CNS

as adult OPC, to regenerate oligodendrocytes throughout life (Levine et al., 1993; Nishiyama et al., 1996; Reynolds and Hardy, 1997).

In the developing CNS: belong to oligodendrocyte lineage

It has been reported that the NG2 cells can be found by E16 throughout the hindbrain and within the basal forebrain (Nishiyama et al., 1996). During the final days of embryonic development, there is a dramatic increase in the number of NG2 cells, so that by birth they are distributed widely throughout the whole CNS. NG2 cells will reach a maximum density in the spinal cord before birth, in the cerebral cortex at postnatal day 3 (P3), and in the cerebellum at P10 (Nishiyama et al., 1996). It has been found that the distribution and number of NG2 positive cells is remarkably similar to those platelet-derived growth factor α receptor (PDGF α R) mRNA-expressing cells (Pringle et al., 1992) which is an accepted marker for oligodendroglial progenitors (Hall et al., 1996). Therefore, the co-expression of NG2 positive cells and PDGF α R in the developing CNS suggests that NG2 cells are a kind of oligodendrocyte progenitors.

The O4 expression occurs at the late progenitor and prooligodendrocyte stage, at which point the cells are still mitotically active (Gard and Pfeiffer, 1990). In the developing CNS, O4 expression was also found in the NG2 positive cells. Thus, the appearance of O4 expression provides additional evidence that the NG2 positive cells in developing CNS are indeed oligodendrocyte progenitors and are capable of differentiation into mature oligodendrocytes *in vivo*.

In the adult CNS: part of oligodendrocyte lineage

The persistence of NG2 positive cells throughout the mature CNS has been demonstrated in lots of studies (Levine and Card, 1987; Levine et al., 1993; Nishiyama et al., 1996; Reynolds and Hardy, 1997). It has been the subjects of much debate for the origins of these cells and their functions in the mature CNS. Up to now, it is already clear that, during development of the CNS, not all NG2 cells differentiate into oligodendrocytes. It is possible that features of the microenvironment regulate the proliferation and differentiation of oligodendrocyte progenitors (Gallo et al., 1996).

NG2 cells in the adult rat CNS have a highly complex morphology which can not easily classify these cells into oligodendrocyte progenitors. They are very unlike the progenitors that populate the CNS (Reynolds and Hardy, 1997). Also, in the developing animal, NG2 expression in adult CNS does not overlap with any expression of markers known to be specific for other glial cell types. Although NG2 cells are frequently observed in close apposition to microglial cells and astrocytes, double labeling with OX-42 (Levine et al., 1993) or GFAP (Reynolds and Hardy, 1997) has not been demonstrated.

All this evidence taken together strongly suggests that NG2 positive cells in the adult CNS are phenotypically different from oligodendrocyte progenitors.

6.2 Pathological changes of brain cells in brain focal injury model

In neuropathological condition, cellular reactions or responses in brain could be observed. The cell types to which the current designed nanodrug delivery system may target is of importance to study.

6.2.1 Microglia

In mature rat brains, resting microglia exists in a characteristic ramified morphology and is responsible for immune surveillance. Microglia become activated in response to inflammatory diseases (Kreutzberg, 1996; Liu and Hong, 2003) and undergoes dramatic morphologic alterations upon activation, changing from resting ramified microglia into activated amoeboid microglia (Kreutzberg, 1996). Further, surface molecules are also upregulated when microglia are activated (Graeber et al., 1988). In addition, activated microglia are capable of releasing a variety of soluble factors, which are pro-inflammatory in nature and potentially cytotoxic. In addition to producing cytotoxic factors such as superoxide (Colton and Gilbert, 1987), nitric oxide (Liu et al., 2002; Moss and Bates, 2001), and tumor necrosis factor alpha (TNF- α) (Lee et al., 1993) in response to immunological stimuli, microglia are also reported to increase neuronal survival through the release of trophic and anti-inflammatory factors (Liao et al., 2005; Morgan et al., 2004).

6.2.2 Astrocytes

In normal brain, astrocytes play important roles in providing glia-neuron contact, maintaining ionic homeostasis, buffering excess neurotransmitters, secreting neurotrophic factors, and serving as a critical component of the BBB (Aloisi, 1999; Hansson and Ronnback, 1995). Contrast to microglia, the pro-inflammatory function of astrocyte is not prominent as well (Lindsay, 1994; Streit et al., 1999), but they also can become activated in response to immunologic challenges or brain injuries and

inflammatory diseases (Aloisi, 1999; Tacconi, 1998). Astrocytes also produce a host of trophic factors (Friedman et al., 1990; Lindsay, 1994), which are crucial for the survival of neurons. However, activated astroglia exhibit increased production of glial fibrillary acidic protein (GFAP), and form glial scars, which may hinder axonal regeneration.

6.2.3 Oligodendrocytes

As adult Oligodendrocytes ensheath neuronal processes to form either myelinated or unmyelinated axons in the white matter, their responses are related to the demyelination in the traumatic neural injured brain (Vick et al., 1992). Both oligodendrocytes as well as precursor-type oligodendrocytes that previously formed a myelin sheath are able to remyelinate in the CNS. Adult oligodendrocytes can gain access to relevant mitogens either in the axonal plasma membrane or in a soluble form and undergo a wave of proliferation; there is good potential for remyelination after neural injury (Levine et al., 2001; Vick et al., 1992).

6.2.4 Neurons

Brain focal injury may directly induce neuronal damage in the CNS, which results in the primary or secondary cell death (Kermer et al., 1999). Injured CNS neurons can release glutamate in great amounts owing to depolarization after cell damage or energy failure. In addition, nitric oxide synthesis was activated and free radical was formed. It is clear that the damage and loss of neurons in the CNS will

lead to some neurodegenerative diseases such as Parkinson's disease or Alzheimer's disease (Reichmann, 2008; Ribe et al., 2008).

6.2.5 NG2 positive cells responses to brain injury

In developing brain, Rhodes found that the oligodendrocyte precursor cells (OPCs) can differentiate into myelinating oligodendrocytes in mature, uninjured rat CNS (Rhodes et al., 2006). Also, the OPCs have synaptic regulatory functions because of the expression of GluR4 glutamate receptor during various developmental stages (Ong and Garey, 1996; Ong and Levine, 1999).

However, when the brains become developed, NG2 cells in the adult CNS represent a population of reactive glial cells. Their reactions to damage or injury include dramatic changes in cell morphology, increases in NG2 immuno-reactivity, and cell proliferation in some cases. In some instances they may be the first cells to react to damage, but, unlike microglia, these reactive changes are spatially restricted to the immediate damage area (Di Bello et al., 1999; Levine, 1994; Levine and Reynolds, 1999). As their responses have been observed in stab wounds (Levine, 1994), viral infection (Levine et al., 1998; Redwine and Armstrong, 1998) and kainate excitotoxicity (Ong and Levine, 1999). The functional significance of this rapid response to brain focal injury is not well understood.

7. Hypothesis

Antibiotics may be a good choice for the treatment of brain infectious diseases

caused by bacterial. However, their applications were limited by the difficulty in penetrating the BBB. The BBB penetration rate may have a significant impact on their final therapeutic efficacy. Using physiologically-based strategy to develop a kind of nanoparticle drug carrier to deliver these antibiotics from the blood to the brain is a feasible solution. Taking into account of all the advantages of self-assembled core shell structured micelles and TAT cell-penetrating peptide, a novel nanoparticle drug delivery system will be designed. The nanoparticle of PEG-*b*-Chol is a kind of PEGylated amphiphilic micelles. It has hydrophobic part (*b*-Cholesterol) and hydrophilic part (PEG chain). Therefore, in aqueous solvent of DI water (H₂O); their molecules of PEG-*b*-Chol can automatically form the core shell structure by self assembly. The hydrophilic PEG forms the coronal outside and the hydrophobic *b*-Cholesterol forms the core inside. The structure of core shell formed by PEG-*b*-Chol was shown by Figure 1.12. TAT peptide can be conjugated to the surface of this nanoparticle by EDC/NHS chemistry. The particle of TAT-PEG-*b*- Chol also can form this core shell structure. This nanoparticle system can be a good drug carrier to deliver the selected antibiotics to cross the BBB and reach brain parenchyma.

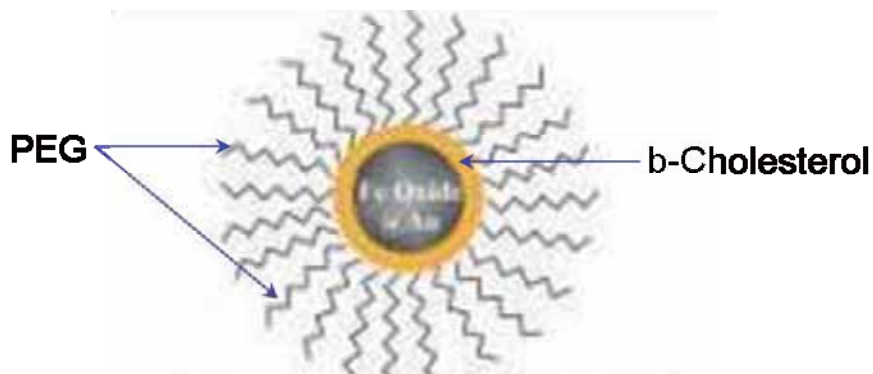


Figure 1.12: The core shell structure formed by PEG-*b*-Chol. The hydrophilic PEG forms the coronal outside and the hydrophobic *b*-Chol forms the core inside.

In this research, hydrophobic molecules such as ciprofloxacin lactate (selected as drug molecules), FITC and QDs (selected as fluorescent markers) will be encapsulated into the core during the process when this structure is formed.

Just as Figure 1.13 shown, when the biologically active micelles which contain drug molecules inside their core meet the cells with appropriate surface receptors, they can be bound by those receptors and enter the cell by AMT or RMT induced. The drug molecules just use this method to cross the BBB.

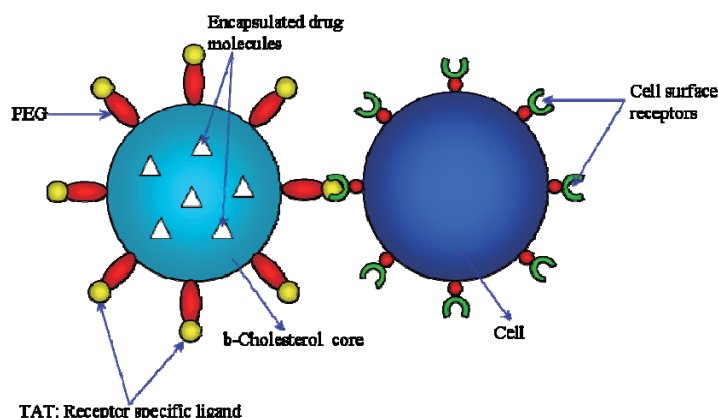


Figure 1.13: Designed drug-nanoparticle system (TAT-PEG-b-Chol)

It is expected that this nanoparticle has good BBB penetration ability but not any cytotoxicity to brain cell. They can be well taken by brain cells after they enter the brain parenchyma. Also, the nanoparticle system can release the drug molecules at pathological site and the release of drug should be well controlled.

Hydrophobic antibiotics such as ciprofloxacin lactate are expected to be well encapsulated into the core of nanoparticles formed and delivered to the target site. However, the encapsulation of hydrophilic antibiotic such as Penicillin G is not so

good. Therefore, another method of delivering hydrophilic antibiotics should be explored. It is hoped that the direct connection of Penicillin G and TAT molecules may be effective. As TAT conjugated CdS:Mn/ZnS quantum dots (Santra et al., 2005) can cross the BBB, it is also of great possibility that TAT-Penicillin G can also penetrate the BBB. Penicillin G has $-\text{COOH}$ group and TAT peptide contains $-\text{NH}_2$ group, it is possible to connect them together just like TAT and PEG-*b*-Chol through EDC/NHS chemistry. Also, the TAT conjugated new compounds are also expected having no cytotoxicity to brain cells.

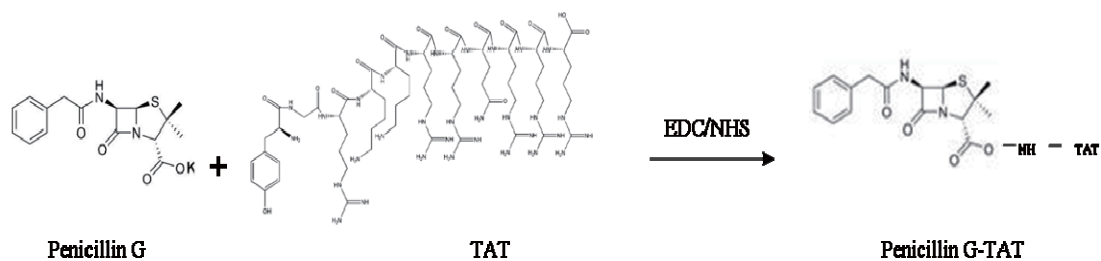


Figure 1.14: Scheme of the Penicillin G-TAT synthesis

For the nanoparticle drug delivery system testing, both *in vitro* and *in vivo* model will be investigated. The higher intake of nanoparticles with TAT group in cultured brain cells will be expected. In addition, those nanoparticles will not show any cytotoxicity to brain cells. For *in vivo* testing, a LPS triggered pathological brain model will be established. After that, the responses of NG2 positive cells in this pathological model will be investigated. Then the nanoparticles carriers will be observed in this study. The most important thing is that these nanoparticles will be supposed to gather at the pathological area and release the drug molecules there. It suggests that this nanoparticle may be an ideal carrier for drug delivery cross the BBB.

The expected sustained drug release from those nanoparticle micelles in pathological area demonstrates their promising applications in future clinical trials.

8. Scope of research

8.1 To synthesize and characterize the core-shell structured micelles of PEG-*b*-cholesterol and TAT-PEG-*b*-cholesterol:

First of all, the amphiphilic copolymer of PEG-*b*-cholesterol (PEG-*b*-Chol) will be synthesized by EDC/NHS chemistry in DCM. In aqueous solution, core shell structured micelles can be fabricated by self assembly method. During the process of fabrication, molecules of an antibiotic (ciprofloxacin lactate) or fluorescent markers (FITC or Quantum dots) will be encapsulated into the central core of PEG-*b*-Chol.

When the amphiphilic copolymer of PEG-*b*-Chol is ready, TAT peptide can be conjugated to PEG to form TAT-PEG-*b*-Chol.. Based on the same methods, the core shell structured TAT-PEG-*b*-Chol also can be formed in aqueous solution, meanwhile the encapsulation of ciprofloxacin lactate or fluorescent marker can be achieved.

The particles size of nanoparticles will be measured and the *in vitro* release of ciprofloxacin lactate from micelles in PBS solution will be studied.

8.2 To study the BBB penetration of PEG-*b*-Chol and TAT-PEG-*b*-Chol

In SD rats, the BBB penetration of FITC and/or QDs encapsulated PEG-*b*-Chol and TAT-PEG-*b*-Chol micelles will be investigated. After the administration of

micelles solution through the femoral vein, their biodistribution in liver, kidney, spleen and brain will be studied. Using cultured endothelial cells and astrocytes, the *in vitro* cellular uptake of those two types of nanoparticle micelles will also be studied. After the nanoparticles enter the brain parenchyma from blood stream, the nanoparticle positive cell types will be identified by immunohistochemical staining techniques.

8.3 To study the primary pharmacokinetics of selected antibiotics and FITC encapsulated TAT-PEG-*b*-Chol *in vivo*

In SD rats, the primary pharmacokinetics of Penicillin G, Ciprofloxacin and Doxycycline in blood plasma will be investigated by High Performance Liquid Chromatography (HPLC). After these antibiotics were injected into the blood stream, at different time points, rat plasma samples will be collected, extracted and analyzed by HPLC. As for FITC encapsulated TAT-PEG-*b*-Chol, after they enter the rat body, rat brain sample also will be collected at different time intervals. Then, brain sections will be processed using histological techniques and observed by a confocal microscope.

8.4 To synthesize and characterize TAT-Penicillin G

Penicillin G is a hydrophilic antibiotic which cannot be encapsulated into the core of TAT-PEG-*b*-Chol. Here, it will be conjugated to TAT directly using EDC/NHS chemistry. After successful conjugation, the cytotoxicity of TAT-Penicillin

G to cultured endothelial cells, microglia, astrocytes, and neuronal cells will be investigated. Also, their penetration to the BCEC and astrocytes will be studied *in vitro*. It will be proved that many more TAT-Penicillin G particles may penetrate or attach to BCEC and astrocytes with the aid of TAT peptide, suggesting that the connection of TAT to Penicillin G is a feasible way to deliver Penicillin G across the BBB.

8.5 To evaluate PEG-*b*-Chol and TAT-PEG-*b*-Chol *in vitro* and *in vivo*

The cellular uptake and cytotoxicity test of PEG-*b*-Chol and TAT-PEG-*b*-Chol micelles will be studied in this part. In addition, a LPS triggered *in vivo* brain pathological model will be established by LPS focal injection. In this model, the delivery of drug molecules by TAT-PEG-*b*-Chol will be investigated. Meanwhile, the responses of NG2 cells in this pathological brain, including the alteration of expression and morphological changes will be investigated. In addition, through the inhibition of microglia complement receptor 3, the possible relationship between NG2 cells and microglia will also be studied.

CHAPTER 2

MATERIALS AND METHODS

1. Fabrication and characterization

1.1 Materials

I . Chemicals

- Cholesteryl chloroformate (*b*-Cholesteryl) (Sigma-Aldrich, USA)
- TAT peptide (GL Biochem Ltd, China)
- Fluorescein5-isothiocyanate (FITC) (Sigma-Aldrich, USA)
- Dichloromethane (DCM) (Sigma-Aldrich, USA)
- Dimethylformamide (DMF) (Sigma-Aldrich, USA)
- Dimethyl sulfoxide (DMSO) (Fluka, USA)
- Triethylamine (TEA) (Fluka, USA)
- N-hydroxy-sulfosuccinimide (NHSS) (Sigma-Aldrich, USA)
- Ciprofloxacin Lactate (Sigma-Aldrich, USA)
- Penicillin G Potassium (Sigma-Aldrich, USA)
- Doxycycline (Sigma-Aldrich, USA)
- BupH MES buffered saline (Pierce, USA)
- Heterobifunctional H₂N-PEG-COOH (PEG: Mn 5000) (Nektar, USA)
- 1-ethyl-3-[3-dimethylaminopropyl] carbodiimide hydrochloride (EDC) (Pierce, USA)

II . BupH MES Buffered Saline Buffer (pH 4.7)

- BupH MES Buffered Saline Packs 1 pack
 Each pack yields 500 ml of 0.1 M 2-[morpholino]ethanesulfonic acid,
 0.9% NaCl (Pierce, USA)
- Deionized water 500 ml

III. 1M NaOH solution

- NaOH (Sigma-Aldrich, USA) 4g
- Deionized water 100ml

1.2 Synthesis procedures

1.2.1 PEG-*b*-Chol

For the synthesis of PEG-*b*-Chol, Cholesteryl chloroformate (0.352g, 0.78mmol) in 20ml of DCM was slowly added to a solution of TEA (100μl) and NH₂-PEG

-COOH (1g, 0.2mmol) dissolved in 20 ml of DCM at room temperature (RT) with vigorously stirring. The mixtures were left to react for 2 days. The crude product was purified by dialysis against DCM for 6 days using membrane with a molecular weight cut-off of 2,000 Da. DCM was then removed by vacuum drying to yield a final product.

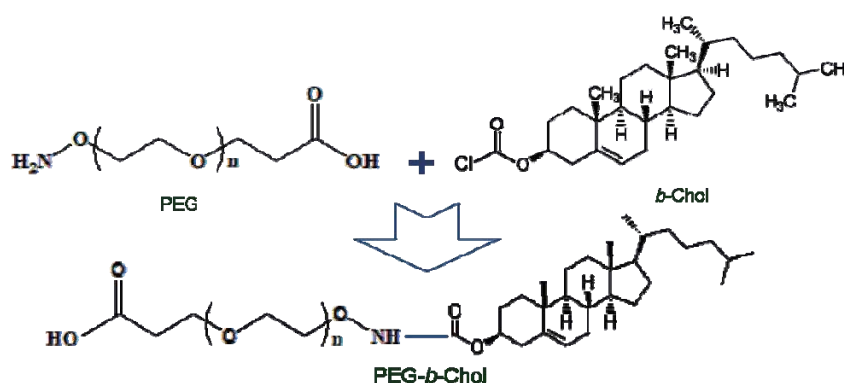


Figure 2.1: Scheme of the PEG-b-Chol synthesis

1.2.2 TAT-PEG-b-Chol

TAT peptide with a sequence of NH₂-YGRKKRRQRRR was conjugated to PEG through its carboxylic acid group. Briefly, EDC and NHSS were dissolved in 0.1 M MES buffer to get 100 and 40mM stock solutions respectively. TAT peptide stock solution was prepared in phosphate-buffered saline (PBS, pH 7.4) at a concentration of 1 mg/ml. PEG-b-Chol (5mg) was dissolved in 400 ml of 0.1 M MES buffer, and incubated with 40 ml of EDC and NHSS solutions for 1 hour (h) at 4°C. TAT peptide solution (250 ml) was then added to the activated PEG solution, and incubated for 3h at RT. The reaction mixture was dialyzed against de-ionized (DI) water to remove byproducts and unreacted TAT peptide molecules by using the membrane with a molecular weight cut-off of 3500 Da. The final product was freeze-dried for 2 days

prior to use.

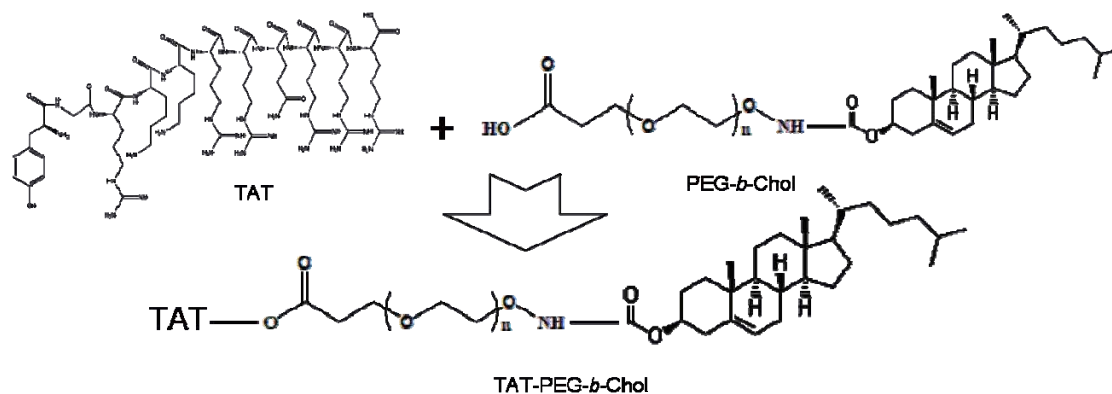


Figure 2.2: Scheme of the TAT-PEG-*b*-Chol synthesis

1.2.3 Encapsulation of FITC or QDs into PEG-*b*-Chol and TAT-PEG-*b*-Chol

FITC and QDs were respectively encapsulated into PEG-*b*-Chol or TAT-PEG-*b*-Chol micelles by a membrane dialysis method. Briefly, the polymers (5mg) were dissolved in 3ml of DMSO. A certain amount of FITC or QDs (2mg to 5mg) was then added. The solution was dialyzed against DI water at 10°C for 48 hours using a dialysis membrane with a molecular weight cut-off of 2,000 (Spectra/Por 7, Spectrum Laboratories Inc.). The water was replaced overnight. After dialysis, the solution in the dialysis bag was collected and freeze-dried for two days.

The antibiotic (ciprofloxacin lactate) was encapsulated into PEG-*b*-Chol or TAT-PEG-*b*-Chol using the same method.

1.2.4 TAT-Penicillin G

TAT was conjugated to Penicillin G potassium *via* EDC/NHS chemistry. Penicillin G potassium (14.8mg) dissolved in 1ml MES buffer (pH=6.0) was slowly added to a solution of EDC (46mg) in 1ml MES buffer (pH=6.0) at RT with vigorous stirring. After 5 minutes reaction at room temperature, 1ml NHSS solution (130mg) was added into the mixed solution and the mixtures were left to react for 30 minutes at RT. After that, the pH value of mixture was adjusted to 7.0 by 1mol/l NaOH solution. TAT peptide was prepared in phosphate-buffered (PBS) saline at 1 mg/ml, then, this TAT solution (25 μ l) was added to the activated Penicillin G potassium solution and incubated for 3 hours at room temperature. Unreacted Penicillin G potassium and other reagents were removed by dialysis against de-ionized (DI) water using the membrane with molecular weight cut-off of 1000 Da for 24 hours. The final product was harvested by freeze-drying.

1.3 Characterization procedures

1.3.1 Morphology of blank or drug-loaded nanoparticles

The morphologies of blank as well as drug-loaded (FITC, QDs and ciprofloxacin lactate) PEG-*b*-Chol or TAT-PEG-*b*-Chol nanoparticles were observed by a field emission scanning electron microscope (SEM) (JEOL JSM-7400F) operated at 5.0 kV accelerating voltage. To prepare SEM samples, 20ml of the nanoparticles solution were placed on a silicon wafer chip, and air-dried at room temperature. The silicon chip was then coated with Pd film and mounted on SEM stud for visualization.

1.3.2 ¹H NMR spectra of nanoparticles

The ¹H NMR spectra were studied using a BrukerAvance 400 spectrometer (400 MHz). For scanning of PEG and PEG-*b*-Chol, chloroform-d (CDCl₃) was used as solvent. Briefly, 5mg of sample was dissolved in 0.6ml CDCl₃ and scanned for 1000 times. As for TAT, TAT-PEG-*b*-Chol, Penicillin G and TAT-Penicillin G, D₂O was chosen as solvent.

1.3.3 MALDI-TOF/MS characterization of Penicillin G and TAT-Penicillin G

To validate the successful conjugation of TAT to Penicillin G molecules, Penicillin G and TAT-Penicillin G were characterized by matrix-assisted laser desorption ionization of time-of-flight mass spectrometry (MALDI-TOF/MS) (Autoflex II, Bruker Daltronics) respectively. The analysis was performed by the dried-droplet method with 2, 5-dihydroxybenzoic acid as matrix. All Penicillin G and TAT- Penicillin G samples were run in reflection positive ionization model

1.3.4 Particle size and zeta potential analysis

The particle size and zeta potential of blank, drug-, FITC- and QDs-loaded PEG-*b*-Chol or TAT-PEG-*b*-Chol nanoparticles in DI water were measured by ZetaPALS/BI-MAS (Brookhaven Instruments Corporation) equipped with a HeeNe laser beam at 658nm (scattering angle: 90°). The concentration of nanoparticles in DI water was about 0.6mg/ml. The intensity of scattered light (in kilo counts per second) was also recorded as a function of polymer concentration ranging from 0.0 to 500.0

mg/l. A stock polymer solution was prepared with a concentration of 500.0mg/l, and diluted using DI water to various concentrations. Each measurement was repeated 5 times, and an average value was obtained and used. The size measurements were performed by multimodel analysis. The zeta potential measurement was repeated for 5 runs per sample and an average value was reported.

1.3.5 *In vitro* drug release of ciprofloxacin-loaded nanoparticles

Ciprofloxacin lactate-loaded nanoparticles solution (20mg in 5ml of PBS, pH 7.4) was poured onto the dialysis membrane with a molecular weight cut-off of 2000 Da. The membrane was then immersed in a beaker containing 50ml of PBS (pH 7.4) with shaking at 80rev/min at 37°C. At specific time intervals, the PBS solution was taken out for analysis of drug concentration by the UV/VIS/NIR spectrophotometer and put back after the measurement. The standard curve was constructed by dissolving ciprofloxacin in PBS in the concentration range from 2.5 to 20.0ppm and r^2 value was 0.999906. The detection wavelength was set at 270nm, and 310nm was used as base line.

2. Cell culture

For the investigation of cellular uptake of nanoparticle micelles, cultured human endothelial cells and brain astrocytes which are the main components of BBB were used. In addition, the technique of cell culture was also applied for the toxicity test of nanoparticle micelles..

2.1 Materials

I .Culture medium and chemicals

- Dulbecco's Modified Eagle's Medium (DMEM, Sigma) 450ml
- 10% Fetal Bovine Serum (Gibco, Invitrogen Life Technologies, USA) 50ml
- 1% Antibiotic-Antimycotic (Invitrogen corporation, USA) 1ml
- 1×Trypsin-EDTA (0.25% Trypsin-0.53mM EDTA, Sigma, USA)
- Dimethyl sulfoxide (DMSO, Sigma, USA)
- PEG-*b*-Chol
- TAT-PEG-*b*-Chol
- Penicillin G potassium (MW: 372.48, Sigma, USA)
- TAT-Penicillin G potassium

II .Cell lines

- Human brain astroglia, SV40 transformed (CRL-8621, ATCC, USA)
- Human cortical neuron (CRL-10442, ATCC, USA)
- Human endothelial cells (Cell system Ltd, USA)
- Bacillus subtilis* (23857, ATCC, USA)
- Escherichia coli* (25922, ATCC, USA)

2.2 General operating procedures

2.2.1 Handing procedure frozen cells

To insure the highest level of viability, thaw the vial and initiate the culture as soon as possible upon receipt. It should be stored in liquid nitrogen vapor phase and not at -70°C. At the beginning, thaw the vial by gentle agitation in a 37°C water bath. To reduce the possibility of contamination, keep the O-ring and cap out of the water. Thawing should be rapid (approximately 2 minutes). Next, the vial was removed from the water bath as soon as the contents were thawed, and decontaminated by dipping in or spaying with 70% ethanol. Last, the vial contents was transferred to a T75 flask

quickly with at least 10ml of fresh medium and incubated the culture at 37°C in a suitable incubator. A 5% CO₂ in air atmosphere was supplied.

2.2.2 Subculture procedure

When cultures reach about 80-90% confluence, subcultures were carried out. First, culture medium was removed and discarded and briefly the cell layer was rinse with 0.25% Trypsin-0.53mM EDTA (1×) solution to remove all traces of serum which contains trypsin inhibitor. Then, 2.0 to 3.0ml of Trypsin-EDTA solution was added to flask and observes cells under an inverted microscope until cell layer was dispersed (usually with 5 to 15 minutes). When cell layer was fully dispersed, 6.0 to 8.0ml of complete growth medium added and the cells were aspirated by gently pipetting. Next, the Trypsin-EDTA solution was removed and cell suspension transferred to centrifuge tube and spined at 2000 rpm for 5 minutes. Last, supernatant was discarded and cells resuspended in fresh growth medium, then culture vessels were place in incubator at 37°C with 5%CO₂.

2.2.3 Cell preservation procedure

The cell suspension after Trypsin-EDTA administration was spined at 2000rpm for 5 minutes. Then the supernatant was discarded and the cells were resuspended with fresh preservation medium (10% complete growth medium+10% FBS+10 DMSO) in preserving vial. After that, the vial was put in the -80°C freezer overnight and transferred into liquid nitrogen in the next morning.

2.3 Procedures of toxicity test

The nanoparticle drug delivery system should not have cytotoxicity to brain cells. Therefore, their cytotoxicity to cultured endothelial cells, astrocytes, microglia and neuronal cells were necessarily checked.

For TAT-Penicillin G, firstly, human brain astrocytes, cortical neuron, brain capillary endothelial cells and microglia were cultured in DMEM media with 10% fetal bovine serum (FBS) and 1% antibiotics. Among them, endothelial cells and astrocytes are the main components of the BBB. These cells were seeded in 6-well plate and incubated at 37°C, 5% CO₂. 24 hours later, Penicillin G potassium-TAT (495µg/mL) and controlled pure Penicillin G potassium (496µg/mL) were added. And another 4 hour incubation of cells and drugs, the medium containing the drug carriers was removed and the cells were washed with 1×PBS solution for 2 times, each time takes 5 minutes. Then, 1ml of 1×Trypsin-EDTA solution was added in each plate for 5 minute reaction at 37°C, 5%CO₂ to disperse the cell layer. Last, 1ml fresh growth medium was added to each plate in order to neutralize the reaction of Trypsin-EDTA. At last, the number and viability of these cells were checked by VCELL viability analyzer instrument (VCELL, USA). Based on the alteration of cell number and viability, the cytotoxicity of TAT-Penicillin G potassium could be determined.

For PEG-*b*-Chol and TAT-PEG-*b*-Chol, 10µl TAT-PEG-*b*-Chol-QDs (0.0375 mg/ml), PEG-*b*-Chol-QDs (0.0375mg/ml) and pure QDs solution (0.0375mg/ml) were added into cultured BVEC and astrocytes (2.2×10⁵ cells/well) respectively. After

incubated at 37°C at 5%CO₂ for 4 hours, their cell number and viabilities were measured with the same method described before.

2.4 Procedures of cellular intake test

To investigate cellular uptake of PEG-*b*-Chol and TAT-PEG-*b*-Chol micelles, human brain endothelial cells and astrocytes were seeded into flask respectively in DMEM with 10% FBS and 1% antibiotics supply. After becoming 80-90% confluent, they were subcultured into 6-well plates with a density of 2x10⁴ cells/well. A piece of the coverslips was placed at the bottom of each well. 100µl nanoparticle solutions (0.1mg/ml) with FITC or QDs fluorescent markers were added and incubated for 1 hour at 37°C with 5% CO₂. Then, cells were fixed with 4% paraformaldehyde solution for 10 minutes. After 2 times' washing with 1×PBS, the coverslips with fluorescence labeled cells were mounted with nonfluorescent mounting medium (DAKO, USA) and observed with Laser Scanning Confocal Microscopy (Olympus FluoViewTM FV1000, Japan) in 488nm (FITC) and 560nm (QDs) respectively.

2.5 Procedures of antibiotic screening

In order to investigate the antibacterial efficacy of TAT-Penicillin G, experiment of antibiotic screening was done. *Bacillus subtilius* (ATCC23857) and *Escherichia coli* (ATCC25922) were grown in tryptic soy broth (TSB) at 37°C. All microorganisms were cultured with 200 rpm shaking to facilitate the growth. Fresh overnight cultures (10µl) of bacteria and yeast were inoculated into 10ml of respective

broth and cultured till reaching the mid-logarithmic-phase for antimicrobial susceptibility testing. The minimum inhibition concentration (MIC) was determined using the method of broth microdilution. Briefly, 50µl of Penicillin G potassium-TAT solution with various concentrations (1.4 and 2.7ppm) and 50 µl controlled Penicillin G potassium solutions with same concentration respectively were placed into each well of 96-well plates respectively. Diluted organism suspensions (50µl) were then added to each well of the microplate. At different time intervals, the optical density readings of ~ 0.1-0.2 at 600 nm were measured. Broth containing cells alone was also used as control to validate the assays The MIC was defined as the lowest concentration of antibiotic that completely inhibited the growth of the organisms. The tests were repeated on three different days.

2.6 Cellular uptake study of Penicillin G and TAT-Penicillin G

The human endothelial cells and astrocytes were seeded into the 6-well palate with a cell density of 1.0×10^5 /well and a culture medium volume of 3ml/well. After 8 hours' incubation at 37°C, 5% CO₂, TAT-Penicillin G (1.4ppm and 2.7ppm) and controlled pure Penicillin G solution with same concentration were added into the culture medium respectively. At different time points (20, 40, 60, 80, 100, 240 and 720 minutes), 100µl medium samples were collected and directly injected into HPLC system for analysis.

3. Histochemistry and immunohistochemistry studies

The main purpose of histochemistry and immunohistochemistry studies is to investigate the nanoparticles BBB penetration in the animal model. In the study, such as the biodistribution of nanoparticles after they enter the body, the cellular uptake of nanoparticles in brain parenchyma and the testing of nanoparticle carriers in pathological brain could be achieved with histological techniques

3.1 Animal and anesthesia procedures

Adult male Sprague-Dawley rats (250~350g, 6~8 weeks) were employed in experiments. All animal work was carried out in accordance with the Singapore Animal Care and Use Committee and performed according to the guidelines set forth in the National Institutes of Health Guide for the Care and Use of Laboratory Animals (NIH Publications NO. 85-23, revised 1996). The minimum number of animals was used for the experiments, and suffering was minimized by the use of analgesia.

Prior to surgery, perfusion or harvesting of tissue samples or cells, all animals were deeply anaesthetized by an intraperitoneal injection of ketamine & xylazine solution (1ml/kg body weight). After 10-15 minutes, a foot pad of the animal was pinched with a pair of toothed forceps to ensure the animal was under full anesthesia. All procedures involving animals were approved by Institutional Animal Care & Use Committee, DSO National Laboratories, Singapore.

Anesthesia knockout solution preparation: 7.5ml Ketamine (100mg/ml), 5.0ml Xylazine (20mg/ml) and 7.5ml MilliQ water were mixed together to form the total

amount of 20ml. For the top-up solution during the surgery, 7.5ml Ketamine (100mg/ml) and 12.5ml MilliQ water together to total amount of 20ml. The dosage for top-up was half of the knockout dosage.

3.2 Perfusion, tissue sampling and sectioning procedures

3.2.1 Fixatives

I .4% paraformaldehyde (PF)	
-Pareformaldehyde	40g
-Phos. Buffer	1000ml
II .Phos. Buffer	
-0.1M Solution 'B'	
(178 g Na ₂ HPO ₄ .2 H ₂ O in 10 litres Deionised H ₂ O)	750 ml
-0.1 M Solution 'A'	
(69 g NaH ₂ PO ₄ . H ₂ O in 5 litres Deionised H ₂ O)	±250 ml
(Add approx 1 volume of 'A' to 3 volume of 'B' till PH 7.4)	

3.2.2 Preparation of gelatinized slides

I .5% gelatin solution:	
-Gelatin	1.5mg
-Chrome Alum	0.15g
-Distilled water	100ml

Slides were first dipped in the acid solution (400 ml of 98% sulfuric acid mixed with 1 tea spoon of potassium dichromate) for 2 minutes, and then washed by running tap water for 10 minutes. The slides were rinsed with distilled water and then baked in an oven at 80°C overnight for drying. The following day, dried slides were dipped in the gelatin solution and then were hung to dry with the clips. Gelatinized slides were kept in an oven at 37°C for histological or immunohistochemical study.

3.2.3 Perfusion

Two reservoirs were used, one containing Ringer's solution and the other appropriate fixative. Each reservoir was connected to a long polythene tube with an air trap interposed between them. A 19G winged needle (Terum Co., Japan), serving as cannula, was connected to the tube. Before introducing the perfusion fluid to the heart, all air bubbles in the tubes connected the two reservoirs were removed. Perfusion was done under gravity with the two reservoirs fixed at a height of 100cm above the perfusion table.

A midline incision of the skin from the level of the suprasternal notch to the level above the symphysis pubis was made. The incision, made through the skin and muscles of the anterior abdominal wall, was extended bilaterally along the subcostal margins to expose the sternum and diaphragm. The latter was then cut along the subcostal margin to fully expose the heart. Care was taken during this process not to damage the lungs. The pericardium was then slit with a pair of fine scissors to fully expose the heart. Perfusion was initiated whereby a cannula with some Ringer's solution dripping slowly from its tip was inserted into the left ventricle and was immediately followed by slitting a portion of the right atrium to let out the blood, and subsequently the perfusate. Once the cannula was secured in place, the flow of the Ringer's solution was turned to full pressure by means of a three-way tap. A total of 100ml of Ringer's solution at room temperature was allowed to flush the vascular system until the lungs and liver were cleared of blood. A total of about 400ml of the fixative (4% PF) at 4°C was administered.

3.2.4 Tissue sampling and sectioning

After perfusion, the brain was dissected, along with this, the liver; spleen and kidney were also removed for examination the distribution of nanoparticles. All the tissues were then postfixed with the same fixative for additional 4 hours. The tissues were subsequently transferred to 0.1M phosphate buffer (pH7.4) containing 15-30% sucrose and kept overnight at 4°C. The tissue samples were mounted on a metal chuck using Lipshaw M-1 embedding matrix (Pittsburgh, USA) and rapidly frozen by quenching in liquid nitrogen. Transverse sections of 30µm thickness of brainstems were cut using a cryostat (Leica CM 3050). The sections were subsequently mounted on gelatinized slides and allowed to dry at room temperature for 1 hour.

3.3 Procedures of immunofluorescent staining

3.3.1 Buffers and solutions

I . 0.1 M PBS	
-Disodium hydrogen phosphate heptahydrate	13.3g
-Sodium chloride	8.5g
-Distilled water	900 ml
(Adjusted to PH 7.4 with 2N HCL and topped up to 1,000 ml with distilled water)	
II . PBS containing 0.1% Triton-X 100 (PBS-TX)	
-PBS	1000 ml
-Triton-X 100	1 ml
III. 5% Normal goat serum	
-Normal goat serum	0.5ml
-Distilled water	9.5ml
IV. BrdU injection solution	
-BrdU (5-Bromo-2'-deoxyuridine) (Upstate, USA)	25mg
-0.9%w/v NaCl solution	1ml
V. Avidin-Biotinylated horseradish peroxidase Complex (ABC)	
-1 drop of A +1 drop of B	50µl +50µl
-PBS-TX	5ml

VI. 0.1M TBS (pH7.6)	
- Tris	6g
- Sodium chloride	8g
- Distilled water	1000ml
(Adjust with 2N or 4N HCl to pH 7.6)	
VII. 1xDAB Solution	
-10xDAB	10ml
-0.1M TBS	90ml
-30% H ₂ O ₂	0.067ml

3.3.2 Antibodies

- Mouse anti-rat CD11b monoclonal antibody (marker for microglia, 1:1000, Chemicon, USA)
- Mouse anti-Glial Fibrillary Acidic Protein (GFAP) monoclonal antibody (astrocytes, 1:1000, Chemicon, USA)
- Mouse anti-CNPase 2',3-cyclic nucleotide 3'-phosphodiesterase monoclonal antibody (oligodendrocytes 1:500, Chemicon, USA)
- Mouse anti-Neuronal nuclei (NeuN) monoclonal antibody (neuron, 1:500, Chemicon, USA)
- Mouse anti-bromodeoxyuridine (BrdU) monoclonal antibody (1:500, Chemicon, USA)
- Monoclonal anti-Tumor Necrosis Factor- α (TNF- α), clone 45418.111 (1:500, Sigma, USA)
- Mouse monoclonal [DB-1] to Interferon gamma (ab22543) (IFN- γ) (1:500, Abcam,UK)
- Rabbit PDGF Receptor- α antibody (1:100, Cell Signaling Technology USA)
- Mouse anti-Transforming Growth Factor- β (TGF- β) monoclonal antibody (1:1000, Chemicon, USA)
- Mouse monoclonal antibody to HIV TAT (ab24778) (1:100, abcam,USA)
- Mouse monoclonal anti-rat IL-1 α antibody (MAB500 1:500, R&D systems, USA)
- Rabbit anti-NG2 chondroitin sulfate proteoglycan polyclonal antibody (NG2 1:500, Chemicon USA)
- Goat anti rabbit IgG (H+L) F(ab')₂ fragments ,Cy3 conjugated affinity purified secondary antibody (1:500, Chemicon, USA)
- Goat anti mouse IgG (H+L) F(ab')₂ fragments ,Cy3 conjugated affinity Purified secondary antibody (1:500, Chemicon, USA)
- Goat anti mouse IgG (H+L) F(ab')₂ fragments, FITC conjugated affinity purified secondary antibody (1:500, Chemicon, USA)

3.3.3 Staining procedure

For immunofluorescent staining, the prepared slides first were washed with PBS-TX for 3 times, each time takes 10 minutes. Then the sections were blocked with 5% normal goat serum for 1 hour and incubated in only one primary antibodies at RT overnight. Next day, after washing the slides with PBS for 3 times, the FITC (for QDs encapsulated particles) or Cy3 (for FITC encapsulated particles) conjugated secondary antibody was added and incubated at room temperature for 2 hours. At last the slides were incubated with DAPI solution (1:5000) for 1-2 minutes. After washing these slides with PBS for 2 times, they were mounted with nonfluorescent mounting medium (DAKO, USA), then viewed and photographed with Laser-Scanning Confocal Microscopy (Olympus FluoViewTM FV1000, Japan) in 488nm (FITC) and 560nm (QDs) respectively.

Immunofluorescent double labeling technique is the best way to determine the co-localization of two different antigens in one cell or tissue preparation. The respective positive staining may merge together in one cell. It suggests that these two antigens are co-localized. For immunofluorescent double labeling process, two primary antibody from different host (such as 1:500 mouse antibody against rat GFAP and 1:500 rabbit antibody against rat NG2) were used together to incubate brain sections in room temperature overnight. After the same washing procedure as before, fluorescent dye conjugated secondary antibodies respectively against their primary were added to the section (1:500 goat anti mouse IgG, FITC conjugated and 1:500 goat anti rabbit IgG, Cy3 conjugated). 2 hours incubation later, the processing and observation procedures are as same as before.

3.3.4 Procedures of DAB staining

The cryo-cut sections were first rehydrated in 1xPBS pH7.4 for 30 seconds, then, quenched with 3% H₂O₂ for 5 minutes, washed in 1xPBS solution, and blocked with 5% normal goat serum in PBS with 0.1% TritonX-100 for 1 hour at RT. The primary antibody (rabbit anti-NG2 1:500) was applied for overnight at RT. Next day, the slides were rinsed in PBS for 10 minutes, 3 times and incubated with secondary antibody (anti-rabbit IgG 1:200) for 1 hour at RT. After rinsed in 1xPBS, the fresh prepared ABC (A and B should be mixed at least 30mins before application) was added into the section and incubated for 1 hour. One hour later, the sections were rinsed in 1xPBS for 2 times and immersed into TBS for half an hour. Last, sections were stained with 1xDAB solution and rinsed with TBS for 10 minutes, 3 times for methyl green staining.

The stained slides firstly were immersed into 0.1M acetate buffer (pH 4.8) for 2-5 minutes. Then, they were put into methyl green solution in 2-4 minutes. It is followed with dehydration process from 75% ethanol, 95% ethanol to 100% ethanol. Each step took 5 minutes around. After immersed into 100% histoclear for 5 minutes, the slides were dried in a fume hood for 20-30 minutes and mounted with Permount slides mounting medium. These slides were observed and photographed with a light microscope (Olympus BX51, Japan).

3.4 Procedures of injection of nanoparticle solution

Adult male Sprague-Dawley rats (250~350g, 6~8 weeks) were anesthetized with ketamine & xylazine solution (1 ml/kg body weight), and their hair near the thigh were shaved. An incision was made on the right side of the thigh to expose the femoral vein. Carefully separating the vein and the artery with small scissor, the lower femoral vein close to the toes was tied. A very small incision was made on the vein and a polyethylene cannula was put inside the blood vessel through this incision. The nanoparticles solution (PEG-*b*-Chol or TAT-PEG-*b*-Chol at 0.054 mg/ml, dissolved in 1×PBS) containing the FITC or QDs were injected into the vein through this polyethylene cannula (the injection volume: 1.5ml/rat). Then the animals were monitored in a heated recovery box until fully conscious. Two hours after the injection of nanoparticles, the animals were sacrificed for sampling and observation.

3.5 Pathological brain model setup procedures

3.5.1 Materials

- I . LPS Solution (1μg/μl)
 - Lipopolysaccharide (E. coli serotype 0127:B8; Sigma, USA) 1mg
 - 1x PBS 1ml

LPS is a bacterial endotoxin released from the surface of replicating and dying gram-negative bacteria into the circulation (Rietschel et al., 1996; Rubenstein et al., 1962). It is known to have a variety of effects on the brain and cerebral circulation. At the molecular level, these changes include activation of transcription factors, changes in gene expression, formation of proinflammatory and anti-inflammatory cytokines, expression of adhesion molecules, and infiltration of leukocytes. Many of

these changes, including the infiltration of leukocytes, are generally thought to contribute to neuronal dysfunction and cell death (Barone and Feuerstein, 1999).

3.5.2 Procedures of LPS and anti-CD11b antibody cortical injection

Male SD rats (10 weeks, 310–400g) were anesthetized with xylazine and ketamine (1ml/kg body weight). After the animals were placed in a stereotaxic frame, their scalp and temporal muscles were reflected and a hollow female Luer-Loc fitting (4.5mm) was fixed rigidly with dental cement to the animal's skull through a craniotomy centered over the left parietal cortex, 2mm lateral to the sagittal suture and 3mm posterior to the coronal suture. This would position the hole parasagittally over the cerebral cortex. The dura was left intact.

As for LPS triggered pathological brain model, LPS was administered to trigger the neuron-inflammation in the cerebral cortex region. After exposing the skull, a small hole (2mm lateral to the sagittal suture and 3 mm posterior to the bregma) was drilled and LPS solution (1 μ g/ μ l, 1 μ g/rat) was injected into the cortex by micro-syringe through this hole. Then, the rat was put back to the cage and 24 hours later used in the experiment. Saline served as the control for the LPS.

As for anti-CD11b antibody blocked and LPS triggered pathological brain model, before the administration of LPS, anti-CD11b antibody solution (1 μ g/ μ l, 1 μ g/rat) was injected into cerebral cortex region. And 24 hours later, LPS solution was injected to the same site.

3.6 BrdU assay procedures

3.6.1 BrdU solution preparation

Warm saline solution (0.9%w/v NaCl in sterile H₂O) to 40–50°C, slowly dissolve BrdU in saline solution by gently vortexing, allowing BrdU injection solution to cool to room temperature (22–25°C) and use them immediately.

3.6.2 BrdU solution intraperitoneal injection

The ideal BrdU injected dosage varies from 50mg/kg to 300mg/kg depending on experiments and animals in use. Here, the dosage of 50mg/kg was used. For an intraperitoneal injection, the lower abdominal cavity must be isolated. A 23-gauge needle and a 5-ml syringe were used. The maximum tolerable intraperitoneal injection volume in the rat was 10ml.

3.6.3 Perfusion and sectioning

After experimental animals were anesthetized, their hearts were exposed by sharp dissecting tools. Then, insert the needle connected to the pump into the left ventricle and made an incision in the right atrium to allow blood to flow out of the animal's body. The animal was perfused with 0.1M PBS at pH7.4. When the draining blood became clear, they were then perfused with 4% paraformaldehyde in 0.1M PBS. The brain sample was sectioned into 30µm slices by cryostat (Leica CM 3050).

3.6.4 DNA denaturation

Denaturation of DNA allows the access for anti-BrdU antibody, so incomplete denaturation may cause problems. There are various denaturation procedures (such as ethanol treatment and enzyme treatment), which may have different effects on the retention of morphology. The acid treatment with an increased temperature generally results in more effective exposure of the halogenated-nucleotide antigen. However, harsh HCl treatment (>2M HCl), in conjunction with high temperature (>65°C) incubation, is detrimental to other antigens, particularly surface antigens and receptors. Moreover, some BrdU antibodies can recognize methylated thymidine under harsh denaturation conditions. This non-specific staining is evident when all or most of the nuclei are stained. Thus, careful adjustments of the denaturation conditions are necessary.

First, sections were rinsed three times, 5 minutes each with 0.1M PBS (at pH 7.4) on a shaker. Then, DNA was denatured by incubating sections in 1M HCl for 30 min at 45°C (or 2M HCl for 15 min at 37°C).

4. HPLC analysis

4.1 Materials

I .Instruments

- Chromatographic HPLC system (Alliance 2695XE separation Module. Water Ltd, USA)
- UV-Vis 2996 photodiode array detector (Water Ltd, USA)
- Atlantis dC18 column (150×2.1mm I.D.; particle size, 3µm. Water Ltd, USA)
- SymmetryShield™ Cartridge Column RP18 (250×4.6mm I.D.; particle size, 5µm. Water Ltd, USA)

II .Chemicals

- 0.01M sodium phosphate (pH4.8)
 - Sodium phosphate monobasic (MW: 119.98, Sigma, USA) 1.20g

Millipore water	1000ml
-5% acetic acid	
Acetic acid (MW: 60.05, USA, 1.05 g/ml)	4.76ml
Millipore water	95ml
-15mM triethylamine	
Triethylamine (MW: 101.19, Sigma, USA)	1.52g
Millipore water	1000ml
-Methanol (HPLC) (MW: 32.04, VWR Prolabo, USA)	
-Acetonitrile (HPLC) (MW: 41.05, VWR, BDH, USA)	
-Ciprofloxacin (MW: 331.34, Sigma, USA)	
-Penicillin G potassium (MW: 372.48, Sigma, USA)	
-Penicillin G-TAT	

4.2 Procedures of injection and sample preparation

Ciprofloxacin and Penicillin G were injected into the animal body through the femoral vein or oral pathway respectively. The dosage of injection is 80 mg/kg body weight. After administration, the rat plasma samples were collected at the time points of 20,40,60,80,100 and 120 minutes respectively.

4.2.1 Sample collection

At different time intervals, 0.5ml rat blood was collected through femoral vein respectively. Then, collected blood samples were centrifuged at speed of 5000 rpm for 5 minutes. The upper clear compartment was extracted for sample preparation.

4.2.2 Sample preparation

Ciprofloxacin: Rat plasma (100µl) samples were spiked with concentration ranging between 0.5 and 10µl/ml of ciprofloxacin and denatured by 200µl of acetonitrile, vortex for 1 minute and centrifuged at 4500rpm for 10 minutes. The supernatant was extracted into a test-tube and dried under nitrogen gas. The resultant

residue was reconstituted in (5% acetic acid+15 mM triethylamine) and injected into the HPLC system for analysis.

Penicillin G: Rat plasma (200µl) samples were spiked with concentration ranging between 1.0 and 50µl/ml of ciprofloxacin and denatured by 200µl of acetonitrile, vortexed for 1 minute and centrifuged at 14,000 rpm for 15 minutes. The supernatant was extracted into a test-tube and dried under nitrogen gas. The resultant residue was reconstituted in (75%0.01M sodium phosphate (pH4.8):25% acetonitrile) and injected into the HPLC system for analysis.

4.3 HPLC analysis method

10µl samples was injected into the HPLC system and analyzed with different column and mobile phase. The Ciprofloxacin was separated on Atlantis dC18 column (150×2.1mm I.D.; particle size, 3µm) at a flow rate of 0.5 ml/min, with mobile phase of 90% (5% acetic acid+15mM triethylamine),10%(Methanol : Acetonitrile) in isocratic program for 13 minutes. The detector was operated at a wavelength of 280nm. As for Penicillin G, the column was also SymmetryShield™ Cartridge Column RP18, and the mobile phase was 75% 0.01M sodium phosphate (pH4.8), 25% acetonitrile. The flow rate and detective wavelength were 1.0 ml/min and 229nm respectively.

5. Statistical analysis

All the experiments were repeated at least in triplicate for statistical purpose, and where appropriate, the data were presented as mean and standard deviation. All quantitative data were statistically evaluated using the Student's *t*-test. The level of significance was set at $p < 0.05$.

CHAPTER 3

RESULTS

1. Fabrication and characterization of nanoparticle micelles

1.1 Synthesis of PEG-*b*-Chol and TAT-PEG-*b*-Chol

As shown in the ^1H NMR spectrum of PEG-*b*-Chol (Figure.3.1), PEG-*b*-Chol was successfully synthesized. The multiple peaks at δ 3.5-3.7 could be attributed to the protons of -CH₂- groups in PEG and the weak and multiple peaks at δ 0.68-1.02 could be attributed to *b*-cholesterol. Figure.3.2 shows the spectra of TAT conjugated PEG-*b*-Chol (TAT-PEG-*b*-Chol), TAT and PEG-*b*-Chol in D₂O. The weak and broad peaks at δ 4.0-4.2 (signal a) could be attributed to the protons of -NH-CH-(CH₂)-CO- in TAT. The peaks at δ 2.52-2.58 (signal b) might be derived from the protons of -CH₂-NH-NH-NH₂ in arginine. The peaks at δ 6.60-6.66 (signal c) and at δ 6.95-7.0 (signal d) could be attributed to the protons from the benzene ring in tyrosine. Based on the peak area ratio of signal c (derived from TAT) to signal e (derived from PEG) and the number of their representative protons, the molar ratio of TAT to PEG in the polymer was estimated to be about 0.9-1.0. After *b*-cholesterol and TAT conjugation, the increase in average molecular weight from 4.96 to 6.72 kDa further proved that synthesis of TAT-PEG-*b*-Chol was successful. The melting points of PEG-*b*-Chol and TAT-PEG-*b*-Chol (54°C and 47°C respectively) were determined.

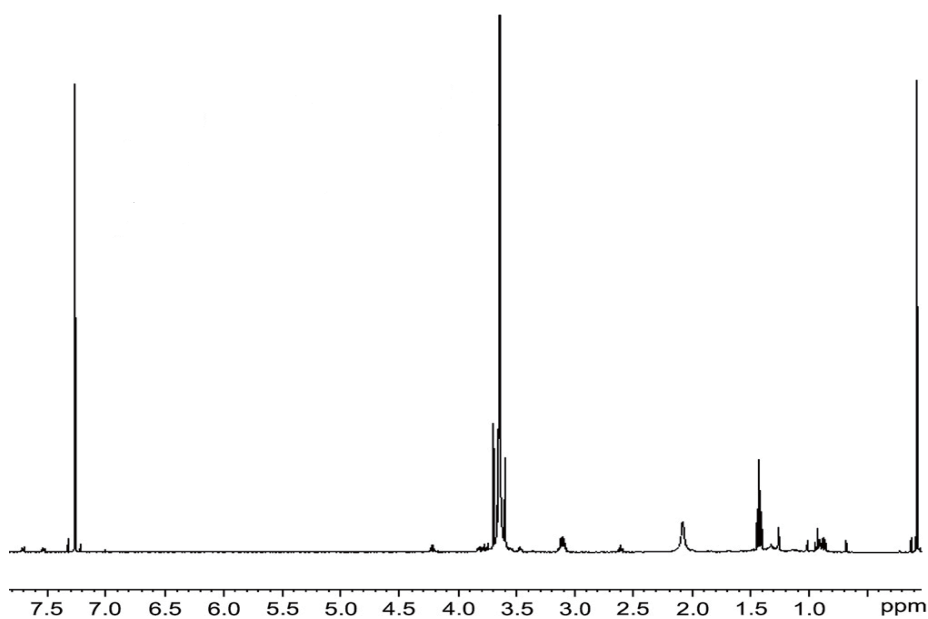


Figure 3.1: ^1H NMR spectrum of PEG-*b*-Chol in CDCl_3 . The PEG-*b*-Chol was successfully synthesized.

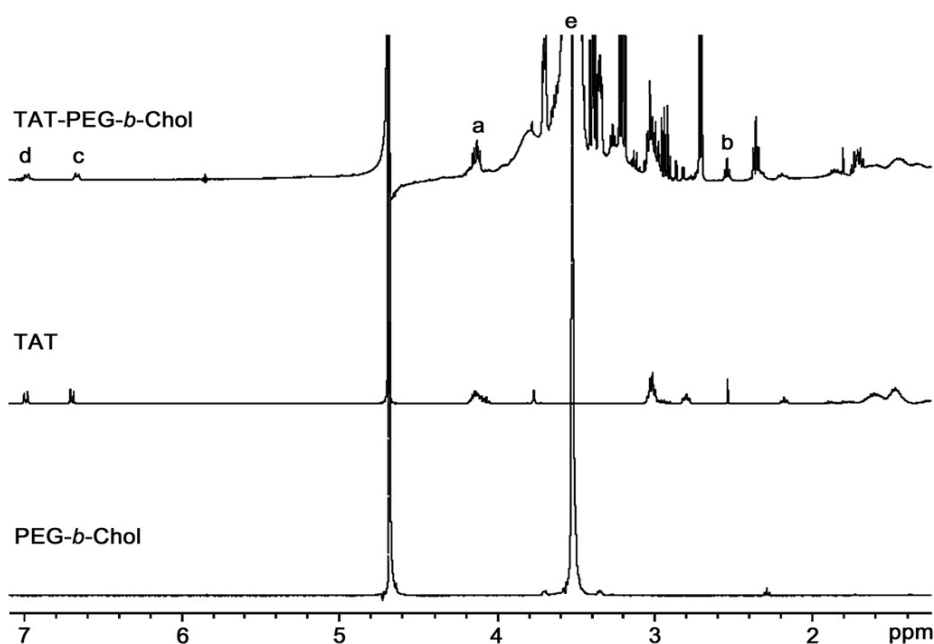


Figure 3.2: ^1H NMR spectrum of PEG-*b*-Chol, TAT-PEG-*b*-Chol and TAT in D_2O . From this spectrum, the synthesis of TAT-PEG-*b*-Chol was also successful.

1.2 Morphology of nanoparticles micelles

The particle size is an important parameter for nanoparticles synthesized to be drug carrier through the BBB. Generally, it is difficult for cells to endocytose particles

with an effective diameter higher than 300nm (Kreuter, 2001). Under the fabrication conditions, the effective diameter of the blank, drug-loaded, QDs-loaded and FITC-loaded nanoparticles was 180,190, 150 and 199nm, respectively. The blank and drug-loaded nanoparticles were spherical in nature, and the size of the nanoparticles increased slightly after drug loading.

The amphiphilic polymers consisting of hydrophilic and hydrophobic segments can self-assemble to form core shell structure in aqueous solutions. The morphology of blank and ciprofloxacin encapsulated nanoparticles formed with PEG-*b*-Chol or TAT-PEG-*b*-Chol was examined with scanning electrical microscope (SEM). Figure 3.3 shows typical SEM images of bland (C) and drug-loaded TAT-PEG-*b*-Chol nanoparticles (A, B and C). In C, the nanoparticles which red arrows pointed had successfully encapsulated drug molecules into their core shell. However, the white small cycles were blank nanoparticles. A and B show the morphology of drug loaded TAT-PEG-*b*-Chol nanoparticles under SEM. The size of the nanoparticles showed in the SEM images was slightly smaller than the results obtained from light scattering possibly because of the shrinking of the shell of the nanoparticles during the process of vacuum drying required for sample preparation and SEM operation.

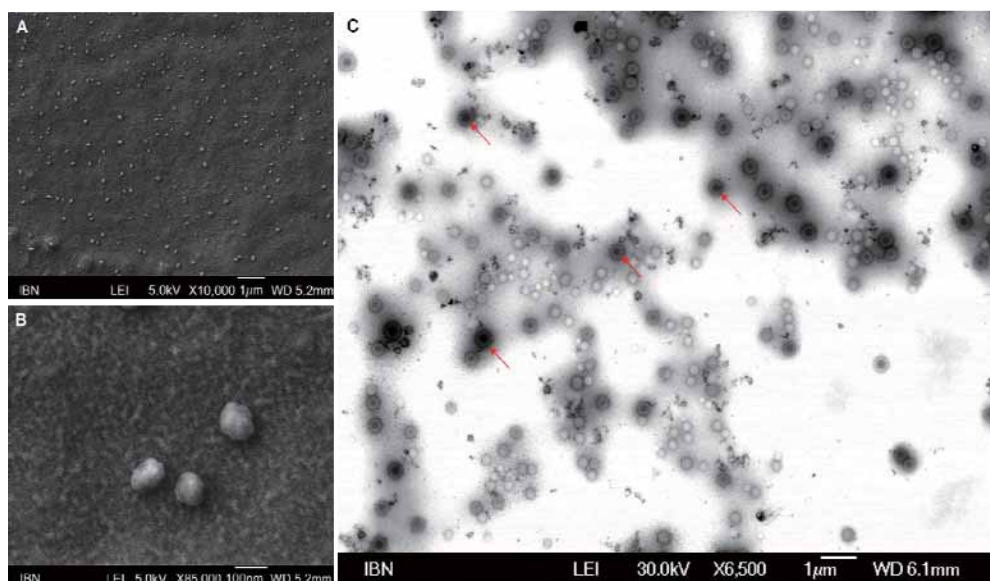


Figure 3.3: A typical SEM images of drug-loaded and blank TAT-PEG-*b*-Chol nanoparticles. A (lower magnification) and B (higher magnification) show the morphology of drug loaded TAT-PEG-*b*-Chol nanoparticles. C shows the nanoparticles which have successfully encapsulated the drug into their core shell (red arrow). Others are blank TAT-PEG-*b*-Chol. (Scale bar: 1μm for A, C and 100 nm for B).

1.3 Drug loading into nanoparticle micelles

Ciprofloxacin was loaded into the nanoparticles at different initial drug loadings (i.e. 3, 5 and 8mg) at RT. Increasing initial drug loading led to an increased actual drug loading level, i.e. 2.3%, 2.7% and 3.2%, respectively. However, the particle size increased as well as the increase of initial drug loading reaching up to the highest of 297nm at the initial loading of 8mg. This size might be too high to yield a prolonged blood circulation of the nanoparticles. The ciprofloxacin-loaded nanoparticles were also fabricated at 10°C with an initial drug loading of 3mg, and an increased drug loading level was achieved (3.7% vs. 2.3%). This may be due to the fact that the solvent removal rate was lower at 10°C so that the drug molecules had more time to assemble into the nanoparticles.

In addition, the particle size of the drug-loaded nanoparticles fabricated at 10°C was smaller (190nm) than those fabricated in room temperature (208nm). Therefore, loading of FITC or QDs into nanoparticles was conducted at 10°C and low initial loading (i.e. 0.75mg) to yield small size particles. Figure 3.4 shows the effect of initial drug (ciprofloxacin) loading on loading capacity of the nanoparticles. When the initial drug loading amount increased from 1 mg to 3 mg, the actual drug loading rate also increased from 12.2% to 13.8%. However, when the initial drug loading amount continued increasing, the actual drug loading rate nearly has no change.

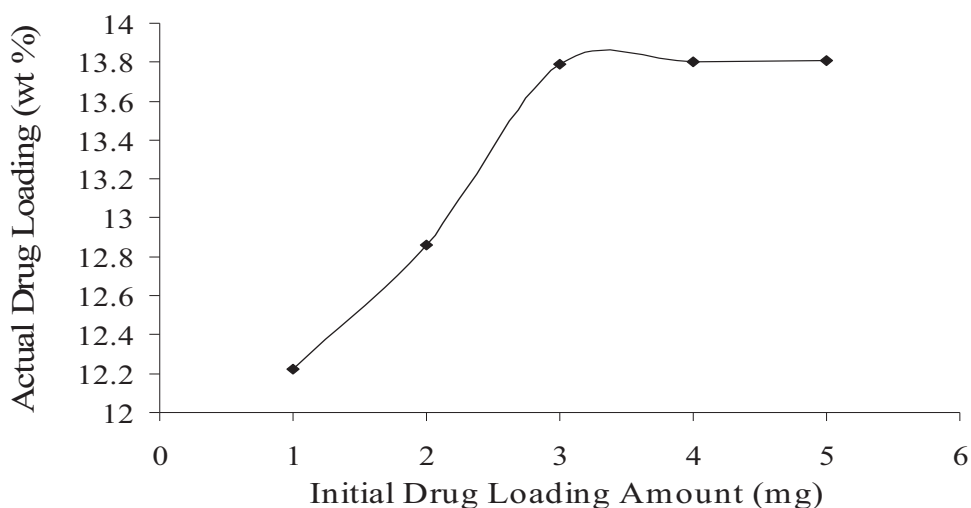


Figure 3.4: Effect of initial drug loading (Ciprofloxacin) on loading capacity of the nanoparticles. When the initial drug loading amount is 3 mg, the actual drug loading rate reaches the highest point.

1.4 *In vitro* drug release in PBS

To get *in vitro* drug release of ciprofloxacin loaded nanoparticle in PBS solution, at specific time intervals, the PBS solution with 20mg drug loaded nanoparticle micelles was taken out for analysis of drug concentration by the UV/VIS/NIR spectrophotometer. The standard curve was constructed by dissolving ciprofloxacin in

PBS in the concentration range from 2.5 to 20.0ppm and r^2 value was 0.999906. Figure 3.5 shows drug release profile from the nanoparticles in PBS (pH 7.4) at 37°C. The release of the drug was sustained over a period of 5 hours. The results indicated that the release of the drug was well sustained. It suggested that after the nanoparticles get into the brain, a sustained release of ciprofloxacin lactate could be achieved. On the other hand, the *in vitro* drug release results also indicated that the drug molecules were well encapsulated into the nanoparticles.

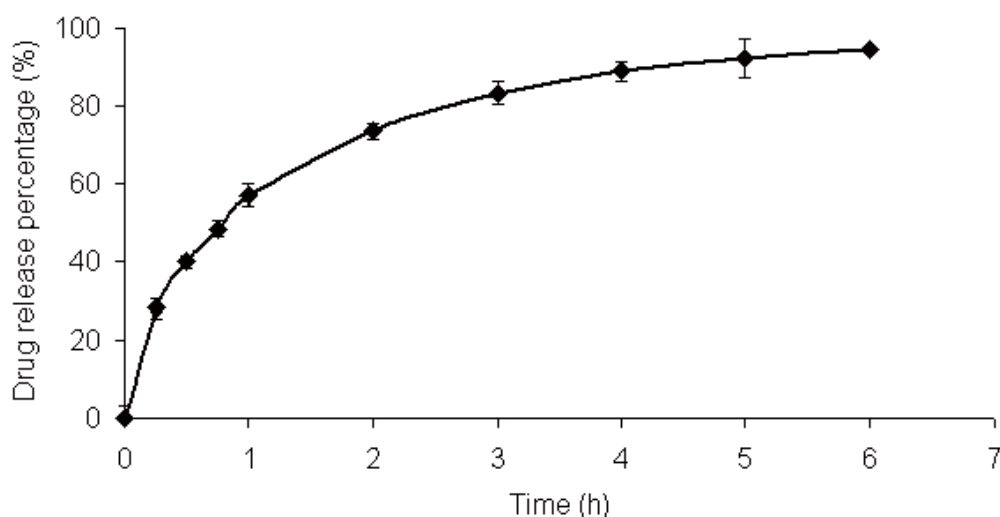


Figure 3.5: *In vitro* ciprofloxacin lactate release from the nanoparticle,, which shows the release of drug molecules was well sustained over a period of 5 hours. It indicates that the drug molecules were well encapsulated into the nanoparticles and a sustained drug release would be achieved.

2. Investigation of BBB integrity

2.1 BBB in developing rat

Qtracker 565 non targeted Quantum Dots are intended for use *in vivo* imaging or the imaging of micro-injected cells. These materials can exhibit long *in vivo* circulation times, non-specific binding and low immune response. In order to

investigate the integrity of developmental rat's BBB, Qtracker 565 was injected into the bodies of rats (Postnatal 1 day, Postnatal 7 days and Postnatal 14 days respectively) as fluorescent marker. Figure 3.6 shows the labeling results in the brain of developmental rat. There were many positive cells (green dots the arrow pointed) in A and B. Although we did not study the type of these positive cells, the results suggest that Qtracker 565 can penetrate the BBB in P1 and P7 rats. It may be because in these stages, the BBB function of rats is not completely developed and can let substance enter the brain. However, in C, there was not any cell labeled with Qtracker 565. It indicates that in P14, the BBB was fully developed and excluded foreign molecules entering the brain.

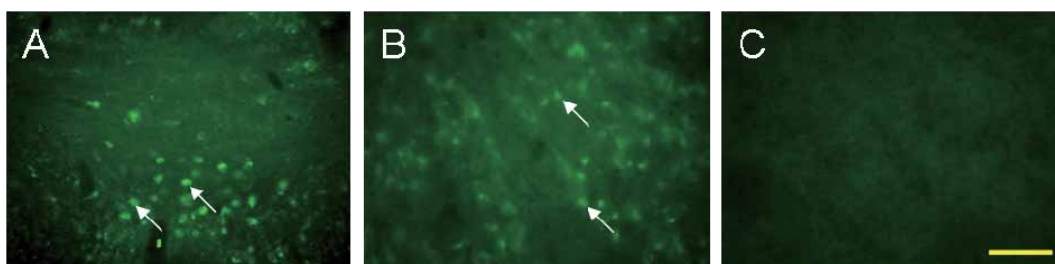


Figure 3.6: Investigation of BBB integrity in developmental rat with Qtracker 565 non-targeted Quantum Dots. The arrows point the positive cells which labeled with Qtracker in brain. (A: Postnatal 1 day; B: Postnatal 7 days; C: Postnatal 14 days. Scale bar: 100 μ m)

2.2 The BBB penetration of Rhodamine B

As rats' BBB become complete from P14 onwards, therefore, fluorescent dyes such as fluorescein or Rhodamine can easily penetrate the BBB before P14. Figure 3.7 shows the images that come from Rhodamine B stained brain of baby rat (postnatal 5). Here, 50 μ l 1% Rhodamine B solutions (A and B) and 0.25% Rhodamine B (C and D) solutions were injected into the rat respectively. 4 hours later,

the brain tissues were collected. In A and B, many brain cells in cerebral cortex were labeled with Rhodamine B (red cells which arrows pointed). In C and D, also many Rhodamine B labeled cells could be found. However, contrast to A and B, the number of Rhodamine B labeled cells in C and D was much lower because of concentration difference in injected Rhodamine B. These results indicate that Rhodamine B really can cross the BBB without any aid in the baby rat. Therefore, some brain drugs such as antibiotics are supposed to enter the brain parenchyma in the developing brain freely.

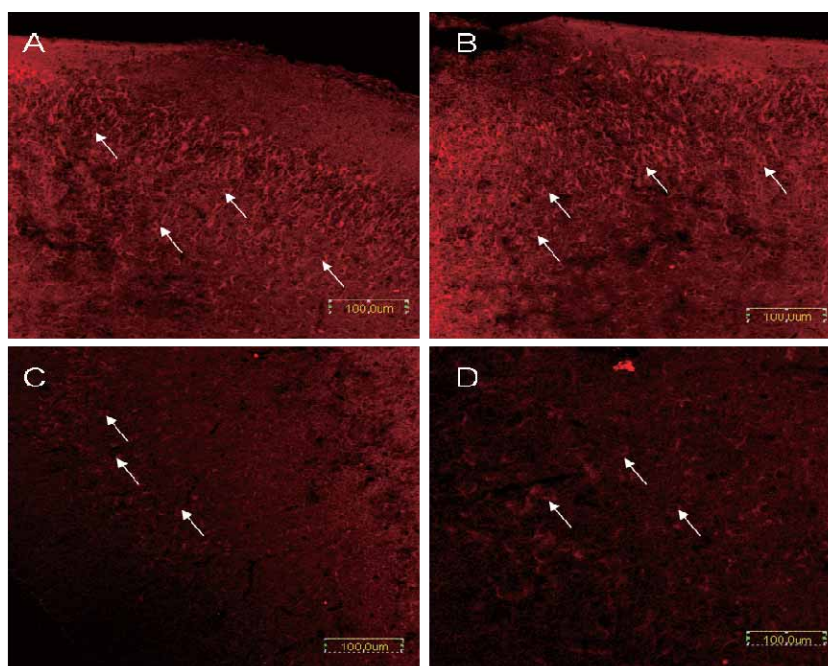


Figure 3.7: The penetration of Rhodamine B through the BBB in P5 rat. A and B: 50 μ l 1% Rhodamine B solutions; C and D: 50 μ l 0.25% Rhodamine B solutions. (Observation area: cerebral cortex. Scale bar: 100 μ m)

3. *In vivo* BBB permeability of nanoparticle micelles

3.1 BBB penetration of FITC Encapsulated nanoparticles

The penetration ability of PEG-*b*-Chol and TAT-PEG-*b*-Chol nanoparticles through the BBB and their distribution in major rat organs has been observed. Firstly,

FITC as a fluorescent trace marker was successfully encapsulated into the core of PEG-*b*-Chol. Then, FITC-PEG-*b*-Chol solution was injected into the body through the femoral vein. Figure 3.8 shows that after entering the blood stream, FITC-PEG-*b*-Chol were distributed in most organs of the body except brain because of the existence of BBB. In the rat brain (A), it is obvious that very few nanoparticle positive cells were found after the administration of FITC-PEG-*b*-Chol. However, many of green fluorescent positive cells could be observed in the liver (E), kidney (C) and spleen (G). It suggests that FITC-PEG-*b*-Chol can be taken by liver, kidney and spleen but not brain.

The TAT peptide has been successfully conjugated with FITC-PEG-*b*-Chol to form the nanoparticle of FITC-TAT-PEG-*b*-Chol. When rats were treated with FITC-TAT-PEG-*b*-Chol through intravenous administration, many cells in liver (F), kidney (D), and spleen (H) could also be labeled by TAT conjugated FITC-PEG-*b*-Chol nanoparticle micelles. In addition, some micelles positive cells with long processes (B) were found in the brain. It suggests that although PEG-*b*-Chol can be excluded entering the brain by BBB, with the aid of TAT group, TAT-PEG-*b*-Chol can penetrate BBB and reach the brain parenchyma. Therefore, the nanoparticle system of TAT-PEG-*b*-Chol may serve as a carrier to deliver drug molecules cross the BBB and reach the brain.

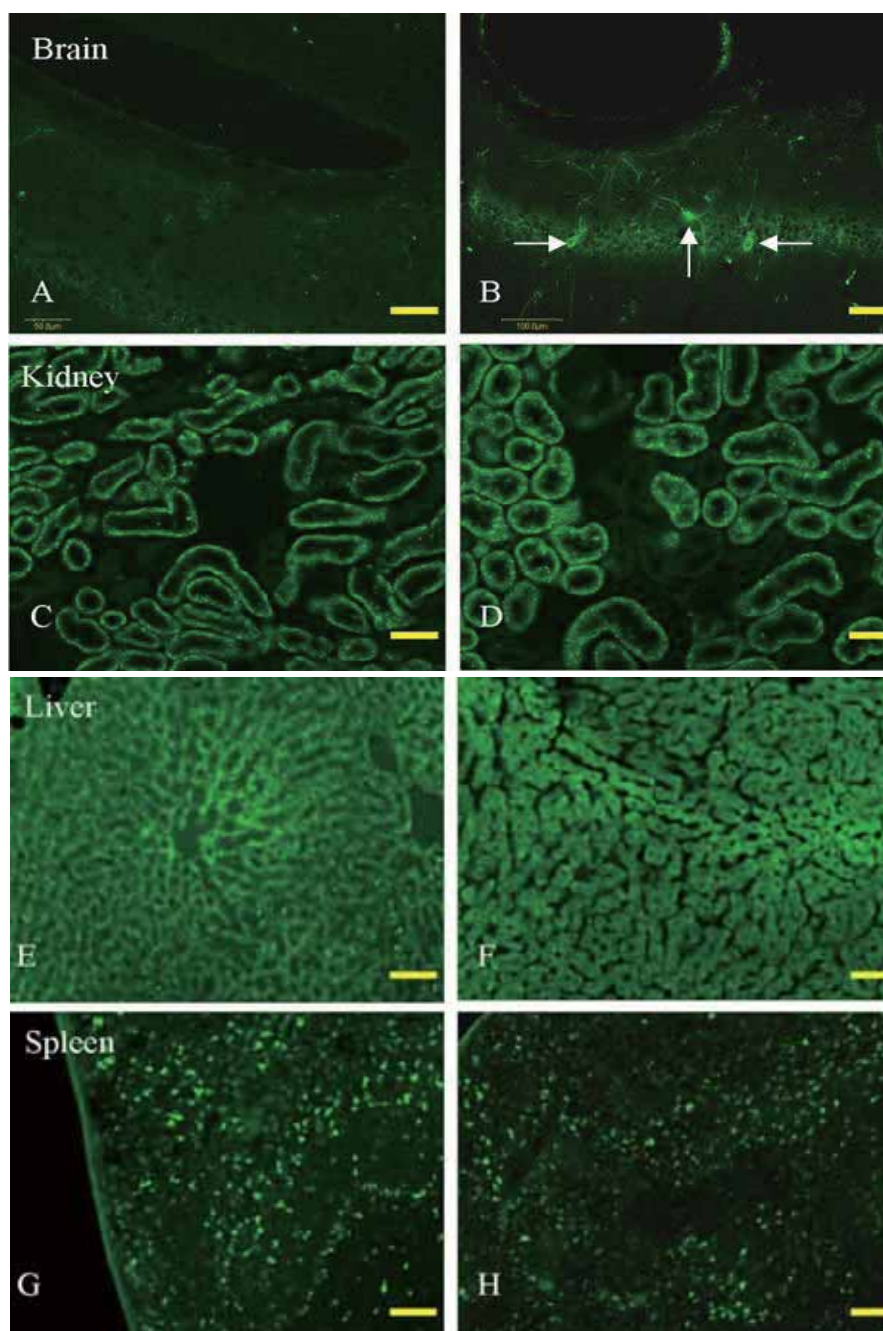


Figure 3.8: Distribution of nanoparticles in rat organs after administration by FITC-PEG-*b*-Chol (A, C, E, and G) or FITC-TAT-PEG-*b*-Chol (B, D, F, and H). Many cells in kidney (C, D), liver (E, F) and spleen (G, H) are labelled with FITC in both groups, but only in TAT-FITC-PEG-*b*-Chol injected rats, some fluorescent positive cells with long extending processes (arrows in B) were detected in the brain hippocampus (A, B). (Scale bar: 50 μ m)

3.2 BBB penetration of QDs Encapsulated TAT-PEG-*b*-Chol

QDs encapsulated TAT-PEG-*b*-Chol was also used to determine whether this kind of nanoparticles could cross the BBB. Here, QDs loaded PEG-*b*-Chol solution

with the same concentration was used as negative control. 4 hours after femoral vein injection, rat the brain sections were sampled and the distribution of fluorescent positive cells were observed under fluorescent microscope. Obviously, only a few traces of QD fluorescence were detected in the section (Figure 3.9 A) treated by QDs-PEG-*b*-Chol. However, the fluorescent intensity increased showed an obvious increase in the brain sections administrated with QDs-TAT-PEG-*b*-Chol nanoparticles (Figure 3.9 B, C and D). The positive staining could be observed to surround the nuclei in many brain cells (Figure 3.9 C, D, white arrows). In addition, the sections of the liver, kidney, heart and lung were also positive for QDs loaded micelles distribution (data not shown) at 4 hours after injection. It suggests that QDs encapsulated TAT-PEG-*b*-Chol could also penetrate the BBB and reach the brain similar like the nanoparticles of FITC loaded TAT-PEG-*b*-Chol.

Figure 3.9 also shows that after QD-loaded TAT-PEG-*b*-Chol nanoparticles crossed the BBB, they mainly surrounded the nuclei of neuronal cells (Figure 3.9 D, white arrows). This finding is in agreement with the results reported in the literature (Santra et al., 2005b), in which TAT-conjugated QDs were detected in the rat brain after QDs injection. The QD-loaded nanoparticles did not enter the cell nucleus of neurons possibly because of the relative large size of the nanoparticles for nuclear pore.

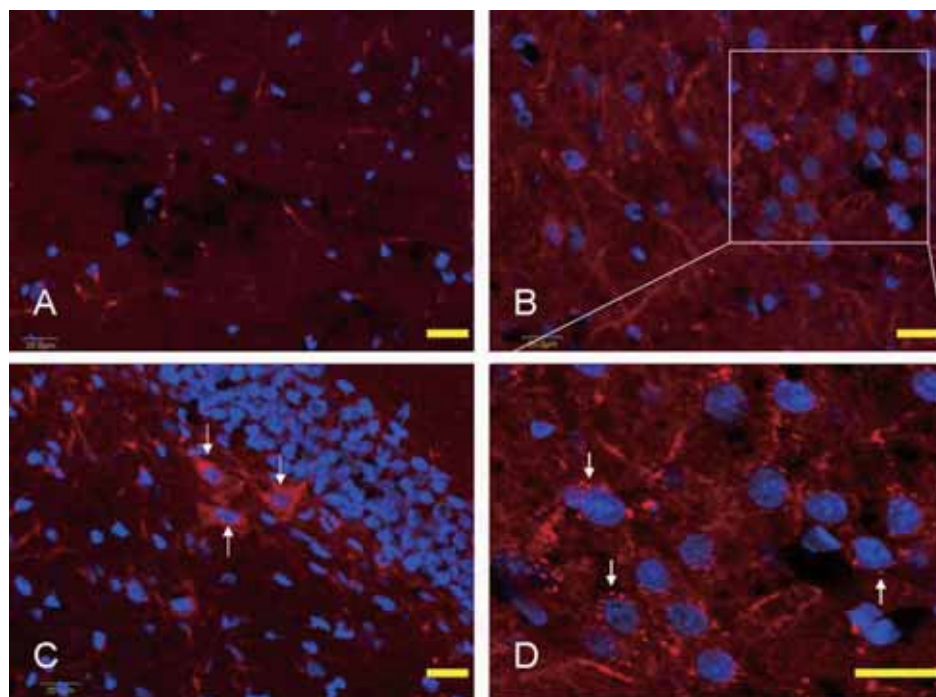


Figure 3.9: Transduction of QDs-PEG-*b*-Chol (A) and QDs-loaded TAT-PEG-*b*-Chol nanoparticles (B-D) across the BBB. A few traces of QD fluorescence were shown in the hippocampus sections of the brain in QDs-PEG-*b*-Chol administrated rat brain (A). Positive fluorescent labeled cells increased significantly when the QDs delivered by TAT-PEG-*b*-Chol particles (B-D). The white arrows (C and D) show the cells in hippocampus of the brain were marked by the QDs loaded micelles and the perinucleus fluorescence indicates the micelles were mainly distributed in the cytoplasm of neuronal cells. (Blue-stained nuclei; Red dots-QDs. Scale bar: 20 μ m.)

3.3 Particle size of micelles for its BBB penetration

The ideal size of drug-loaded nanoparticle system for delivery through the BBB should be lower than 300 nm. Otherwise, it may be difficult to be endocytosed by a cell (Olivier, 2005). In the process of FITC-TAT-PEG-*b*-Chol fabrication, extending the dialysis time and lowering the reaction temperature are providing a better condition to produce nanoparticles with evenly distributed sizes. The FITC encapsulated nanoparticles with diameters lower than 200 nm can be achieved. In order to investigate the relationship between BBB permeability and nanoparticle size, FITC encapsulated nanoparticles with different sizes were prepared and used. Figure

3.10 shows FITC encapsulated nanoparticles in the brain cortex. It is obvious that, in A (particle size 151.7nm), many more nanoparticle positive cells were found in cerebral cortex contrast to the same area of B (particle size 354.6nm). Also, these nanoparticle positive cells in the A emitted a stronger fluorescence than those cells in the B. It indicates that FITC-TAT-PEG-*b*-Chol with smaller diameters (151.7nm, A) could pass the BBB easily than those with larger diameters (354.6 nm, B).

Generally, nanoparticles with small particle size have stronger nanoparticle bioadhesion to human vascular endothelial cells (Lohbach et al., 2006), they showed highest binding percentage than those particles with higher diameters. Therefore, with the aid of TAT peptide group, small-sized nanoparticles can more easily be taken up by endothelial cells and penetrate the BBB. For brain drug delivery, most successful nanoparticle carriers have the size under 200nm (Liu et al., 2008a; Rao et al., 2008; Reimold et al., 2008).

It was clear that TAT can help nanoparticle of PEG-*b*-Chol cross the BBB (Liu et al., 2008a). The differences in *in vivo* brain uptake between FITC-TAT-PEG-*b*-Chol (A and B) and FITC-PEG-*b*-Chol (C) are also shown in Figure 3.10. Although there were still some sporadic positive cells were labeled by FITC-PEG-*b*-Chol (C) contrast to saline injected brain (D), many more FITC-TAT-PEG-*b*-Chol micelles could enter the brain parenchyma and label brain cells with the aid of TAT peptide group (A and B).

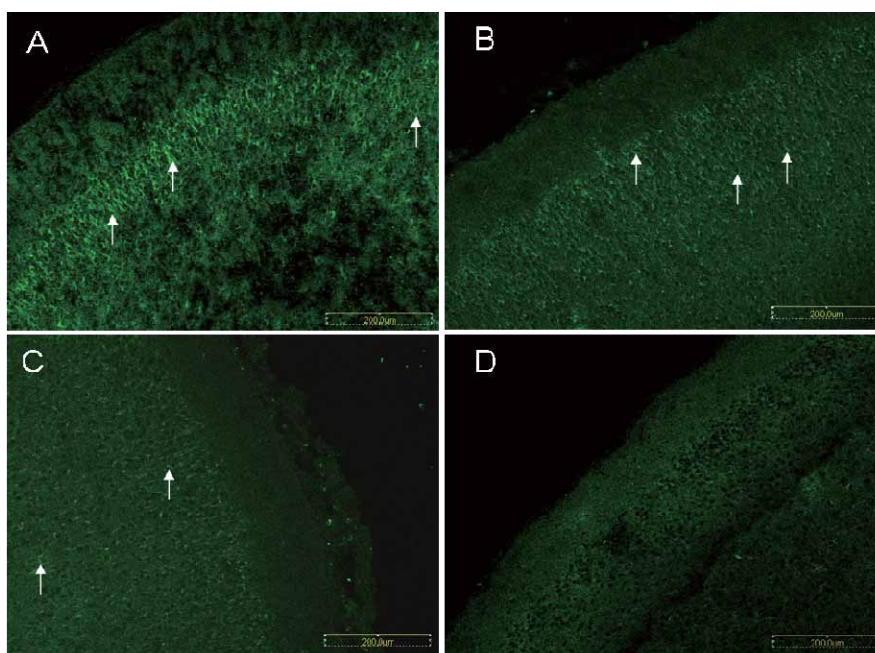


Figure 3.10: Particle size and BBB penetration. A: FITC-TAT-PEG-*b*-Chol, particle size: 151.7nm, concentration of FITC: 0.45mg/ml. B: FITC-TAT-PEG-*b*-Chol, particle size: 354.6nm, concentration of FITC: 0.45mg/ml. C: FITC-PEG-*b*-Chol, particle size: 187.9nm, concentration of FITC: 0.45mg/ml. D: Control: 0.9% Saline injection. There were more FITC-positive cells in the rats administered with nanoparticles with lower diameter (<200nm, A) than those with high diameter (>300nm, B). Also, TAT peptide group (A and B) can help more particles enter the brain contrast to those without this group (C). (Scale bar: 200µm)

4. Further *in vivo* investigation of TAT-PEG-*b*-Chol

4.1 Identification of cell types of nanoparticle positive cells in Brain parenchyma

The current results have shown that FITC and/or QDs encapsulated TAT-PEG-*b*-Chol nanoparticles could penetrate the BBB and intake by brain tissue. Here, the micelles positive cell types were further identified. The anti-CD11b for microglia (Figure 3.11 A, B and C), anti-NG2 for NG2 cells (D, E and F) and anti-GFAP for astrocytes (G, H and I) were applied to the brain sections from FITC-TAT-PEG-*b*-Chol administered rats respectively. Very few co-localization between nanoparticle

positive cells (green) and stained brain cells (red) was observed, suggesting that cells take up the nanoparticles of FITC-TAT-PEG-*b*-Chol (white arrows pointing in A, D and G) were not microglia (white arrows pointing in B), NG2 cells (E) and astrocytes (H). The results of Figure 3.11 indicated that these three kinds of brain cells seldom uptake FITC-TAT-PEG-*b*-Chol when these nanoparticles reach the brain parenchyma.

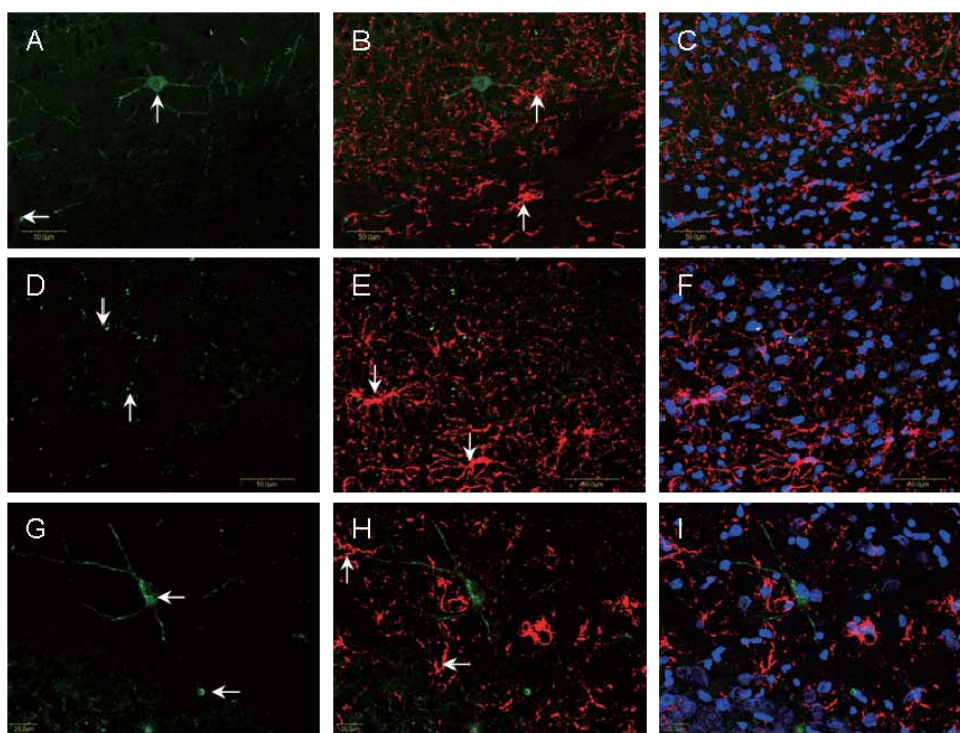


*Figure 3.11: Cell type identification. Double labeling of FITC-TAT-PEG-*b*-Chol nanoparticles (A, D and G, green) and anti-CD11b (for microglia, B and C, red), anti-NG2 (for NG2 cells, E and F, red), anti-GFAP (astrocytes, H and I, red) in the brain section of the rat. Hardly any CD11b, GFAP or NG2 positive cells (arrows pointing cells in B, E, and H) are co-labeled with FITC (arrows pointing cells in A, D, and G) in respective immunohistochemical staining. It suggests that microglia, NG2 cells and astrocytes seldom absorbed the FITC-TAT-PEG-*b*-Chol when these nanoparticles reached the brain parenchyma. (Blue: stained nuclei with DAPI, Scale bar: 50 μ m)*

Figure 3.12 shows the dual labeling results of anti-MAP2 antibody (marker for neurons) and FITC-TAT-PEG-*b*-Chol positive cells. In the brain cortex area (A, B and C) and hippocampus area (E, F and G), the nanoparticle positive cells (A and E,

green) were co-localized with the neuronal cells (B, C and F, G, red). It suggests that FITC-TAT-PEG-*b*-Chol were mainly taken up by neurons.

As TAT transduction domain came from HIV transactivator of transcription protein and was non-cell-specific (Schwarze et al., 1999), theoretically, the TAT conjugated nanoparticles can be taken up by all types of cells in the brain. However, the current results showed that most nanoparticles showed that most nanoparticles in the brain parenchyma were distributed in neuronal cells. The reason for this selective distribution is still unknown. It may be because the intake of micelles is competitive and neurons possess the most suitable membrane receptor which can well recognize TAT peptide and induce the AMT/RMT.

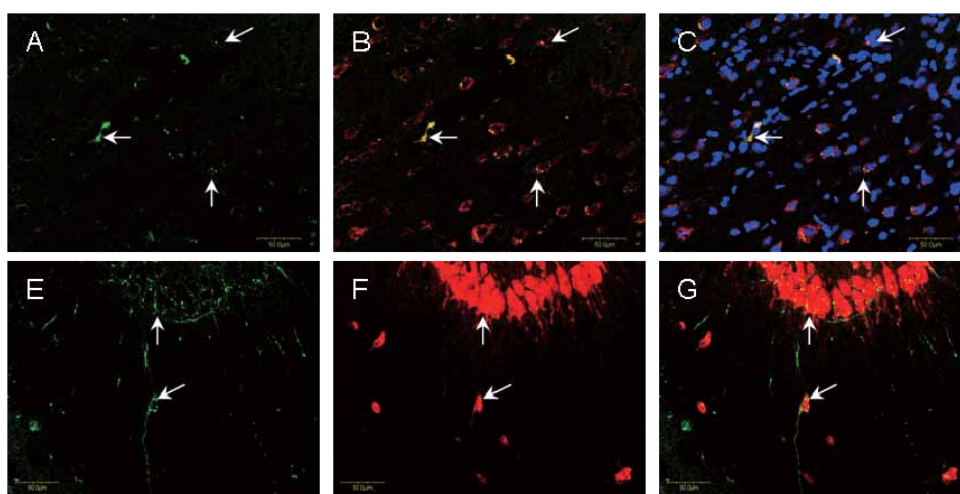


*Figure 3.12: Double labeling of FITC-TAT-PEG-*b*-Chol nanoparticles (A and E, green) and MAP2 positive neuronal cells (B, C and F, G, red) in the cortex (A-C) and hippocampus (E-G) of brain sections from 10 weeks old SD rat. Some cells with the FITC fluorescent positive (arrows in A and E) are double labeled with the MAP2 (arrows in B and F), suggesting that intravenous injected TAT-PEG-*b*-Chol were mainly taken up by neurons. (Blue: stained nuclei with DAPI, Scale bar: 50 μ m)*

4.2 The cellular uptake of TAT-PEG-*b*-Chol by neurons

As mentioned before, TAT-PEG-*b*-Chol nanoparticles could be taken up by neuronal cells concentrated in the area of cerebral cortex and hippocampus. Figure

3.13 shows the detailed distribution of FITC-TAT-PEG-*b*-Chol in these two areas. The positive green cells in A, B and E were located in hippocampus area and those in C and D were located in cerebral cortex area (white arrows pointing cells). In hippocampus (A, B and E), neurons that uptake FITC-TAT-PEG-*b*-Chol have longer processes than those in cerebral cortex. These cells might be internal neurons located in the hippocampus area. However, in cerebral cortex area, these cells may be cortical neurons. Figure 3.13 also demonstrated that these FITC encapsulated nanoparticles only distributed in cytoplasm of neurons but not nuclei. This result is also in agreement with results in the Figure 3.10.

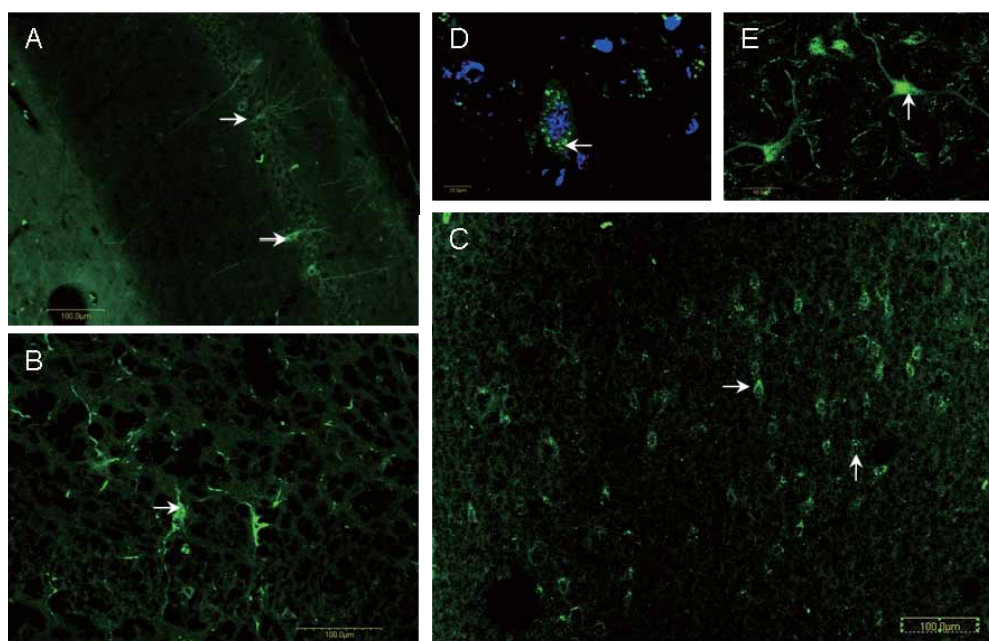


*Figure 3.13: The uptake of FITC-TAT-PEG-*b*-Chol in hippocampus area (A, B and E) and cerebral cortex area (C and D). Those neurons which absorbed the FITC-TAT-PEG-*b*-Chol in brain hippocampus have longer processes than those neurons in cerebral cortex, suggesting they are different type of neurons. (Scale bar: A, B and C 100 μ m; D 1 μ m; E 50 μ m. Blue: stained nuclei).*

Similar results were acquired when QDs-TAT-PEG-*b*-Chol penetrated the BBB and reached the brain parenchyma. Figure 3.14 shows the QDs-TAT-PEG-*b*-Chol

nanoparticle positive neurons in the same two areas. These nanoparticles also distributed mainly in hippocampus area (A, B) and cerebral cortex (C, D). Both neurons with long process (A and B in hippocampus) and those without processes (C and D in cortex) could absorb these nanoparticles. In addition, in the area between the hippocampus and cerebral cortex (Figure 3.14, E), both these two kinds of neurons were found.

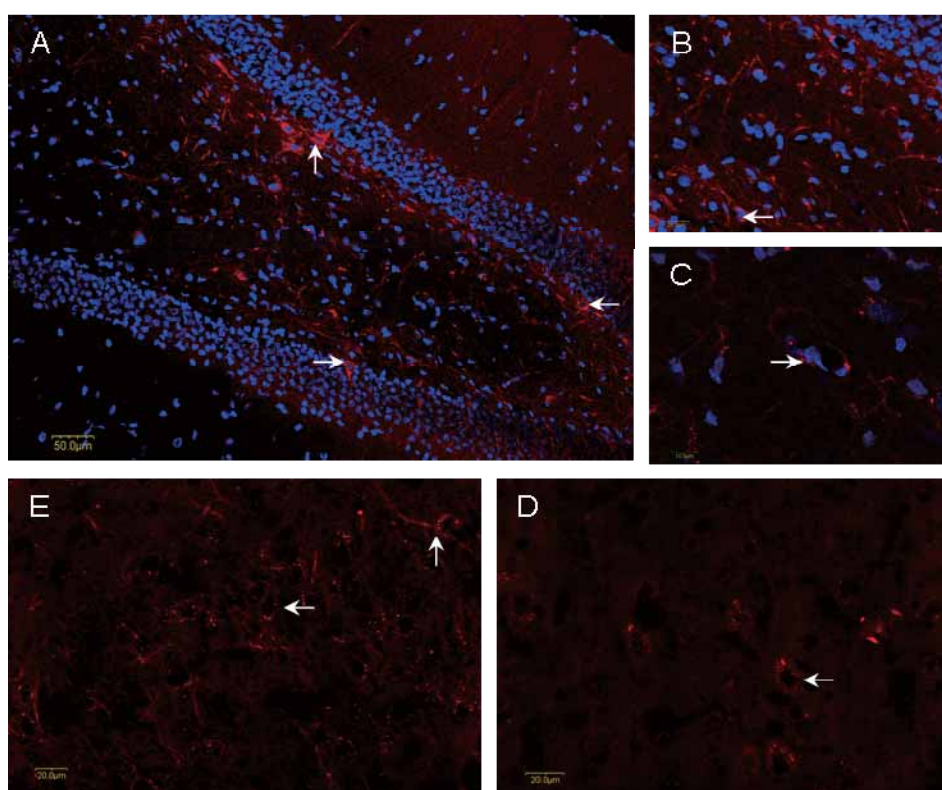


Figure 3.14: The distribution of QDs-TAT-PEG-b-Chol positive neurons in hippocampus (A and B) and cerebral cortex areas (C and D). In the area between hippocampus and cerebral cortex (E), two types of neuron that could absorb nanoparticles were found. (Scale bar: A 50 μ m; B, D and E 20 μ m; C 10 μ m. Blue: stained nuclei).

4.3 Primary *in vivo* kinetics of the BBB penetration of nanoparticles

In the study of BBB penetration of nanoparticles, the brain samples were generally collected 4 hours after intravenous injection. Because the previous *in vitro* staining experiments (data not shown) showed that the absorbance of fluorescent

particles reaches the highest point after 4 hour incubation. However, Schwarze believed that particles with TAT group can rapidly enter the brain shortly within 30 minutes (Schwarze et al., 1999). In order to clarify the dynamic BBB penetration of TAT-PEG-*b*-Chol, the rat brain samples were respectively collected at different time points (5, 15, and 30 minutes) after intravenous injection of these FITC encapsulated nanoparticles. Figure 3.15 shows the results of penetration of these three time points. 5 minutes after injection, the nanoparticles had already entered the blood stream, but they only existed in the blood and perhaps were absorbed by the endothelial cells of the blood vessels (Figure 3.15, A, B). It suggests that the FITC-TAT-PEG-*b*-Chol had not yet penetrated the BBB 5 minutes after they enter the body.

However, from 15 minutes, the positive cells with green dots were already found both inside (write arrow points) and outside the blood vessel (yellow arrow points) (green in Figure 3.15, C and D). It indicated that the BBB penetration of FITC-TAT-PEG-*b*-Chol began between 5 and 15 minutes after they were injected into the blood stream. 30 minutes later since injection (Figure 3.15 E and F), the nanoparticles also existed both inside the blood vessel and in the brain parenchyma. It might because the process of penetration was slowly and stable course that could last 30 minutes or more.

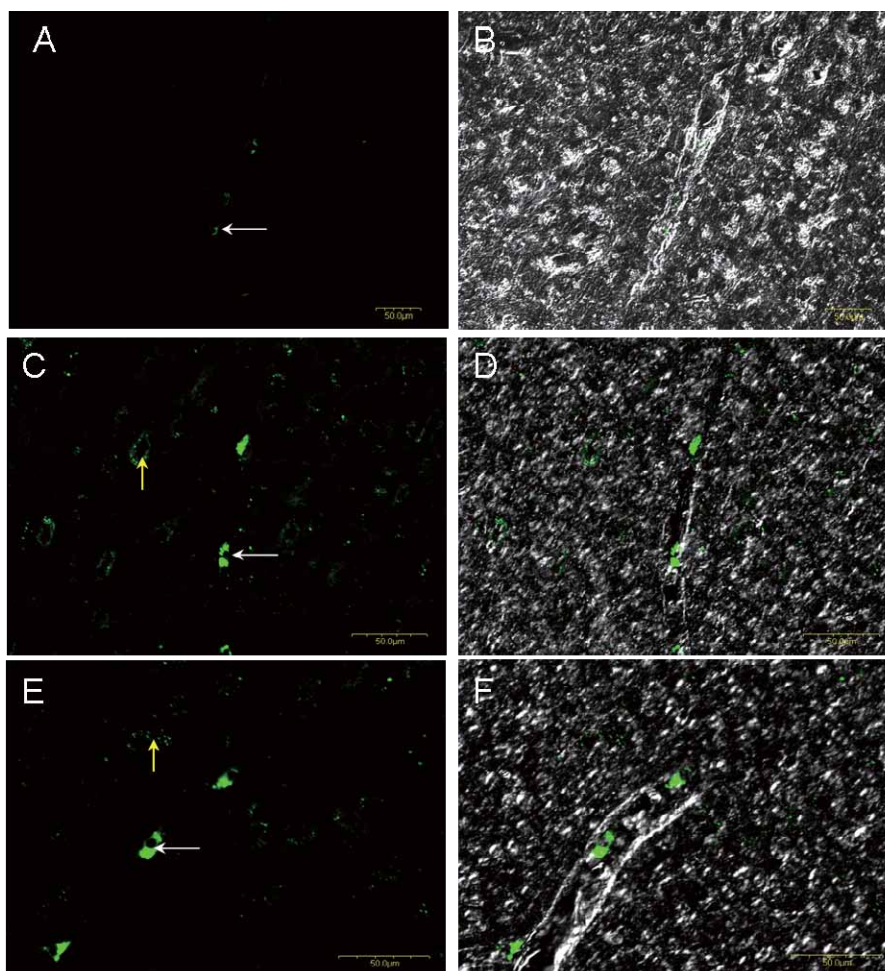


*Figure 3.15: Primary in vivo kinetics of nanoparticle penetration through the BBB. The white arrows pointing cells are endothelial cells which taken the nanoparticles of FITC-TAT-PEG-*b*-Chol in the blood vessels. The yellow arrows pointing cells are neuronal cells in brain parenchyma which absorb the nanoparticles. The results indicated that BBB penetration of FITC-TAT-PEG-*b*-Chol began between 5 and 15 minutes after they entered the blood stream. (Scale bar: 50 μ m)*

As Figure 3.16 shown, the QDs encapsulated TAT-PEG-*b*-Chol also was firstly found outside the blood vessel around 10-15 minutes after they entered the rat body. Just as FITC-TAT-PEG-*b*-Chol, QDs-TAT-PEG-*b*-Chol also began to penetrate the BBB at the time point of 10-15 minutes. Here, FITC conjugated Lectin protein staining results clearly displayed that QDs-TAT-PEG-*b*-Chol dots (red) were completely constrained inside the blood vessels at 5-minute time point (Figure A and B). However, 15 minutes and 30 minutes later, many nanoparticles could be seen both

inside and outside the blood vessels. They may be respectively taken by endothelial cells inside the blood vessel (Figure C, D, E and F, white arrows pointing cells) and cortical neurons in the brain parenchyma (Figure 3.16 C, D, E and F, yellow arrows pointing cells). These results also proved that the designed nanoparticles (TAT-PEG-*b*-Chol) can cross the BBB shortly within 15 minutes since their entry into the body.

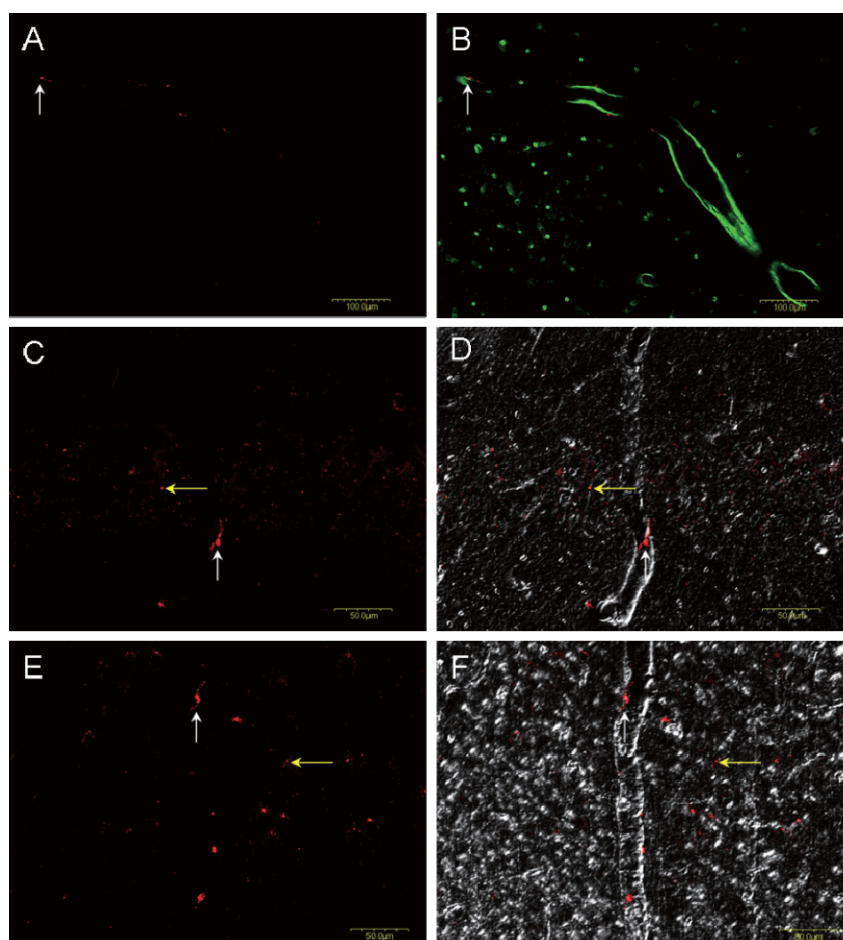


Figure 3.16: The BBB penetration of QDs-TAT-PEG-*b*-Chol in 5 minutes (A, B), 15 minutes (C, D) and 30 minutes (E, F) after intravenous injection. The QDs encapsulated nanoparticles (red in A, C, and E) were only seen inside the blood vessel (green in B and D) in 5 minutes. However, they could be seen both in the blood vessel and brain parenchyma 15 minutes later. (Scale bar: A and B: 100 μm, C, D, E and F: 50 μm)

5. *In vitro* characterization of nanoparticle micelles

5.1 Uptake of nanoparticles in cultured cells

The brain capillary endothelial cells and astrocytes are main components of the BBB. Therefore, they are widely used in some *in vitro* studies related to the BBB. Here, cultured endothelial cells and astrocytes were used to investigate *in vitro* cellular intake of TAT-PEG-*b*-Chol and PEG-*b*-Chol. As shown in Figure 3.17, in cultured endothelial cells (Figure 3.17 A and C) and astrocytes (B and D), both nanoparticles with (C and D) and without TAT peptide (A and B) could enter the cells after 1 hour incubation. However, the uptake of the nanoparticles with TAT peptide was higher as the fluorescent intensity of the cells incubated with FITC-TAT-PEG-*b*-Chol (C and D) was much stronger compared to that of the cells incubated with FITC-PEG-*b*-Chol (A and B). It suggests that many more nanoparticles with TAT group could attach to the surface of cells or enter the cells. It might be because the presence of TAT cell penetrating peptide on the surfaces of the nanoparticles promoted their cellular uptake by endothelial cells and astrocytes. This finding is also in accordant with those results *in vivo*, suggesting TAT peptide could facilitate penetration of nanoparticles through the BBB.

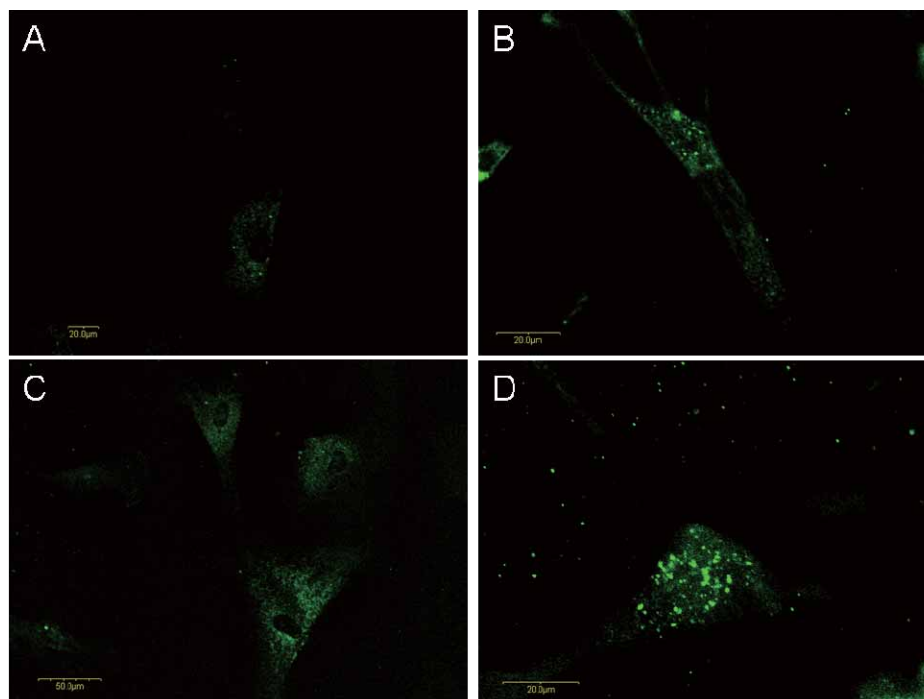


Figure 3.17: Uptake of FITC-TAT-PEG-*b*-Chol and FITC-PEG-*b*-Chol by cultured endothelial cells (A, C) and astrocytes (B, D). Although both nanoparticles without (A, B) and with (C, D) TAT peptide group could enter cultured cells, those cells administrated with TAT group emitted a relatively stronger fluorescence (C, D). It suggests that many more nanoparticles with TAT group (FITC-TAT-PEG-*b*-Chol) could attach to the surface of cells or enter the cells than FITC-PEG-*b*-Chol. (Scale bar: A, B, D 20 μm , C 50 μm)

5.2 The cytotoxicity of nanoparticle micelles

An ideal nanoparticle drug carrier should hardly have toxicity to body and cells. In current *in vivo* study, no rat died during the experiment, suggesting that TAT-PEG-*b*-Chol was not fetal to those animals. In Figure 3.18 A and B, *in vitro* cytotoxicity of QDs loaded TAT-PEG-*b*-Chol was investigated with cultured endothelial cells and astrocytes. Pure QDs solution administration was selected as control group. Here, QDs-TAT-PEG-*b*-Chol (0.0375mg/ml) and pure QDs (0.0375 mg/ml) were added into cultured endothelial cells and astrocytes (2.2×10^5 cells/well) respectively. 12 hours later, the cell number and viability of endothelial cells (A)

hardly changed, suggesting that QDs-TAT-PEG-*b*-Chol was not toxic to endothelial cells. However, significant decreases in cell number and viability have been observed in astrocytes (B). But the decrease of cell number and viability might be due to cytotoxicity came from pure fluorescent QDs (Hoshino et al., 2007). Its toxicity may be caused by released cadmium and selenium, two of the most widely used constituent metal in the QDs core crystal (Lovric et al., 2005). Indeed, when the administration of FITC-TAT-PEG-*b*-Chol particles was applied, no change of cell number and viability was detected for both endothelial cells and astrocytes (Figure 10 C, D). This result suggested that, at the same time fame, TAT-PEG-*b*-Chol nanoparticle was not toxic *in vitro*.

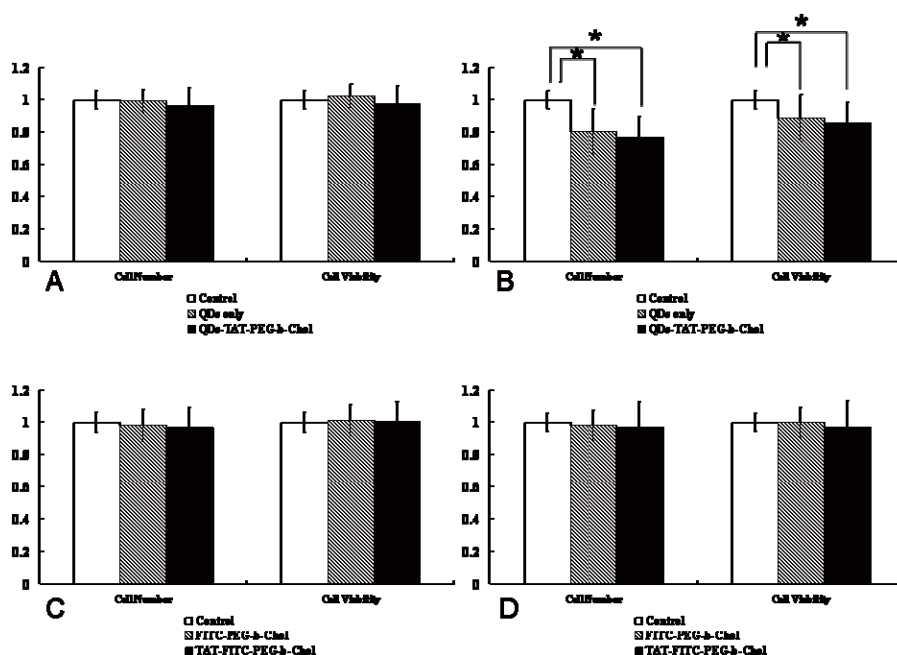


Figure 3.18: The cytotoxicity investigation of QDs-TAT-PEG-*b*-Chol (A,B) and FITC-TAT-PEG-*b*-Chol (C,D) in cultured endothelial cells (A,C) and astrocytes (B,D). The cell number and cell viabilities hardly changed after the treatment of these nanoparticles. It means that the nanoparticle of TAT-PEG-*b*-Chol has no cytotoxicity to cultured brain endothelial cells and astrocytes. (* $P < 0.05$)

6. Synthesis and characterization of TAT-Penicillin G

Hydrophilic antibiotics, Penicillin G potassium can not be encapsulated into the core of PEG-*b*-Chol. As Penicillin G has –COOH group and TAT peptide has –NH₂ group, therefore, using EDC/NHS chemistry, it is feasible to directly connect Penicillin G molecules to TAT peptide to form TAT-Penicillin G. With the aid of TAT cell penetrating peptide, this complex was supposed to cross the BBB and reach the brain parenchyma.

6.1 ¹H-NMR spectrum of TAT-Penicillin G potassium

Figure 3.19 showed the ¹H-NMR spectra of TAT peptide, Penicillin G potassium and TAT-Penicillin G potassium. In the ¹H-NMR spectra displayed, TAT-Penicillin G molecules presented characteristic peaks from both TAT and Penicillin G. In the spectra of TAT-Penicillin G, signal a, b, c and d came from TAT peptide. The weak and broad peak at δ 4.0-4.2 (signal c) can be attributed to the protons of –NH-CH(CH₂)-CO- in TAT. The peaks at δ 2.52-2.58 (signal d) might be derived from the protons of -CH₂-NH-NH-NH₂ in arginine. The peaks at δ 6.60-6.66 (signal b) and at δ 6.95-7.0 (signal a) could be attributed to the protons from the benzene ring in tyrosine. However, the peaks at δ 5.30-5.41 (signal e) came from Penicillin G; it might be derived from –CO-NH- in Penicillin G potassium. The result suggests that the synthesis of TAT-Penicillin G was successful.

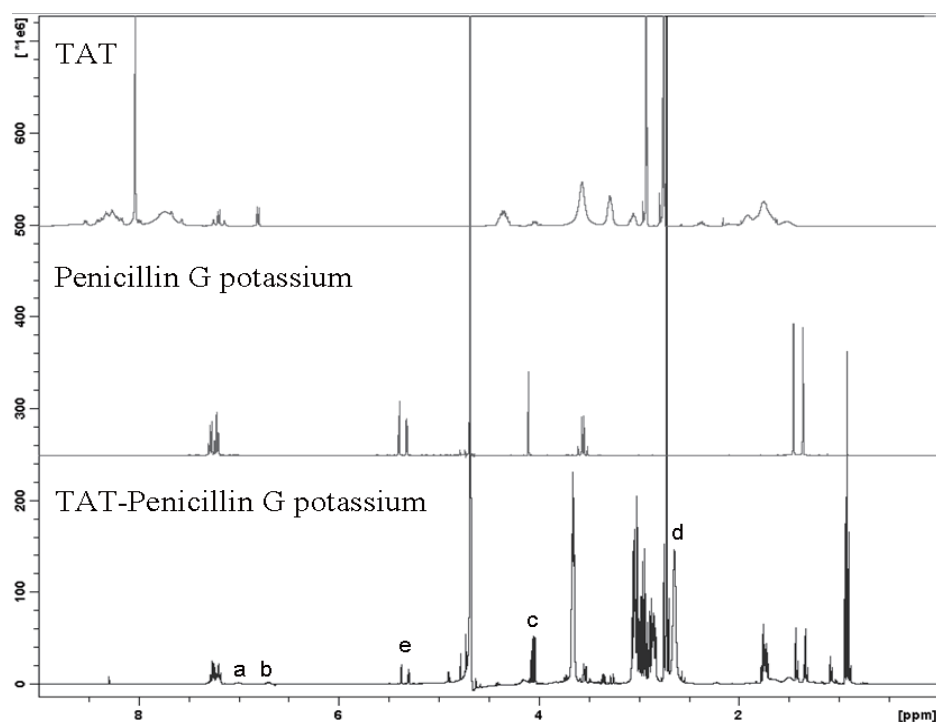


Figure 3.19: ^1H NMR spectra of TAT peptide, Penicillin G potassium and TAT-Penicillin G potassium. TAT-Penicillin G molecules presented characteristic peaks from both TAT and Penicillin G. It proved that the synthesis was successful.

6.2 Determination of molecular weight of TAT-Penicillin G

The molecular weight of TAT-Penicillin G potassium was determined using MALDI-TOF mass spectrometry. The MALDI-TOF mass spectrum of TAT peptide was used as a control to estimate the results obtained for TAT-Penicillin G potassium conjugate. The molecular weight of TAT peptide is 1560, after conjugation of Penicillin G, the molecular weight of TAT-Penicillin G potassium should be around 1875. Figure 3.20 shows the MALDI-TOF spectrum of TAT-Penicillin G (Figure 3.20 A) and TAT (B). A narrow distribution from 1850 to 1888m/z was found in the mass spectrum of TAT-Penicillin G, The existence of those peaks not only suggested the conjugation of TAT to Penicillin G was successful but also verified the ratio of TAT and Penicillin G was 1:1.

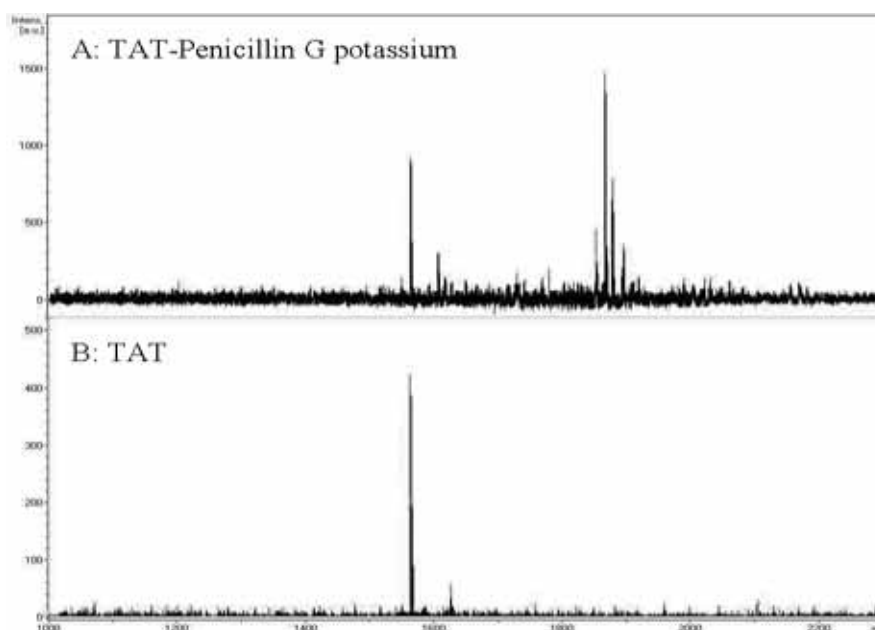


Figure 3.20: The MALDI-TOF spectrum of TAT-Penicillin G (A) and TAT (B). The peaks around 1560 (A and B) represent the TAT molecules, particularly in B. It may be attributed to some un-reacted TAT molecules. Peaks around 1875 represent TAT-Penicillin G.

6.3 The cytotoxicity of TAT-Penicillin G potassium

Figure 3.21 shows the results of cytotoxicity investigation of TAT-Penicillin G potassium to 4 types of brain cell lines: neuron (A, NSC-34); microglia (B, BV2); astrocytes (C) and endothelial cells (D). It was obvious that after microglia, astrocytes and endothelial cells were treated by TAT-Penicillin G, their numbers and cell viabilities had hardly changed (B, C, and D) It suggested that TAT-Penicillin G was not toxic to those cell types. However, the number of neuronal cells (A) decreased to some extent contrast to that of control group after the administration of TAT-Penicillin G, although their cell viability remained as high as those controlled cells. Because when neurons were treated by pure Penicillin G, their number nearly remained unchanged. Therefore, it was not Penicillin G that resulted in the cell number decrease. As it was reported that the HIV-1 TAT protein is neurotoxic to the

cultured rat midbrain fetal neurons (Aksenova et al., 2006), it was believed that it was free TAT peptide that lead to the decrement. The free TAT may come from the tiny amount of unreact TAT peptide that were not removed by the method of membrane dialysis. Here, no direct evidence proved whether TAT-Penicillin G was toxic to cultured neurons. Further investigation is required to clarify this issue or TAT fragment might be modified to reduce its toxicity.

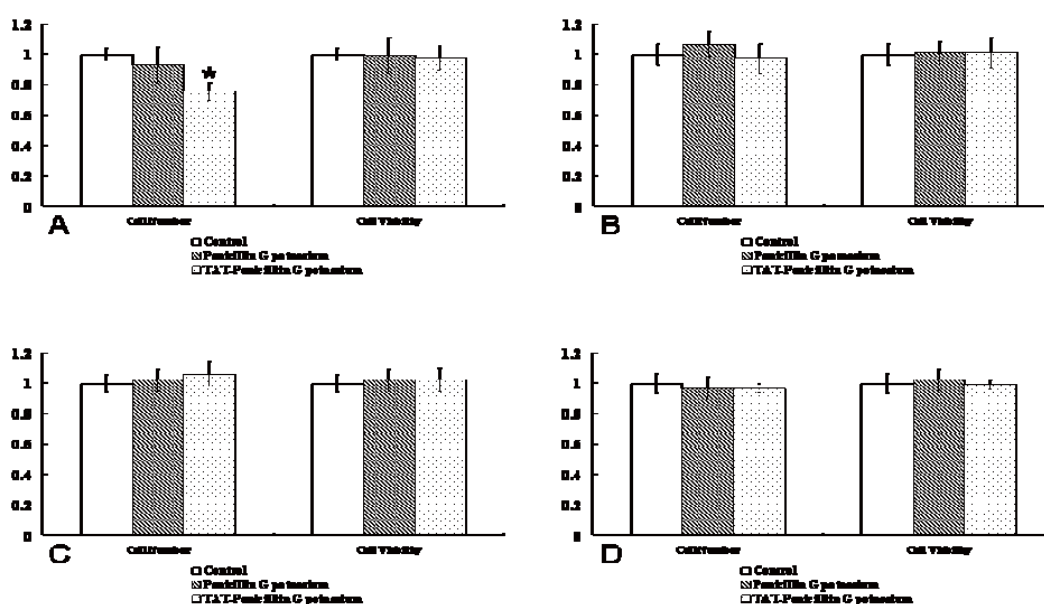


Figure 3.21: Cytotoxicity investigation of TAT-Penicillin G potassium in neuron (A, NSC 34); microglia (B, BV2); astrocytes (C) and endothelial cells (D). The concentration of Penicillin G and TAT-Penicillin G (counted with Penicillin G) used are $500\mu\text{g}/\mu\text{l}$. (* $P < 0.05$)

7. Application of TAT-Penicillin G

7.1 Antibacterial efficacy test of TAT-Penicillin G

B. subtilis and *C. albicans* were used in the antibacterial efficacy test of TAT-Penicillin G. The concentration of microorganism was determined using the method of broth microdilution. Here, the OD value at 600 nm was measured at

different time points after the treatment of TAT-Penicillin G. Those values which come from the treatment of pure Penicillin G were set as the control.

Figure 3.22 respectively shows the anti-*B. subtilius* (A) and anti-*C. albicans* (B) efficacy test of TAT-Penicillin G at 0, 2, 4, 6 and 13 hours after the administration. In this experiment, *B. subtilius* or *C. albicans* treated with 1.4ppm and 2.7ppm TAT-Penicillin G were used as experimental groups and those microorganisms without any treatment were used as control. In A, at the beginning, OD values of all groups were 0.1. Two hours later, the OD value of all three groups began to increase, but the control group increased faster than other two groups, suggesting that 2.7ppm TAT-Penicillin G could prevent the growth of *B. subtilius* more effectively than other two groups. At the time points of 4, 6 and 13 hours, the OD values of 1.4ppm TAT-Penicillin G group, 2.7ppm TAT-Penicillin G group and non-treatment group continued increasing, however, those of non-treatment group increased fastest, next the 1.4 ppm TAT-Penicillin G group and the last 2.7ppm TAT-Penicillin G group. It is obvious that the sequence of anti-*B. subtilius* efficacy was 2.7ppm TAT-Penicillin G > 1.4ppm TAT-Penicillin G > non-treatment control group. It suggests that just as pure antibiotics, TAT conjugated Penicillin G as well has the ability to inhibit the growth of some infectious microorganisms.

When *C. albicans* was administrated with TAT-Penicillin G, till 13 hours after the treatment, the OD value of three groups increased sharply. Similar as before, the values of two TAT-Penicillin G treated group were smaller than non-treatment control group. However, nearly no difference was observed in anti-*C. albicans* efficacy of

2.7ppm and 1.4ppm TAT-Penicillin G group. It is because that the minimum inhibition concentration (MIC) of TAT-Penicillin G to *C albicans* was much smaller than 1.4ppm. These two groups can obtain almost same inhibition efficiency to *C albicans*. Overall, as well as pure Penicillin G, the TAT-Penicillin G also has the ability to inhibit the growth of some infectious microorganisms.

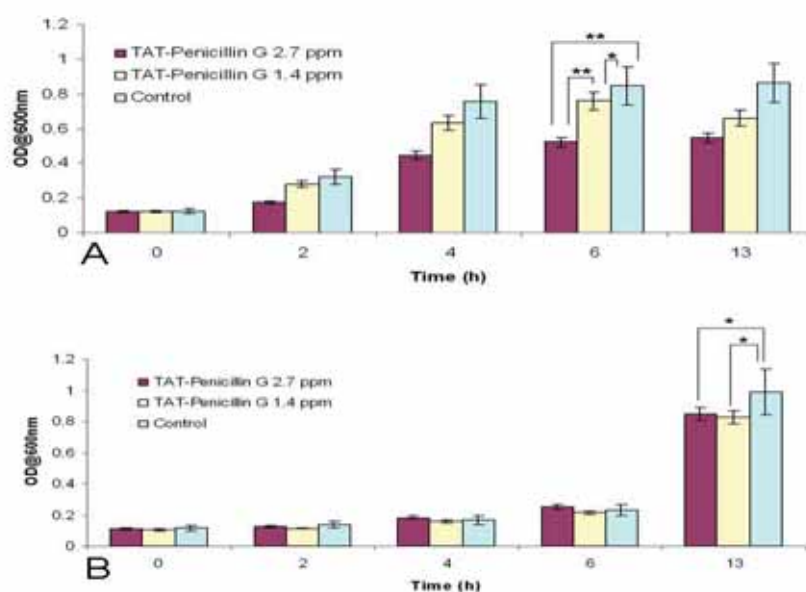


Figure 3.23: The anti-*B subtilius* (A) and anti-*C albicans* (B) efficacy test of TAT-Penicillin G. 2.7ppm of TAT-Penicillin G has higher inhibition efficiency to *B subtilius* than 1.4 ppm of TAT-Penicillin G and non-treatment control group. But for *C albicans*, although those two groups of TAT-Penicillin G both obtained good anti-*C albicans* efficacy than non-treatment control group, they two had no difference. (* $P < 0.05$, ** $P < 0.01$)

7.2 In vitro uptake of TAT-Penicillin G

Figure 3.24 shows the cellular uptake of TAT-Penicillin G and pure Penicillin G in cultured brain capillary endothelial cells. In this study, TAT-Penicillin G and pure Penicillin G solution with same concentrations were added into BCEC seeded 6-well plates (2.2×10^5 cell/well). The initial concentrations of drugs in the culture medium

were set as 100%. At different time intervals (0, 20, 40, 60, 80, 100, 240 and 720 minutes), 100µl medium was collected respectively and analyzed by HPLC. The percentage of absorption by endothelial cells was indirectly calculated from the difference between drugs concentrations remained in collected medium samples and the initial concentration added.

For 1.40ppm (Figure 3.24 A red line) and 2.7ppm (Figure 3.24 B blue line) pure Penicillin G groups, the concentrations of Penicillin G has little change within the first 4 hours when they were added. It may be because that Penicillin G was nearly not taken up by endothelial cells in this period. Until 12 hours after the administration, only about 4% (1.4ppm) and/or 6% (2.7ppm) were endocytosed into the cell or attached to the cell membrane.

However, when these cells were administrated with TAT-Penicillin G (black lines in A and B), the drug concentration in the culture medium began to decrease early in 1 hour after the add-in. 12 hours later, there was only around 85% of TAT-Penicillin G remained in the medium. It suggests that already about 13% (1.4 ppm group) and/or 17% (2.7ppm group) of added drugs may be endocytosed into the cell or attached to the cell membrane. Using cultured astrocytes, similar results were obtained. It was obvious that many more TAT-Penicillin G molecules were taken up by endothelial cells or astrocytes than pure Penicillin G. It may be because TAT peptide helps TAT-Penicillin G to enter the cell body easily or be attached to the cell membrane. The result suggests that the conjugation of TAT may enhance the ability of Penicillin G to penetrate membrane of brain cells.

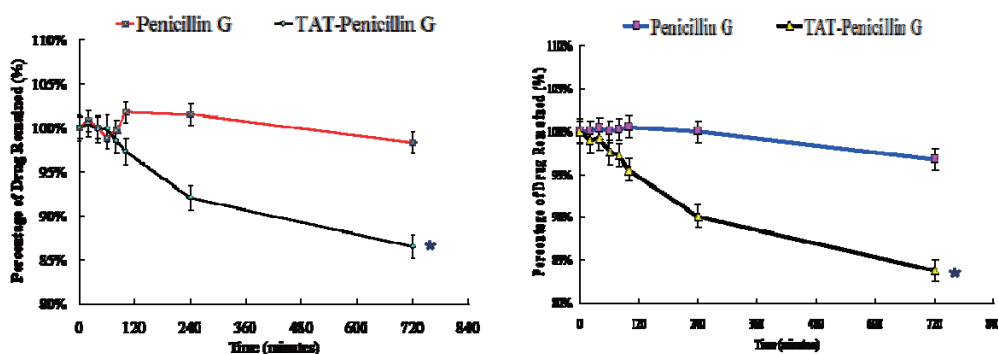


Figure 3.24: *In vitro* uptake of TAT-Penicillin G and pure Penicillin G. 12 hours after the treatment with TAT-Penicillin G or pure Penicillin G respectively, much more TAT-Penicillin G was taken than pure Penicillin G. It suggests that this TAT compound can facilitate Penicillin G to penetrate brain cells which are main components of the BBB.

8. Pharmacokinetics investigation of selected antibiotics

8.1 HPLC spectra of Penicillin G, Ciprofloxacin and Doxycycline

Figure 3.25 are the HPLC spectrums of two selected antibiotics: Penicillin G (A) and Ciprofloxacin (B). When scanning Penicillin G with UV from 210nm to 400nm, its highest UV absorbance was at 229nm. Therefore, the detective wavelength of Penicillin G was set as 229nm. When analyzed by SymmetryShield™ Cartridge Column RP18 column, the peak of Penicillin G came out in 8.5 minutes (retention time). As Figure 3.26 shown, the retention time of Ciprofloxacin was around 11.1 minutes analyzed by Atlantis dC18 column and detected at a wavelength of 280nm.

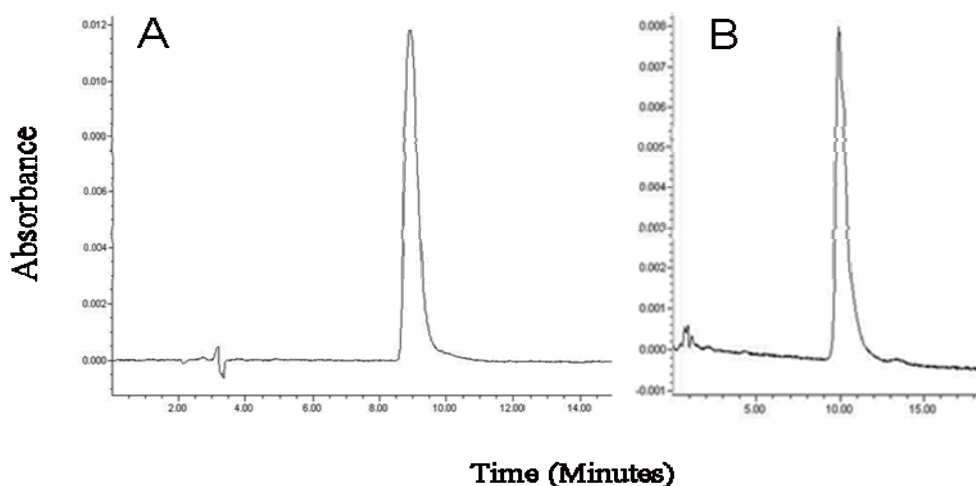


Figure 3.25: HPLC spectra of Penicillin G (A) and Ciprofloxacin (B). Their retention time and detective wavelength were 8.5 minutes (at 229nm) and 11.1 minutes (at 280nm) respectively.

8.2 Within and between day assay validation (n=5)

Table 2 shows the results of within- and between-day assay validation of selected antibiotics. The object of this validation is to validate the feasibility of antibiotics analytical methods. Coefficients of variation (CV) and Accuracy are two important parameters to evaluate the feasibility. Here, CV (%) was defined as the ratio between SD and Mean value ($CV = SD/Mean \times 100\%$). For a good analytical method, the value of CV must be lower than 10%. The accuracy was defined as the ratio between mean of the drug concentration measured and initial standard drug concentration added ($Accuracy = Mean/Standard \times 100\%$). The value of accuracy must fall into the zone between 95% and 105% for a proper analytical method.

As the validation results shown, the values of CV and accuracy of the four added concentration almost met the requirements. It suggests that the established analytical methods for Penicillin G and Ciprofloxacin are feasible and can be used for the pharmacokinetics research of these antibiotics.

Table 2: Validation of the selected antibiotics

Added concentration (µg/ml)	Measured concentration (µg/ml)				
	Within-day		Between-day		Accuracy (%)
	Mean ± SD	CV (%)	Mean ± SD	CV (%)	
<i>Penicillin G</i>					
1.0	1.0 ± 0.08	8.0	1.1 ± 0.09	8.2	100, 110
5.0	5.0 ± 0.07	1.4	5.1 ± 0.20	3.9	100, 102
10.0	10.1 ± 0.17	1.7	10.0 ± 0.16	1.6	101, 100
50.0	49.8 ± 0.36	0.7	49.7 ± 0.44	0.9	99.6, 99.4
<i>Ciprofloxacin</i>					
0.5	0.54 ± 0.05	9.3	0.56 ± 0.05	8.9	108, 112
1.0	1.10 ± 0.07	6.4	1.02 ± 0.08	7.8	110, 102
5.0	4.80 ± 0.10	2.1	4.80 ± 0.19	4.0	96, 96
10.0	10.1 ± 0.07	0.7	10.1 ± 0.13	1.3	101, 101

Note: Within and between day assay validation (n=5) of Penicillin G and Ciprofloxacin. The values of CV and Accuracy suggest the analytical methods are feasible.

8.3 Inter-Assay precision for the analysis of Penicillin G in rat plasma

Before *in vivo* investigation of pharmacokinetics of Penicillin G, the methods of Penicillin G extraction from rat plasma and analysis by HPLC should be established. Also, the inter-Assay Precision for the analysis of Penicillin G in rat plasma should be done. Here, different amounts of pure Penicillin G were added into the fresh rat plasma to form standard solutions. Using extraction method described before, the extracted samples were injected into the HPLC system and analyzed.

Figure 3.26 shows the standard curve of Penicillin G in rat plasma extracted and analyzed by HPLC. It was obvious that this curve displayed a perfect linear relation between the concentration and the peak area.

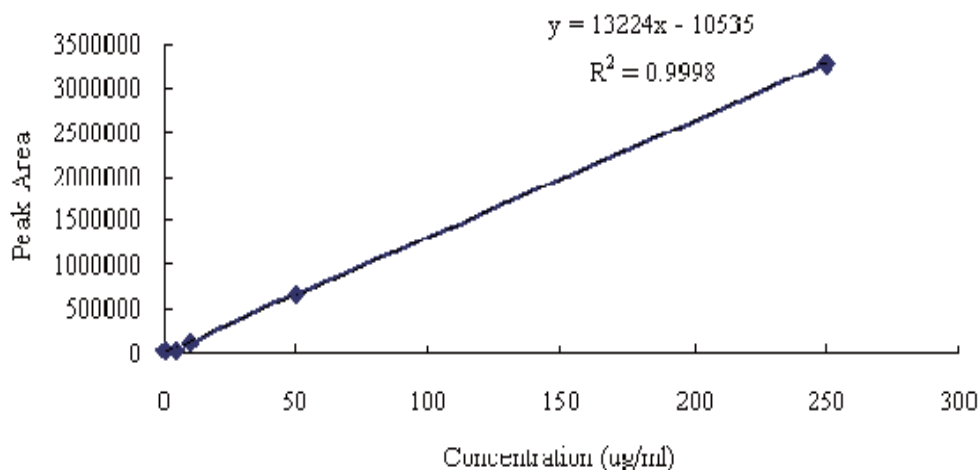


Figure 3.26: Standard curve of Penicillin G analysis in rat plasma. The curve shows a perfect linear relation between the concentration and the peak area.

The table 3 shows the results of inter-Assay Precision for the analysis of Penicillin G in rat plasma. When the concentration of Penicillin G was low in the rat plasma (1.0-5.0µg/ml), the value of CV was higher than 10%. As well, their values of accuracy were not in the zone between 95% and 105%. However, with the increase of Penicillin G concentration in the rat plasma, ideal CV and accuracy values could be acquired. It suggests that when the concentration of sample lies between 10µg/ml and 250µg/ml, the concentration measurement results by HPLC with the current established method are creditable.

Table 3: Inter-Assay Precision for the analysis of Penicillin G in rat plasma

Added concent ration (µg/ml)	Measured concentration in Rat Plasma(n=3, µg/ml)					
	Day 1 (Within-day)			Day 2 (Between-day)		
	Mean ± SD	CV	Accuracy	Mean ± SD	CV	Accuracy
1.0	0.899 ± 0.21	23.1%	89.9%	1.041 ± 0.17	16.3%	104.1%
5.0	5.292 ± 0.56	10.6%	105.8%	3.869 ± 0.37	9.6%	77.4%
10.0	10.06 ± 0.44	4.3%	100.6%	8.776 ± 0.27	3.1%	87.8%
50.0	52.07 ± 1.83	3.5%	104.1%	49.38 ± 0.89	1.8%	98.8%
250.0	251.25 ± 4.11	1.6%	100.5%	248.35 ± 5.23	2.1%	99.3%

Note: Inter-Assay Precision for the analysis of Penicillin G in rat plasma. The results suggest that when the concentration of sample lies between 10 μ g/ml and 250 μ g/ml, the HPLC measured concentration results with our established method are creditable.

8.4 Pharmacokinetics of selected antibiotics after intravenous injection

Figure 3.27 shows the pharmacokinetics results of Penicillin G (A) and Ciprofloxacin (B) when they were intravenous injected into the rat body through the femoral vein. The dosage of injection was 80 mg/kg body weight. At different time points, the rat plasma samples were collected and analyzed by HPLC. As the figure shown, the concentration of these three antibiotics in the plasma greatly decreased in the first 40 minutes since administration. It may be because that the antibiotics were taken by the some organs such as liver and digested by the cells inside. After 60 minutes, the trend of decrease became smooth, suggesting that the plasma concentration of antibiotics was getting balanced with the concentration in other organs.

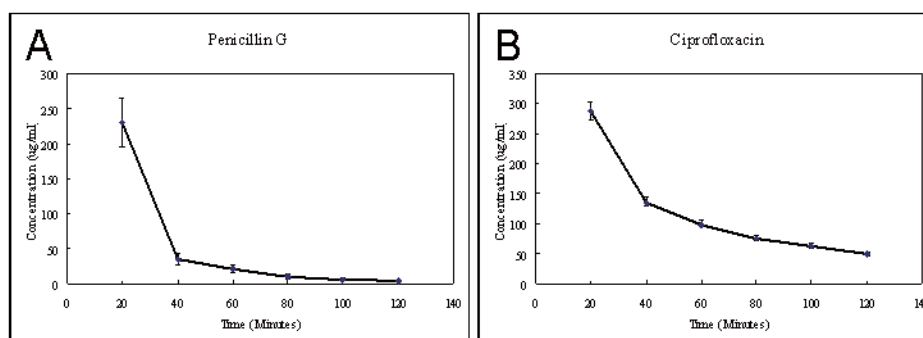


Figure 3.27: Plasma concentration–time curves for Penicillin G (A) and Ciprofloxacin (B) of 80 mg/kg in rat after intravenous injection.

9. Establishment of brain pathological model

Microglia is a brain cell type in the CNS with the capacity of full immunocompetence. Resting microglia has a unique ramified morphology. However, microglia can react to various CNS injury rapidly accompanied with the changing of morphology from ramified to amoeboid microglia. Therefore, the morphology change of microglia may be an obvious symbol to show the status of CNS: normal or pathological. As LPS is a highly proinflammatory molecule that elicits a wide array of responses, including the upregulation of cytokines, adhesion molecules, and tissue factor (Bannerman and Goldblum, 2003), the administration of LPS to the animal brain may certainly result in the brain injury. Also, the administration of LPS can damage the BBB through the action of gelatinase B (Mun-Bryce et al., 2002). Therefore, the intracerebral injection of LPS can be used to establish the brain pathological model and the activation of microglia can serve as a sign of successful establishment. In Figure 3.28, after the focal injection of LPS to the rat brain, it was obvious that the shapes of ramified microglia in non-LPS-administration side (A) had greatly transformed to round amoeboid microglia (B). It suggests that microglia had been activated after the LPS administration. This result demonstrated that the establishment of rat brain pathological model was successful.

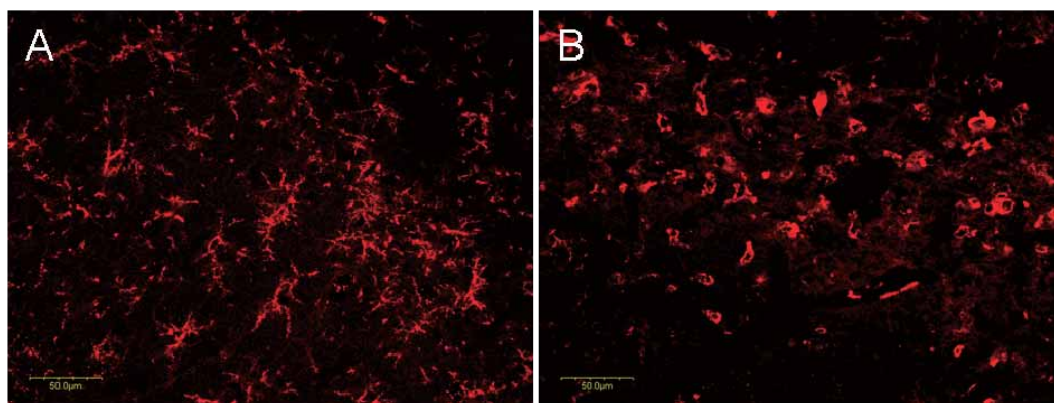


Figure 3.28: Alteration in microglial cells morphology in LPS focal injected pathological brain model. A: Normal side; B: LPS administration side. The shapes of ramified microglial cells in A had greatly changed into round amoeboid microglia in B, suggesting that microglia was activated and the model establishment was successful. (Scale bar: 50.0 μ m)

10. NG2 cell responses in LPS treated pathological brain

10.1 NG2 cell responses

The real function of NG2 cells in the CNS is still unclear now. Some scientists considered the NG2 cells as progenitor cells for oligodendrocytes while others thought that these cells were a specific type of glial cells (Dawson et al., 2000; Politto and Reynolds, 2005). Therefore, it is of great interest to investigate the NG2 cell responses in pathological brain to learn their possible responses and functions. In addition, this investigation may be useful to future drug delivery through BBB to targeted cell type in the brain. Figure 3.29 has shown that in the surrounding region near LPS injection site (B and D), the body size of NG2 cells become enlarged and the upregulation in expression of NG2 molecules was observed, compared with those in normal side (A) as well as saline administration side (C). Meanwhile, the number of the cells seemed increased in contrast to that in normal side and saline injected side. It suggests that, the NG2 expressing cells were responding to the stimulus in the brain

as well as microglial cells. Their morphology greatly changed and their expressions were upregulated. However, the reason is unknown and needs to be elucidated in the future.

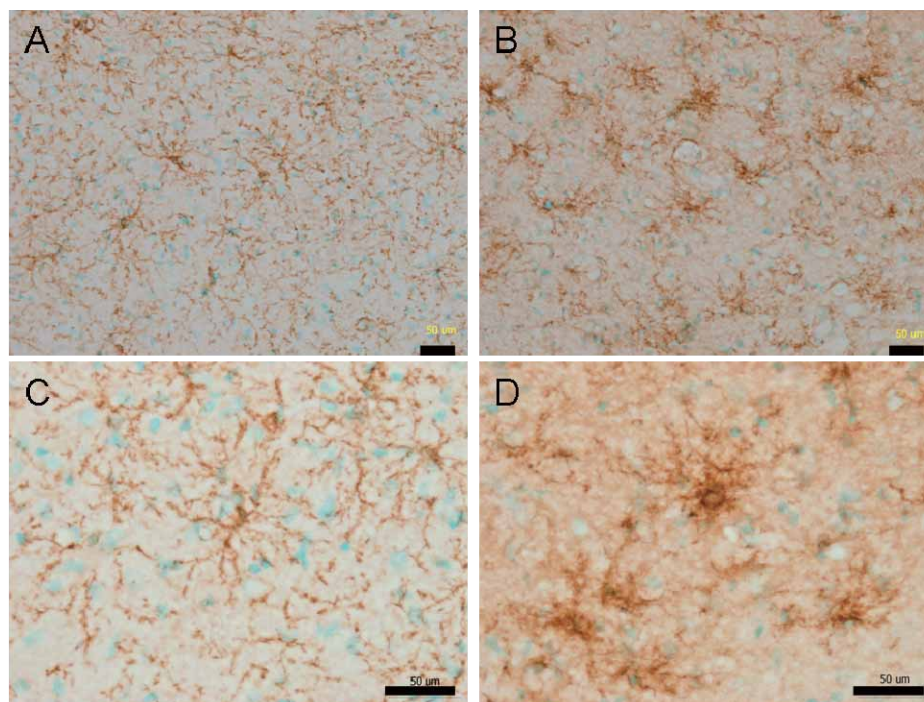


Figure 3.29: The NG2-positive cells, after LPS challenge, increased their sizes of cell body. NG2 positive staining became more intense (B, D) in comparison with those in the normal side (A) and saline injected side (C). The cell number also increased in LPS administration side as obvious increase in the intensity of the NG2 positive cell population. (Scale bar: 50.0 µm Blue: Stained nuclei)

In the further investigation of NG2 cells response to brain injury, the average NG2 cells' numbers in LPS injected area, saline injected area and controlled non-injected area were counted respectively. In Figure 3.30, contrast to the normal side, the cell number in LPS or saline administrated sides both increased around 50%. It means that the injury of injection also resulted in the upregulation of NG2 cells expression. However, after administration of LPS, the number of NG2 cells significantly increased in LPS injected area. LPS administration to the rat brain could promote the increment of NG2 cells number both in LPS injected side and non-

injected side. Overall, this result suggested that in the pathological brain, the focal injection of LPS can activate NG2 positive cells and increase the number of NG2 cells in the surrounding region near LPS injection site

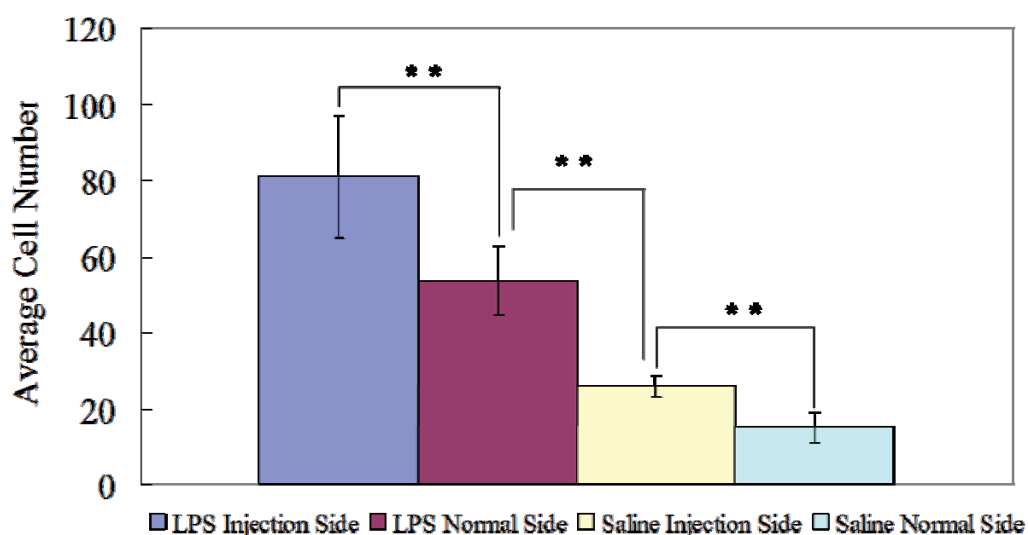


Figure 3.30: Cell number counting of NG2 positive cells in LPS and saline administrated rat brain. As the injury caused by the injection also resulted in an increase in the number of NG2 cells, after administration of LPS, the number of NG2 cells significantly increased in LPS injected area. (Average counting area: 0.357 mm^2 , * $P < 0.01$)

10.2 The activated NG2 cells do not produce some cytokines

Brain cells, such as microglia or astrocytes can secrete cytokines when they are activated under pathological condition in response to brain injury (Lee et al., 1993; Lindsay, 1994). An overwhelming number of animal studies indicated that there were chronic elevation of certain inflammatory cytokines, including $\text{IFN-}\gamma$, $\text{IL-1}\alpha$, $\text{TGF-}\beta$, and $\text{TNF-}\alpha$ by activated microglial cells in the inflammatory area (Lee et al., 1993). As the previous study shows, NG2 cells can be activated in pathological brain. Can these cells also produce some cytokines just as microglial cells? In the current study,

the NG2 cells were double stained with IFN- γ (Figure 3.31 A), IL-1 α (B), TGF- β (C), and TNF- α (D) respectively by immunohistological techniques. As Figure 3.31 shows, there was no any co-localization observed in either LPS administrated side, saline administrated side or non-LPS injected side (not shown) in the brain. However, a significant upregulation in these cytokine expressions could be recorded. The result suggests that, unlike microglia or astrocytes, the activated NG2 cells do not produce the detected cytokines in this LPS focal injected brain.

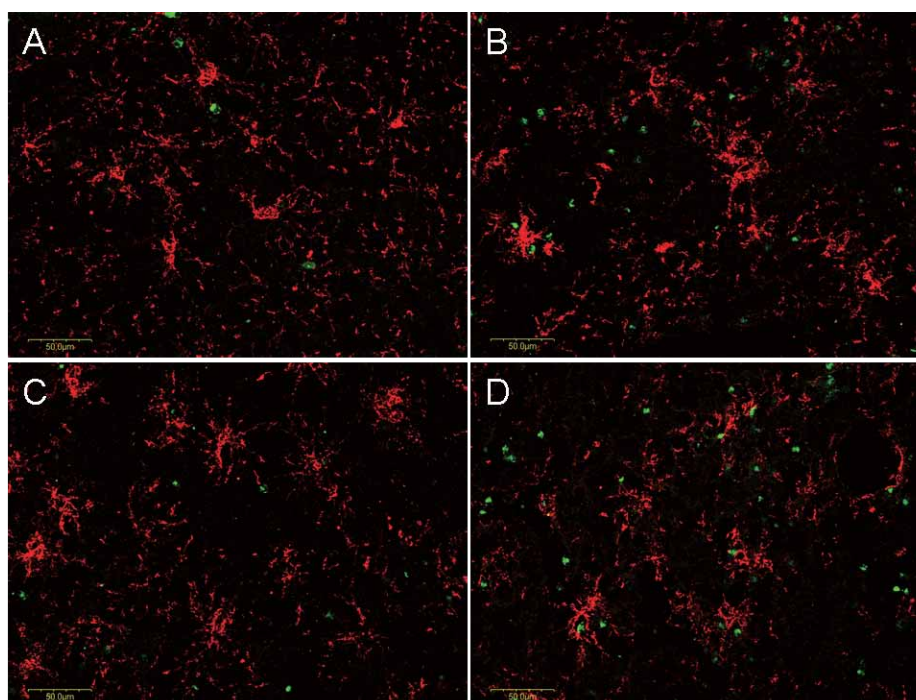


Figure 3.31: Double labeling of NG2 cells and selective cytokines. No colocalization of NG2 positive cells (red) with IFN- γ (green dots in A), IL-1 α (green dots in B), TGF- β (green dots in C) and TNF- α (green dots in D) were detected after LPS administration, suggesting activated NG2 cells did not expression the detected cytokines. (Scale bar: 50.0 μ m)

10.3 Expression of BrdU in NG2 cells after LPS administration

The increment of the number of NG2 cells may be attributed to the cell proliferation in pathological areas both in brain cortex and hippocampus. Here, in order to certify this hypothesis, BrdU solution was injected into the rats body at the

same time when LPS was administered to the brain. Figure 3.32 show the results of double staining of NG2 cell (red) and BrdU (green) in brain sections. A and B are sections from LPS injected brain cerebral cortex. C and D came from hippocampus area just near LPS injection site. As Figure 3.32 shows, the green BrdU positive cells were seldom co-localized with red NG2 cells in both cortex and hippocampus, indicating that BrdU was not mainly expressed by NG2 cells. It suggests that the LPS induced increment of NG2 cells number was not due to proliferation.

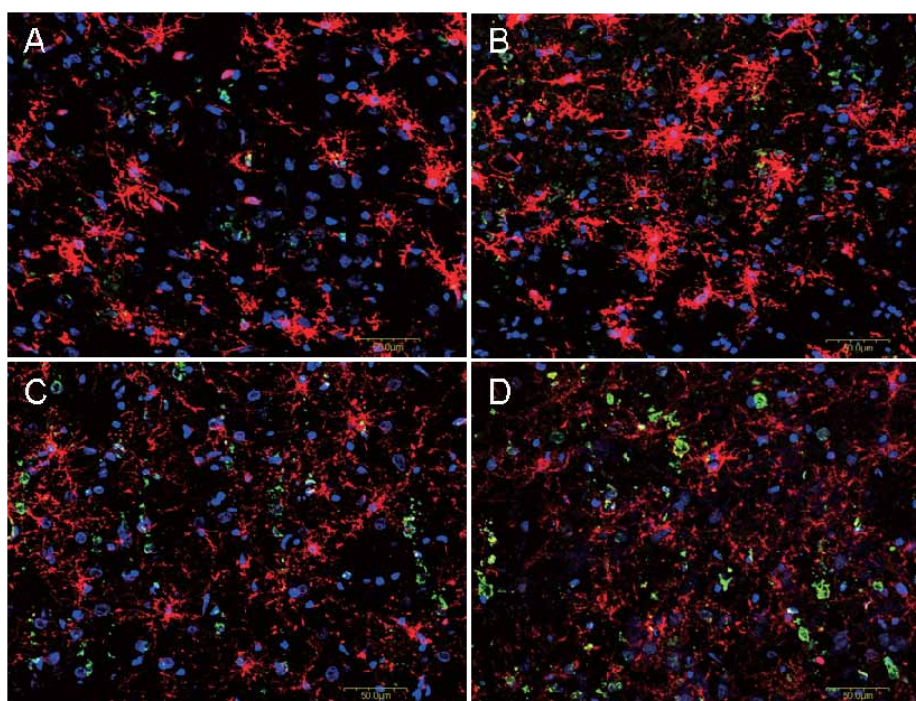


Figure 3.32: Expression of BrdU in brain after LPS administration. A and B: Cerebral cortex; C and D: Hippocampus area. Obviously, the BrdU positive staining was seldom co-localized with NG2 cells in these two affected areas. It suggests that the upregulation of NG2 cells after LPS administration can not be attributed to their proliferation. (Scale bar: 50.0 μ m).

11. NG2 cell responses after blockage of microglial complement receptor type 3 in LPS treated brain

11.1 The change of NG2 positive cells' expression

It has been reported that microglia has reactive responses in various brain pathologies including neuron-inflammation (Kreutzberg, 1996; Liu and Hong, 2003). Microglial activation has been observed in the current study in the brain pathological model triggered focal injection of LPS. As well as microglia, NG2 cells also can be activated in response to brain injury in LPS focal injected pathological brain. Anti-CD11b antibody, as a specific marker of microglia, can recognize and bind the complement receptor type 3 of microglial cells. In order to investigate the possible relationship between microglia and NG2 cells, microglia were blocked by the focal injection of anti-CD11b antibody to the cortex 24 hours before the LPS administration at the same site. The reactions of NG2 cells were studied.

As previous result shows, the expression of NG2 positive cells was upregulated contrast to the expression in non-LPS administration side. Figure 3.33 also confirm this conclusion. However, after the administration of anti-CD11b antibody and LPS, the increase in the number of NG2 cells was significant inhibited contrast to LPS administration only. Just as Figure 3.33 shows, the total number of NG2 cells decreased significantly. As the detailed mechanism was still unknown, this result suggested that microglia may participate in the activation of NG2 cells in the pathological brain. It plays a role in the NG2 cells' responses to brain injury. Their relationship need to be studied in future work.

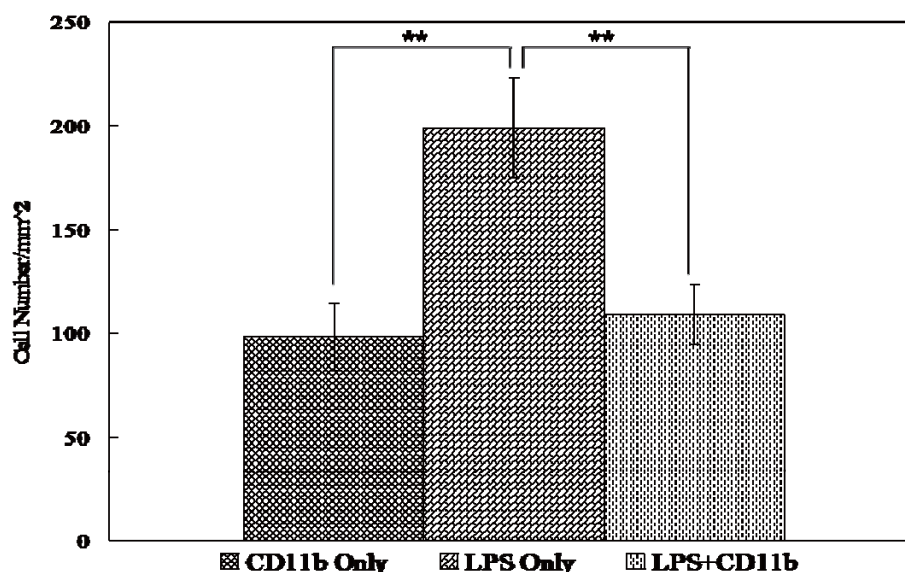


Figure 3.33: NG2 positive cell number counting when the rat was treated with anti-CD11b antibody only; LPS only and anti-CD11b antibody+LPS. After the administration of anti-CD11b antibody and LPS, the increase in the number of NG2 cells was significantly inhibited contrast to LPS administration only, suggesting that microglia may participate in the activation of NG2 cells in the pathological brain. (** $P < 0.01$)

11.2 Morphology of NG2 cells after anti-CD11b antibody+LPS treatment

As Figure 3.34 A and C show, the difference in the morphology of NG2 cells were also observed after anti-CD11b antibody+LPS administration compared to those only treated by LPS. NG2 positive cells in LPS-administrative areas increased their cell body sizes (A and C) in contrast to the NG2 cells in non-administrative area (B and D). Also, the processes of cells in A and C also became short in contrast to the long processes of those cells in normal side (B and D). The area presented in the Figure 3.34 C was the surrounding region near the needle track. There were some round amoeboid microglia (green) found in this area, suggesting they were activated by LPS there. However, at the same place in the normal side (D), the shape of

ramified microglia (green) was remained. The results of morphological alteration of NG2 cells after anti-CD11b antibody+LPS treatment were consistent to those of LPS administration only. It suggested that microglia blockage by anti-CD11b antibodies may hardly affect the morphological transformation of NG2 cells under the existence of LPS.

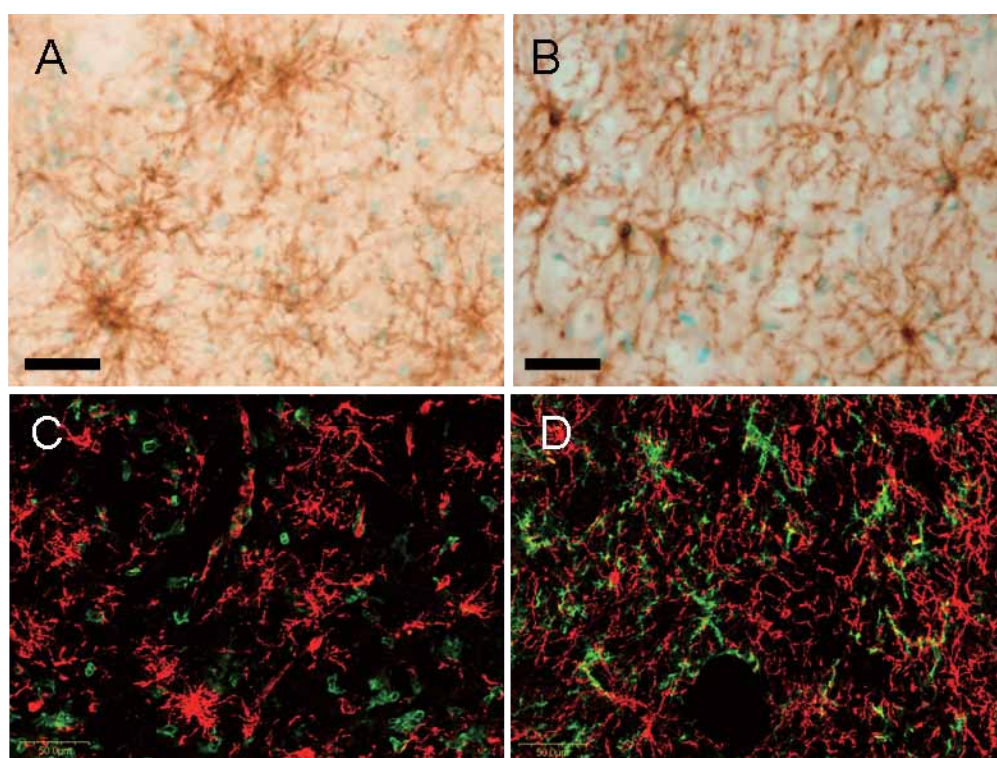


Figure 3.34: The morphological alteration in NG2 cells after anti-OX42 antibody+LPS treatment. After treated by LPS only, NG2 cells became hypertrophic and the processes also shortened. It suggests that the anti-OX42 antibody blockage may have little effect to the morphology transformation of NG2 cells under the existence of LPS. (Scale bar: 50 μ m)

11.3 The cells near the needle track

In the area near the anti-CD11b antibody and LPS focal injection site (the area inside the frame in Figure 3.35 D and E), things became different contrast to surrounding region (A, B and C). After the treatment of anti-CD11b antibody+LPS in

the brain cortex, the microglia near the injection site changed their morphology from resting ramified to amoeboid microglia as well (A, arrow pointing). Also, the NG2 positive cells increased their body sizes (B) and their numbers increased as well. However, in the center of needle track, there was no any microglia (D) found. Only few of amoeboid microglia (D, arrow pointing) were seen near the center. It might be because of inhibition of anti-CD11b antibody injected in this site. However, it was surprised that there was not any NG2 cell labeled in the same site (E), as well as microglia, only a few of NG2 positive cells can be found near the center (E, arrow pointing). The real reason is still unknown. Perhaps the expression of NG2 in the needle track area was suppressed by the blockage of complement receptor type 3. This finding may be useful to future function investigation of NG2 cells in pathological brain.

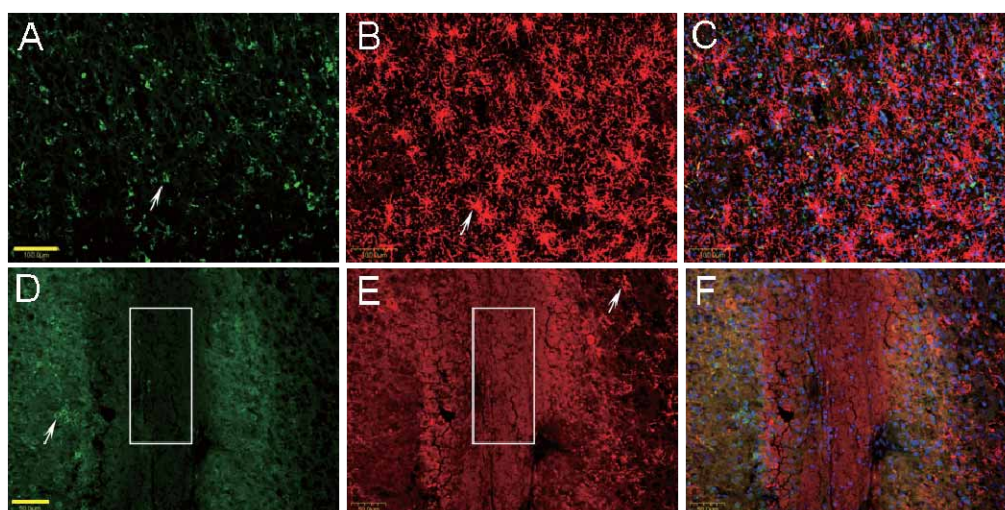


Figure 3.35: The cells in the injection site. After the administration of anti-CD11b antibody and LPS, in this area, neither microglia (green) nor NG2 cells (red) were observed. This finding may be useful to future function investigation of NG2 cell in pathological brain. (Scale bar: A, B and C: 100 μ m, D, E and F: 50 μ m)

12. Distribution of TAT-PEG-*b*-Chol nanoparticles in LPS triggered pathological brain

12.1 The permeability of TAT-PEG-*b*-Chol

It was known that brain damage or diseases can increase the permeability of foreign substance such as protein or big organic molecules because of compromise of the BBB in pathological condition (Hawkins and Davis, 2005; Persidsky et al., 2006). Here, in order to investigate the permeability of designed nanoparticle drug carrier in pathological brain, TAT-PEG-*b*-Chol was injected into the rat body *via* femoral vein. These rat brains had already been treated with LPS focal injection to the cerebral cortex 24 hours before. Rat brain sample was collected just 5 minutes after injection. The staining results in Figure 3.36 showed that the nanoparticles positive cells had already been found both inside the blood vessel (A, left) and in the brain parenchyma (A, right). Previous data had proved that in normal rats brain whose BBB are intact, the TAT-PEG-*b*-Chol positive cell can only be seen till 10-15 minutes after the injection. It suggested that, in the LPS triggered pathological brain, the nanoparticle of TAT-PEG-*b*-Chol can penetrate the BBB much quickly than in normal rats. This result will be of great importance for future clinical use of TAT-PEG-*b*-Chol in drug delivery to the pathological brain.

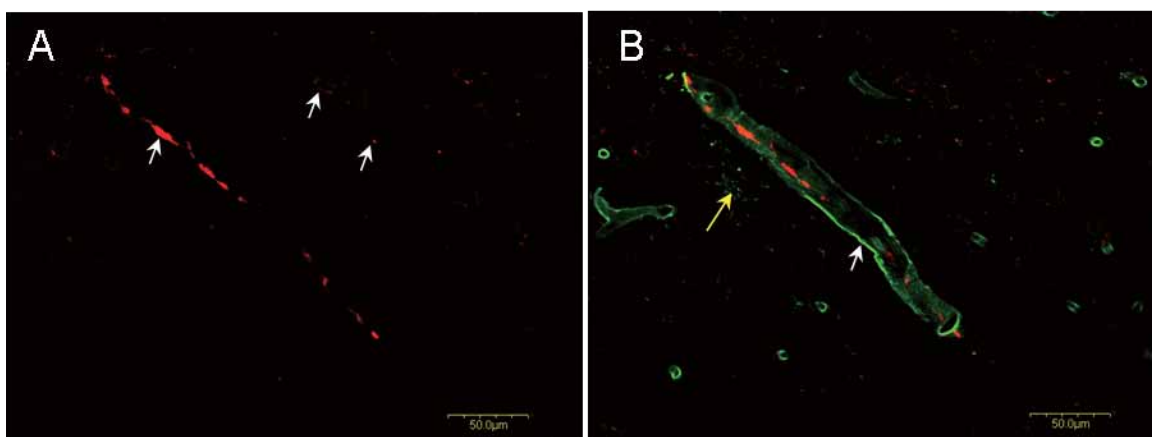
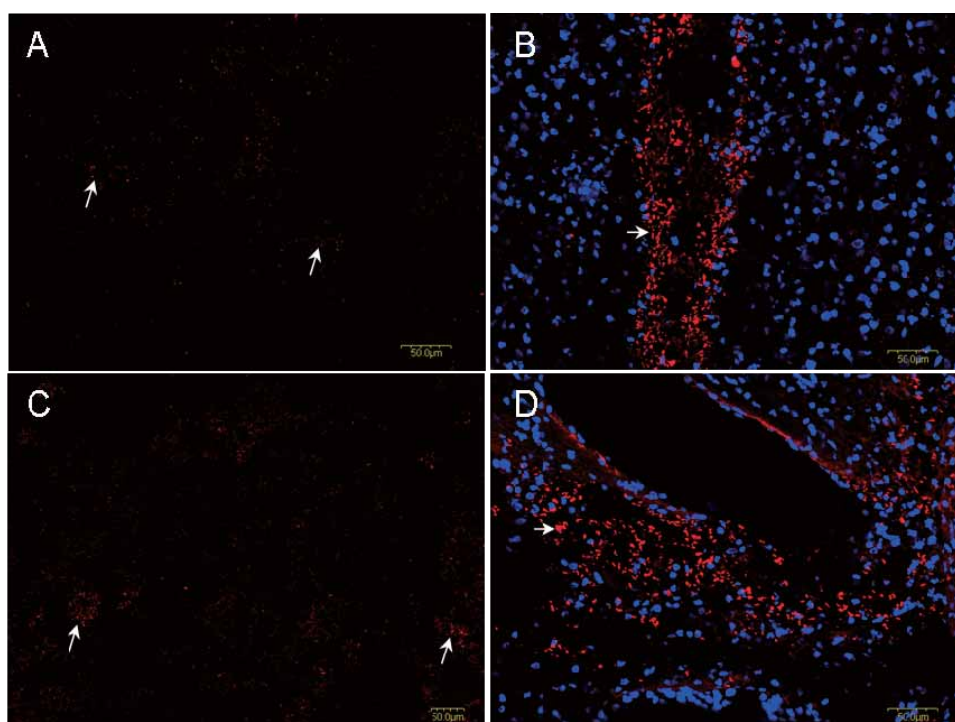


Figure 3.36: The permeability of TAT-PEG-b-Chol in pathological brain in 5 minutes. A: Staining results of TAT-PEG-b-Chol using Mouse anti-TAT antibody, Cy3 conjugated second antibody was also used. B: Staining of blood vessel (white arrow pointing) and microglia (yellow arrow pointing, there were round amoeboid microglia, suggesting they were activated) by FITC conjugated Lactation protein. It suggests that, in our established brain pathological model, TAT-PEG-b-Chol could penetrate the BBB much quickly than in normal rats whose BBB were intact.

12.2 The distribution of TAT-PEG-b-Chol

An ideal nanoparticle carrier and delivered drug system should target the pathological area specifically and release the drug molecules there. Therefore, it may be of importance to study the distribution of TAT-PEG-b-Chol micelles with drug molecules after they penetrate the BBB in pathological brain. Figure 3.37 shows their distribution in different areas within LPS triggered brain pathological model when they reached the brain parenchyma. Figure A and B are images from the cerebral cortex and C and D from hippocampus. The distribution of TAT-PEG-b-Chol in this pathological brain is different contrast to their distribution in normal brain. Although it is not easy to determine the cell types here which uptake these particles, it is obvious that many more nanoparticles were found in the pathological areas (B and D, the red dots which arrows pointed). However, only few red dots were sporadically distributed in non-LPS administration areas (A and C, arrows pointing). The result

suggested that in this pathological brain, the nanoparticles of TAT-PEG-*b*-Chol can assemble in the pathological area and may release drugs there to take the therapeutic effect. Although the reason of this distribution is not clear, this result indicates that TAT-PEG-*b*-Chol micelles can be an ideal targeting drug carrier which can deliver drug molecules through the BBB and release them in special targeted pathological zone.



*Figure 3.37: The distribution of TAT-PEG-*b*-Chol in pathological brain. The anti-TAT antibody staining results showed that there many more nanoparticle of TAT-PEG-*b*-Chol congregated in pathological areas (B and D) either in cortex (A and B) or hippocampus (C and D). It suggests that TAT-PEG-*b*-Chol can be an ideal targeting drug carrier which can deliver drug molecules through the BBB and release them in special targeted pathological zone.*

CHAPTER 4
DISCUSSION

1. PEG-*b*-Chol and TAT-PEG-*b*-Chol system

1.1. Critical micelle concentration value of nanoparticle micelles

Critical micelle concentration (CMC) value is an important parameter, above which an amphiphilic copolymer forms core shell structured micelles. The amphiphilic polymers consisting of hydrophilic and hydrophobic segments can be self-assembled core shell structure in aqueous solutions. In this study, although the NMR spectrums of polymers had proved that the synthesis was successful, other evidences are required to show that the formation of core shell nanoparticles with PEG-*b*-Chol and TAT-PEG-*b*-Chol was achieved. Therefore, CMC values of these formations were detected by a fluorescence technique, where pyrene was chosen as a fluorescent probe.

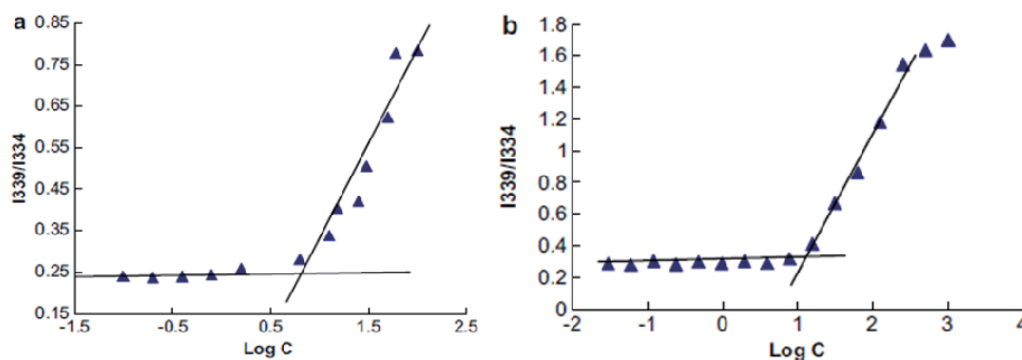


Figure 4.1: Plot of I_{339}/I_{334} ratio as a function of logarithm of polymer PEG-*b*-Chol (a) and TAT-PEG-*b*-Chol (b) concentration ($\text{Log } C$) in DI water.

The peak intensity increased markedly when the polymer concentration was above 6.2 mg/l ($\text{Log } C \approx 0.8$) for PEG-*b*-Chol or 7.8 mg/l ($\text{Log } C \approx 0.9$) for TAT-PEG-*b*-Chol. At low concentrations, the intensity ratio of I_{339}/I_{334} changed slightly. However, as polymer concentration increased, the intensity ratio increased sharply,

indicating the partitioning of pyrene into the hydrophobic core of the nanoparticles. As shown in Figure 4.1, the CMC values of PEG-*b*-Chol and TAT-PEG-*b*-Chol in DI water were about 6.6 and 11.2 mg/l, respectively. The low CAC values indicate that the core shell nanoparticles can be formed at low concentrations because of the strong hydrophobicity of cholesterol, allowing their use in much diluted media, such as body fluids. The presence of TAT led to a slight increase in the CMC. This is because more cholesterol molecules are probably needed to interact and to form the core of nanoparticles due to the strong interactions between TAT and water molecules, and the repulsion force between TAT molecules.

1.2. Particle size control in the nanoparticles fabrication

The size of nanoparticles prepared from self assembly method for targeted drug delivery is normally distributed between 100 to 200nm (Liu et al., 2007), even smaller than 100nm (Chen et al., 2008). It has been consistently shown that PEGylated nanoparticles with smaller particle size are easier to be taken up by cells. Also, these nanoparticles with small sizes can reduced plasma protein adsorption on their surface and also reduce hepatic filtration, which makes them have a long blood residence time to avoid taking by other cells in the body. In addition, the nanoparticles with smaller size have a high rate of extravasation into permeable tissues (Alexis et al., 2008). In this project, under the fabrication conditions, the effective diameters of the blank, drug-loaded, QDs-loaded and FITC-loaded nanoparticles were 180, 190, 150 and 199 nm, respectively. It demonstrates that the designed nanoparticles can achieve effective and targeted drug delivery with a longer circulating time.

During the process of blank and ciprofloxacin lactate loaded PEG-*b*-Chol micelles fabrication, extending the dialysis time up to 48 hours and changing the DI water outside the dialysis bag frequently may be good to achieve ideal micelles with smaller and even-distributed particle size. In addition, a lower environmental temperature for dialysis (10°C) may also benefit the formation of core shell structured nanoparticles. In this project, the formed blank and drug-loaded nanoparticle micelles were spherical in nature. Their size of slightly increased after drug and FITC loading.

In the core shell structure formation of PEG-*b*-Chol and TAT-PEG-*b*-Chol, the dialysis bags were put into 10°C DI water with stirrer bar in medium speed. However, in the conjugation of TAT peptide to Penicillin G, the environmental temperature hardly affects on the connection rate of TAT-Penicillin G. For sake of the stability of Penicillin G, the dialysis time can not exceed 24 hours. Although the dialysis time was half as before, current results showed that TAT-Penicillin G could be well endocytosed by cultured brain cells. It suggests that total size of designed TAT-Penicillin G system is acceptable.

1.3 The length of PEG chain and TAT-PEG-*b*-Chol BBB penetration

Properties of PEGylated nanoparticles such as size, hydrophilicity, surface charge, morphology, PEG chain length and homogeneity may affect the relationship between nanoparticles and cell membrane (Mosqueira et al., 2001a). For our designed TAT-PEG-*b*-Chol nanoparticles, we have examined the effect of PEG chain length to the BBB penetration ability of nanoparticle micelles.

In this study, TAT-PEG₃₂₉₀-*b*-Chol and TAT-PEG₅₀₀₀-*b*-Chol were successfully synthesized and used to investigate the effect of PEG chain length *in vivo* and *in vitro*. Our previous results had showed that both TAT-PEG₃₂₉₀-*b*-Chol (Liu et al., 2008b) and TAT-PEG₅₀₀₀-*b*-Chol (Liu et al., 2008a) can penetrate the BBB and reach the brain parenchyma. Few differences were found in the cellular uptake of TAT-PEG₃₂₉₀-*b*-Chol and TAT-PEG₅₀₀₀-*b*-Chol at the time point of 2 hours. However, as the Figure 2 shows, 15 minutes after venous injection, the number of FITC-positive cells which uptake the TAT-PEG₃₂₉₀-*b*-Chol nanoparticles (FITC encapsulated) was more than those uptake the TAT-PEG₅₀₀₀-*b*-Chol in the same brain area, suggesting that more nanoparticles of TAT-PEG₃₂₉₀-*b*-Chol could penetrated the BBB and uptake by brain cells in a shorter time frame. Regarding the nanoparticle micelles designed, shorten their PEG chain length may further improve their permeability through the BBB which in concert with the results from Mosqueira (Mosqueira et al., 2001b).

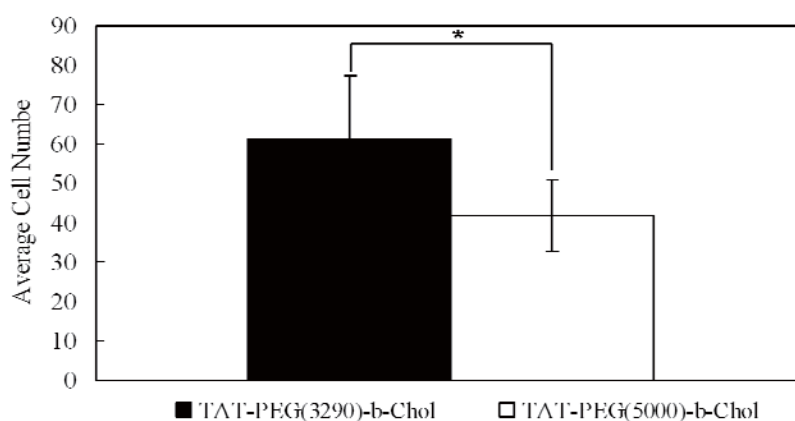


Figure 4.2: The number of FITC positive cells 15 minutes after venous injection of FITC-TAT-PEG₃₂₉₀-*b*-Chol (black) and FITC-TAT-PEG₅₀₀₀-*b*-Chol (white). The concentrations of both injected nanoparticles solution were 0.045 mg/ml. There were many more FITC positive cells in the brain cortex after intravenous injection of TAT-PEG₃₂₉₀-*b*-Chol particles in comparison that of FITC-TAT-PEG₅₀₀₀-*b*-Chol particles. * $P < 0.05$

Figure 4.3 shows the *in vitro* results of cellular uptake of TAT-PEG₃₂₉₀-*b*-Chol-FITC (A), TAT-PEG₅₀₀₀-*b*-Chol-FITC (B), PEG₃₂₉₀-*b*-Chol-FITC (C) and pure FITC (D). They share the same initial concentration and incubation time. It was obvious that astrocytes incubated with TAT-PEG₃₂₉₀-*b*-Chol-FITC (A) presented much stronger fluorescence intensity than those astrocytes incubated with TAT-PEG₅₀₀₀-*b*-Chol-FITC (B). It also proved that nanoparticles with shorter PEG chain length could be prone to be taken up by cultured cells.

In addition, in figure 4.3, it was observed that cells incubated with nanoparticles linked with TAT peptide (A and B) emitted stronger fluorescence contrast to cells incubated with nanoparticles without TAT (C) or pure FITC (D), indicating that TAT may play an important role in nanoparticles penetrating the BBB.

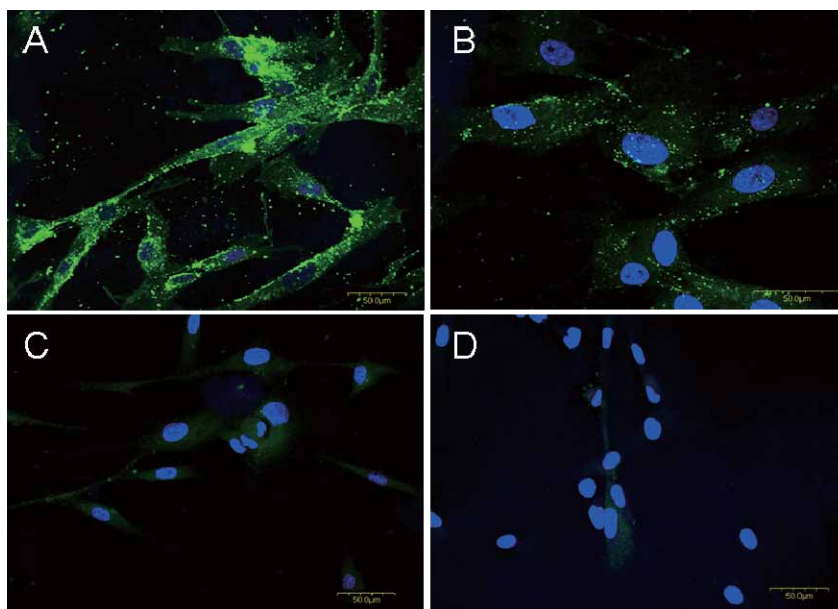


Figure 4.3: Cultured astrocytes can uptake many more FITC-TAT-PEG₃₂₉₀-*b*-Chol particles (A) than FITC-TAT-PEG₅₀₀₀-*b*-Chol (B), FITC-PEG₃₂₉₀-*b*-Chol (C) and pure FITC (D) particles. It suggests that PEGylated nanoparticles with shorter PEG chain length may penetrate the cell easily than those longer ones. Nanoparticles were incubated for 1 hour at 37°C. (Scale bar: 50 μ m, blue: stained nuclei with DAPI)

1.4 Ciprofloxacin and ciprofloxacin lactate

It has been reported that the leading causes of bacterial meningitis are gram-positive *Streptococcus pneumoniae* (Editorial, 2003), gram-negative *Escherichia coli* (Regoes et al., 2004) and *Neisseria meningitides* (Tzankaki et al., 2006) since 1990s. Ciprofloxacin ($C_{17}H_{18}FN_3O_3$) may be one of the most effective antibiotics and has a wide spectrum of these bactericidal activities. It functions by inhibiting bacterial chromosome replication (Torriero et al., 2006a; Torriero et al., 2006b). For example, an *Escherichia coli* O18:K1:H17 susceptibility test revealed that minimum inhibition concentration (MIC) of ciprofloxacin was 0.03ppm, whereas ampicillin and streptomycin were 8 and 32ppm respectively. Therefore, in our study, ciprofloxacin was firstly chosen as an antibiotic drug that will be encapsulated into the core of TAT-PEG-*b*-Chol.

However, ciprofloxacin has poor solubility in DMSO which is the main solvent for encapsulation. It will directly result in low loading efficiency of drug molecules into the core. It is necessary to find solutions for this problem. Ciprofloxacin lactate is another antibiotic within the ciprofloxacin family. As well as ciprofloxacin, ciprofloxacin lactate is also a kind of fluoroquinolone antibiotics. Contrast to the molecular structure of ciprofloxacin, ciprofloxacin lactate has an added lactate group connected in one of carbon atom (marked with * in Figure 4.4 B) with weak physical force. The ciprofloxacin lactate can be well dissolved in DMSO and the lactate group was in dissociative status when it was in DMSO. Because ciprofloxacin lactate and ciprofloxacin both possessed crucial element of fluoroquinolone group which can kill

the bacteria through its binding to bacterial DNA topoisomerase, they may almost obtain the same antibacterial efficacy. We had investigated the MIC of ciprofloxacin lactate to *Bacillus subtilis* and *Escherichia coli*. The result shows that ciprofloxacin lactate displayed the lowest MIC (0.2ppm) when compared with penicillin G potassium (MIC: 156ppm) and doxycycline monohydrate (MIC: 6.25ppm) (Liu et al., 2008b). Therefore, ciprofloxacin was finally substituted by ciprofloxacin lactate with good solubility in DMSO as the antibiotic chosen in the encapsulation into TAT-PEG-*b*-Chol.

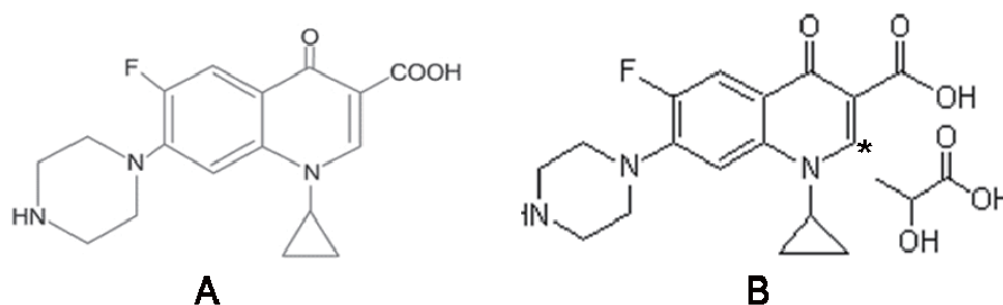


Figure 4.4: The chemical structure of ciprofloxacin (A) and ciprofloxacin lactate (B). The only difference of structure lies in the existence of lactate group in ciprofloxacin lactate.

1.5 Consideration in injecting and sampling methods for application of nanoparticles in BBB penetration

Collective results in the current study have demonstrated that TAT-PEG-*b*-Chol could easily cross the BBB into the brain parenchyma. From these observations, most of those nanoparticles that already reached the brain parenchyma were distributed in cerebral cortex and hippocampus area. However, in the project, there still many nanoparticles were found in other organs such as liver, spleen or kidney. It may be due to the intravenous injecting method (through femoral vein) adopted in the

research. This intravenous injection would increase amount of nanoparticles within the blood stream, resulting the drug distribution in the whole body. As the cells in liver, spleen and kidney can also uptake these nanoparticles, the loss of nanoparticles into other cells may eventually reduce the amount of drug in the brain and therefore affect therapeutical efficacy.

In the quantitative investigation, shifting way of injection from femoral vein (or tail vein) injection to common carotid artery (CCA) infusion may decrease the loss of injected nanoparticles (Santra et al., 2005b). However, up to now, the research of TAT conjugated nanoparticles mostly focused on qualitative investigation (Santra et al., 2005b; Schwarze et al., 1999; Torchilin et al., 2001) because of the difficulties in pharmacokinetics research *in vivo*. So that, more research efforts should be spent on studying new way of delivery of the TAT conjugated systems.

Microdialysis technique is a well developed sampling method *in vivo* in either awake, free moving or anesthetic animals (Fillenz, 2005; Justice, 1993; Mas et al., 1996; McKenzie et al., 2002; Olson and Justice, 1993; Watson et al., 2006; Zhou et al., 1995). In this project, this technique was used to sample the drug in the brain. However, during the pre-testing process of measuring nanoparticle concentration, only around 5% of nanoparticles can be sampled in 90 minutes. Perhaps only 5% can cross through the membrane of microdialysis probe. Pure antibiotics (Penicillin G potassium or ciprofloxacin lactate) were injected into the animal body (dosage: 80 mg/kg) and the whole rat brain were collected without any blood flushing. Even though, there is only about 0.03% of injected antibiotics was detected (including

antibiotics both in the blood and brain parenchyma) after 15 to 20 minutes (data not shown). That indicates to use microdialysis, only $5\% \times 0.03\% = 0.0015\%$ of injected nanoparticles can be sampled and then analyzed by HPLC. As the amount of synthesized nanoparticles is far from the dosage requirement of injection, the microdialysis technique can not sample enough nanoparticles from brain for the next analysis by HPLC.

Therefore, it is difficult to quantitatively investigate the penetration percentage of TAT-PEG-*b*-Chol through BBB at present. However, the current histological staining results revealed that this penetrating ratio may not be so low. In future study, other more sensitive methods, like radio labeling technique, should be employed to determine this percentage. For future clinical application, in order to increase the penetration ratio across the BBB, except for reducing the circulation time in blood stream, the blockage of the binding site for nanoparticles in the cells from other organs (for instance the liver, spleen or kidney) or finding other specific biological ligand to specific surface receptors of brain cells should be considered.

1.6 The cellular uptake of TAT-PEG-*b*-Chol in brain parenchyma

TAT-PEG-*b*-Chol positive cells were mainly distributed in cerebral cortex and hippocampus area after this nanoparticle reached the brain parenchyma. In this project, obviously many FITC or QDs, loaded nanoparticle positive cells were observed in these two areas. It is clear that the cells which can uptake TAT-PEG-*b*-Chol are abundant in these two areas than other areas, suggesting the designed TAT-PEG-*b*-Chol carrier system might be region-preferable. Although the relevant

mechanism for this phenomenon is still not understood, the designed drug carrier system may be a good candidate for the purpose of targeting to specific pathological region in the brain after drug administration.

Histological double staining results had already demonstrated that it was neurons that mainly uptake these nanoparticles. However, other brain cells, such as microglia, astrocytes, oligodendrocytes and NG2 cells also can uptake some tiny amount of TAT-PEG-*b*-Chol. Our study discovered that those intake generally fulfilled by cells near the blood vessel. In Figure 3.13, both cortical neurons in cortex and internal neurons can be labeled with FITC encapsulated TAT-PEG-*b*-Chol. Perhaps neuronal cells have specific surface receptors in their cell membrane, which can bind the TAT ligand specifically and induce the transcytosis.

Previous research had discovered that TAT peptide can rapidly translocate through the plasma membrane and accumulate in nucleus (Brooks et al., 2005; Santra et al., 2005b; Vives et al., 1997). However, in this research (Figure 3.10 D and Figure 3.13 D), the nanoparticles of TAT-PEG-*b*-Chol were not seen inside the nuclei, but mainly surrounding the nuclei. The uptake of nanoparticles by cultured brain cells (astrocytes and endothelial cells) also certified this finding (Figure 3.17). The FITC or QDs encapsulated TAT-PEG-*b*-Chol did not enter the nuclei possibly because of their relatively big sizes. The particles might be too big to pass through the nuclear pores.

1.7 Dynamic transport of TAT-PEG-*b*-Chol *in vivo*

In 1999, Schwarze discovered that particles of FITC-TAT can rapidly enter the brain within 30 minutes since injection (Schwarze et al., 1999). In 2005, Santra found that the TAT conjugated Quantum dots (CsS:Mn/ZnS) can also rapidly and effectively label the brain tissues after 5 minutes pump infusion (Santra et al., 2005b). The findings in the current project are in agreement with these previous findings. Within 15 minutes after injection, these nanoparticles could be found in brain parenchyma. When the nanoparticles of TAT-PEG-*b*-Chol were injected into the blood stream, because of the non-specificity of TAT peptide, they can be taken up by cells in other organs before they reach the brain. The nanoparticles with smaller particle size have longer blood residence time (Alexis et al., 2008) to avoid taking by liver cells or kidney cells. In addition, TAT-PEG-*b*-Chol particles with relative shorter PEG chain length also can shorten the time from blood to brain. Therefore, in future clinical application, the drug encapsulated TAT-PEG-*b*-Chol system with smaller particle size and shorter PEG chain length can rapidly deliver the drug to the pathological site of the brain. The rapid delivery of the designed nanoparticle carrier system through the BBB may be an important feature to benefit treatment effects for brain diseases and injuries.

1.8 Drug transport with TAT-PEG-*b*-Chol in pathological brain

It has been reported that LPS can disrupt the BBB through the action of gelatinase B (Mun-Bryce et al., 2002). The opening of BBB makes the entry of substance through the BBB easier, including the entry of drug molecules. The current results have demonstrated that the nanoparticles system of TAT-PEG-*b*-Chol can

rapidly penetrate BBB and reach the brain parenchyma within 15 minutes. In the current focal injury model plus LPS stimulation, the time for the nanoparticle delivery was shortened to only around 5 minutes. It was the damaged BBB that make the entry of TAT-PEG-*b*-Chol so fast. The rapid penetration will minimize the decrement of effective drug concentration to achieve better delivery outcome.

The most interesting finding is the congregation of TAT-PEG-*b*-Chol nanoparticles in LPS administration area. It indicated that TAT-PEG-*b*-Chol can bring most of drug molecules encapsulated cross the BBB and may release drugs in the pathological areas. However, in current experiments, only the congregation of nanoparticles carrier in the pathological site was confirmed. The release of drug molecules from the core shell of TAT-PEG-*b*-Chol should be further investigated. *In vitro* drug release data in PBS had shown that only 10% of drug inside the core shell was released after 10 minutes. So it is of great possibility that most nanoparticles accumulated in the pathological area still contained the drug molecules. As pH value, temperature or other features can affect the drug release from micelles (Blanco et al., 2008), the use of the pathological model will be ideal for the investigation of drug delivery and release in the brain. Although the reason why TAT-PEG-*b*-Chol and drug system accumulated in the brain pathological area is not known yet, it is of great significance for their clinical application in future drug targeted delivery. Therefore, in pathological brain, the drug molecules loaded TAT-PEG-*b*-Chol nanoparticles may quickly penetrate the BBB to avoid the significant loss before they were delivered to

targeted brain area. Their congregation in the pathological areas may achieve better therapeutic results.

1.9 HPLC analytical and detective method for nanoparticle system

Current research has successfully established the HPLC analytical methods of selected two antibiotics. Because all those antibiotics have benzene-like groups in their chemical structures, they can show strong absorption in UV zone at special wavelength. Therefore, photodiode array detector can be used to measure their respective concentration in samples. This detective method also can be used to analyze the concentration of antibiotics loaded TAT-PEG-*b*-Chol or PEG-*b*-Chol. But for the HPLC analysis of FITC or QDs encapsulated nanoparticles (PEG-*b*-Chol or TAT-PEG-*b*-Chol), fluorescent detector (Waters, USA) may be used in future study. From the inter-assay precision analysis results for these three antibiotics, it can be concluded that the established methods are feasible for the antibiotics concentration analysis. They can be used in future for quantitative investigation of pharmacokinetics of antibiotics encapsulated in TAT-PEG-*b*-Chol nanoparticles.

1.10 Application of nanoparticle micelles for gene targets delivery

Successful gene delivery into the targeted cells or organs is the most important step in the treatment of diseases caused by genetic disorders, mutation or genetic defects such as leukemia and tumors (Yi-Yan et al., 2006). Since 1990, little progress had been made because of the difficulties in the development of gene delivery vector.

Up to now, the research of gene delivery vectors only constrain inside the laboratory and has not proven successful in clinical trails.

In the research of gene delivery vector development, non-viral have recently received increasing attention. Recent years, nanoparticle as a promising non-viral gene delivery vector has fully developed. Those vectors, such as polyethylenimine (PEI) (Kleemann et al., 2004), cationic polymer micelles (Wang et al., 2007a; Wang et al., 2007b), self-assembled oligopeptide nanoparticles (Seow et al., 2009; Wiradharma et al., 2009) and peptide-functionalized carbon nanotubes (Pantarotto et al., 2004; Singh et al., 2005), have proven to deliver transgenes into targeted cells successfully.

For the successful delivery of gene to targeted cells or organs by nanoparticle micelles, there are three things need to be concerned. The first is the fabrication of gene into vectors. Nanoscaled complexes of cationic polymer and DNA can be fabricated by simply mixing these cationic polymer solutions with DNA (Yi-Yan et al., 2006). However, the encapsulation of DNA fragments into the core of TAT-PEG-*b*-Chol was not so simple. As hydrophobic *b*-Chol form the central core, if the gene could be well dissolved in organic solvent and can be successfully encapsulated into the central core, these TAT-PEG-*b*-Chol nanoparticle micelles also can be used for gene delivery. The second is the cytotoxicity. As it had proved by previous data, TAT-PEG-*b*-Chol micelles were nontoxic. And the last is the gene transfection efficiency. It was reported that conjugation of HIV-1 Tat cell penetrating peptide to nanocomplexes could improve cellular uptake of gene vectors and

enhanced gene transfection efficiency of neurons (Jabbari, 2009; Suk et al., 2006). We have reasons to believe that because of the existence of TAT peptide, TAT-PEG-*b*-Chol micelles also can achieve high gene transfection efficiency when they were used as gene delivery vectors.

2. TAT-Penicillin G potassium system

2.1 Encapsulation of hydrophobic and hydrophilic antibiotics

The polymer micelles of PEG-*b*-Chol were synthesized in DCM which is a hydrophobic organic solvent. In hydrophobic organic solvent such as DCM, these polymers are not in the form of core shell structure. However, when they are in aqueous solvent, core shell structure will be automatically formed by self assembly method. During the process of formation, hydrophobic *b*-Cholesterol formed the core inside and hydrophilic PEG formed the coronal shell outside. Therefore, only drugs that could be dissolved in hydrophobic organic solvent with PEG-*b*-Chol could be encapsulated into the core during this process. In current project, FITC, QDs and ciprofloxacin lactate all had good solubility in non-aqueous solvent and therefore could be well encapsulated into the core of PEG-*b*-Chol or TAT-PEG-*b*-Chol. But regarding hydrophilic antibiotics, such as Penicillin G, the encapsulation was not so good.

Because of this fact, the application of TAT-PEG-*b*-Chol nanoparticles was unfortunately limited the delivery of hydrophobic drug molecules. Therefore, other kind of nanoparticles or liposomes should be explored for encapsulation and delivery

of hydrophilic antibiotics through the BBB in the future. However, as far as Penicillin G concerned, a substitutable method of direct conjugation using TAT penetrating peptide comes out.

2.2 Conjugation of TAT to Penicillin G potassium

In this study, the TAT peptide has been successfully conjugated to the surface of PEG-*b*-Chol nanoparticles and antibiotics such as ciprofloxacin lactate were successfully encapsulated into the core, and then delivered through the BBB (Liu et al., 2008a; Liu et al., 2008b). The connection of TAT to PEG-*b*-Chol was based on the EDC/NHS chemistry. As for the chemical structure of Penicillin G, it processes the carboxyl group (-COO) in the terminal of β -lactams as well as PEG-*b*-Chol. Therefore, it makes the direct connection of Penicillin G to the amido (-NH₂) of TAT peptide *via* EDC/NHS chemistry possible.

In order to conjugate TAT peptide to Penicillin G successfully, a three-step reaction was taken to achieve this goal: activation, conjugation and dialysis. During the processes of synthesis, many different factors, such as temperature, pH value, may take effect to the final production. Previous data had showed that reaction temperature hardly affected the final connection efficiency. Therefore, the synthesis temperature was chosen at room temperature. However, the pH value may affect the connection efficiency much more than temperature. More TAT peptide molecules could be conjugated with Penicillin G in a higher pH value buffer environment, especially in the second step. It is because that although the EDC reactions were usually performed in MES buffer at pH at 4.7-6.0, the reaction of Sulfo-NHS-activated molecules with

primary amines was most efficient at pH 7.0-7.5. To get best results, the first step of reaction (EDC reaction) was performed in MES buffer at pH 5-6, then adjusted it to 7.0-7.5 with 1M NaOH solution immediately in the second step (Sulfo-NHS reaction). Therefore, in the first step of activation, the reaction was started with a pH value 6 MES buffer. After this step completed, the pH value had already been changed to 5.4. Before the second step of adding TAT peptide solution, the pH value should be adjusted to 7.0 around, but must be lower than 7.5 (Grabarek and Gergely, 1990). Under this circumstance, the TAT conjugation rate may reach the highest value in theory.

In addition, the molar ratio of Penicillin G: TAT peptide: Sulfo-NHS: EDC also affect the final connection rate. In current experiments, when this ratio increased from 1:0.5:4:1.6 to 1:0.5:15:6, the connection efficiency also greatly improved. This indicated that higher concentration of Sulfo-NHS and EDC may result in the increment of conjugation of TAT peptide.

2.3 Cytotoxicity of TAT-Penicillin G

Cytotoxicity test of TAT-Penicillin G to astrocytes, endothelial cells, neuron and microglia had demonstrated that TAT conjugated Penicillin G was nearly not toxic to these brain cells. However, Aksenova found that the HIV-1 TAT protein is neurotoxic to the cultured rat midbrain fetal neurons in 2006 (Aksenova et al., 2006). In addition, in rat hippocampus cell culture, the expression of D1 dopamine receptor can be very low also because of the existence of TAT protein (Silvers et al., 2007). It means that TAT protein may be of some toxicity to some specific cell type.

Although full-length TAT protein exerts a toxic action on primary rat neuronal cultured cells, however, it was completely nontoxic to microglia, astrocytes and oligodendrocytes (Strijbos et al., 1995). In addition, TAT peptides which come from TAT protein with different amino acid also differ in their toxicity. In 2004, it was found that TAT (47–57) which selected in this project turned out to be non-toxic for concentrations of up to 100 μ M (Trehin and Merkle, 2004). Therefore, the toxicity comes from TAT peptide part may be minimized.

During synthesis of TAT-Penicillin G, the superfluous Penicillin G and unconjugated TAT were removed by means of membrane dialysis. However, for sake of the stability of Penicillin G molecules, the dialysis time should be limited within 24 hours. Therefore, it was very difficult to completely remove free TAT in the final product. The spectrum of TAT-Penicillin G (Figure 3.20) also verified this point. Perhaps it is the reason why the cell number of neurons (Figure 3.21 A) decreased to some extent when treated with TAT-Penicillin G. However, for pure TAT conjugated Penicillin G, there was no evidence to prove that it was toxic to cultured neuron. In future study, when the concentration of unconjugated TAT is determined, the cultured neuronal cells can be treated with the pure TAT solution with the same concentration determined. If the number of neuron decreases to the same extent as current results (Figure 3.21 A), then suggesting that it is not TAT-Penicillin G but TAT results in the number decrement.

Current results had demonstrated that TAT-Penicillin G did not cause significant damage to rat brain cells. It may be a feasible way to deliver Penicillin G through the BBB.

2.4 Antibiotics screening of TAT-Penicillin G

The antibiotics screening is a method to determine value of minimum inhibition concentration (MIC) to bacteria or fungi (Fabio et al., 2007; Foroumadi et al., 2003). Here, the MIC was defined as the lowest concentration of antibiotic that completely inhibited the growth of the organisms (Liu et al., 2008b).

In this project, for the anti-bacterial efficacy test of TAT-Penicillin G, *B.subtilius* and *C.albicans* were used as the bacterial organisms. The results demonstrated that just as pure antibiotics, TAT conjugated Penicillin G as well has the ability to inhibit the growth of some infectious microorganisms. However, it still needs to know whether the chemical conjugation of TAT to Penicillin G affect its anti-bacterial efficacy to those organisms. Previous discovery has showed that the MIC of pure Penicillin G to *B.subtilius* was 156ppm (Liu et al., 2008b). It was found when *B.subtilius* was incubated with 50ppm pure Penicillin G, no inhibitory effect on the growth of *B.subtilius* was observed. However, after the 2.7ppm of TAT-Penicillin G was applied to the same *B.subtilius* solution, an inhibition on the growth was achieved. This result means that the anti-bacterial ability of 2.7ppm TAT-Penicillin G is higher than 50ppm pure Penicillin G. As it suggests that the MIC of TAT-Penicillin G *B.subtilius* may be much smaller than 156ppm, we do believe that for TAT-Penicillin G

and pure Penicillin G with same concentration, the anti-bacterial ability of the former will be much higher because of the conjugation of TAT peptide.

Similar result was obtained when *C. albicans* co-incubated with TAT- Penicillin G (Liu et al., 2008b). Sader found the MIC of Penicillin G to *C. albicans* was 64ppm in 2004 (Sader et al., 2004). In current project, when 2.7ppm or 1.4ppm TAT conjugated Penicillin G was applied to *C. albicans*, obvious inhibition effect on the growth of *C. albicans* was observed. It means that TAT-Penicillin G with much lower concentration than MIC of pure Penicillin G still had strong anti-bacterial efficacy. It was clear that MIC of TAT-Penicillin G to *C. albican* was much smaller than that of pure Penicillin G. In summary, these results both indicated that TAT-Penicillin G had a higher anti-bacterial efficacy than pure Penicillin G because of the TAT peptide conjugation.

The conjugation of TAT peptide could enhance its anti-bacterial efficacy both to *B.subtilius* and *C.albicans*. Possibly because the conjugation of HIV-1 TAT cell penetrating peptide could improve cellular uptake of particle-complex and enhanced uptake efficiency of cells (Jabbari, 2009; Suk et al., 2006). The increased cellular uptake result in that many more TAT-Penicillin G could attach or enter the cell and function there. Perhaps the existence of TAT remaining in the product of TAT-Penicillin G may contribute to the inhibition effect to *B. subtilius* and *C.albicans* due to antibacterial action of TAT (Jung et al., 2008). In fact, this effect in this project may be very small and could be neglected. First, the amount of remaining unconjugated TAT was very low after 24 hour dialysis. Second, when pure TAT

peptide solution with same concentration as TAT-Penicillin G (2.7ppm) was used in screening test, very little inhibition to the growth of bacteria was observed (Data now shown). Therefore, the remaining amount of free TAT should have no affect on the growth of bacteria in the experiments. Therefore, the conjugation of TAT to Penicillin G not only might increases its BBB penetration ability, but also might enhance its anti-bacterial efficacy.

2.5 *In vitro* uptake of TAT-Penicillin G

The cell penetrating peptide TAT can promote efficient intercellular delivery when it is on the surface of liposome (Torchilin et al., 2001). Therefore, when Penicillin G was coupled with this TAT peptide vector, it may be possible for the new compound easily taken up by cells. The current results for *in vitro* uptake of TAT-Penicillin G (astrocytes and endothelial cells) have validated the hypothesis. Here, the HPLC was used to detect the remaining drug concentration in culture medium at different intervals after incubation. From the amounts of drugs decreased from the culture medium, the amount of drug taken up by the cultured cells can be quantified indirectly. The uptake of TAT-Penicillin G and pure Penicillin G at five different concentrations was measured in the current study. The results demonstrated that when the concentration added was higher than 10ppm, perhaps the saturated uptake of drug made the relative uptake ratio very small contrast to initial lower drug concentrations (data not shown). It may result in the difficulty in discriminating real value from measurement error. So Penicillin G with initial drug concentrations lower than 10ppm should be used to investigate *in vitro* uptake. As it is not easy to

determine the drug concentration completely inside the cells by HPLC using extraction process from cultured cells, the remaining drug concentration in the culture medium was used to measure the cell drug intake. Although this concentration decreased in medium may be attributed to both those drugs inside the cells and those on the cell surfaces, they all displayed TAT peptide's affection on the enhancement of *in vitro* uptake.

2.6 The *in vivo* labeling of TAT-Penicillin G

Some recent studies of TAT drug delivery system focus on the conjugation of TAT to fluorescent particles, such as FITC (Schwarze et al., 1999) and CdS: Mn/ZnS quantum dots (Santra et al., 2005b). However, no fluorescent marker has been conjugated with the TAT-Penicillin G for observation of the drug trace *in vivo* or *in vitro*. Without such visible marker, it difficult to track the designed TAT-Penicillin G after they enter the blood stream and penetrate the BBB. Up to now, there is still no direct evidence to show that TAT-Penicillin G is able to penetrate the BBB and reach the brain parenchyma for the treatment of inflammation there. The conjugations of TAT to FITC or/and CdS: Mn/ZnS quantum dots have already proved that with the aid of TAT peptide, these particles can definitely cross the BBB (Santra et al., 2005b; Schwarze et al., 1999). The conjugation of TAT to proteins (Fawell et al., 1994; Schwarze et al., 1999), oligonucleotides (Astria-Fisher et al., 2002), plasmid DNA (Hellgren et al., 2004) or nanoparticles (Liu et al., 2008a; Santra et al., 2004; Santra et al., 2005a; Zhao et al., 2002) has also proved this point. Therefore, it is believed that the conjugation of TAT to Penicillin G can also promote their penetration through the

BBB. In future research, if possible, the radio-labeling technique may be used in labeling of TAT-Penicillin G *in vivo* in the investigation of their BBB penetration and pharmacokinetics studies.

3. Application of TAT conjugated drug delivery system

In current project, TAT peptide conjugated PEG-*b*-Chol can encapsulate FITC, QDs or ciprofloxacin lactate into the core of the micelles. During the process of encapsulation, no covalent bond formed between the drug molecules and cholesterol molecules that formed the core. This may be beneficial feature for release of encapsulated drug after entering the brain. Once the core shell structure of nanoparticles was broken in brain parenchyma, the drug molecules would be released out. The properties of drug molecules would not be affected. Therefore, other hydrophobic antibiotics or chemical drug molecules can also be encapsulated into the core if they had suitable particles size. In addition, peptide or protein may also be considered for such encapsulation and be carried through BBB using this micelles system. In future application, perhaps packed DNA fragments or gene can be encapsulated into these nanoparticles and delivered to targeted brain site.

TAT directly conjugated Penicillin G has been shown in the current study to possess the ability to penetrate BBB. So, the method of direct conjugation of TAT peptide with drug molecule provides another possible solution for delivery of some drugs through the BBB. In general, chemical drugs, peptide drugs or protein drugs all could be coupled with TAT, in taking advantage of TAT role in facilitating increase

permeability of the BBB. In the future, after understanding of the function of TAT transduction domain and the interaction between TAT and their receptors, new protein drug compounds infusing with the functional domains of TAT peptide may be developed for treatment of brain diseases or injuries.

4. LPS focal injected rat pathological brain model

4.1 The responses of NG2 expressing cells

The current results had shown that the responses of NG2 positive cells in LPS triggered pathological brain mainly lay in three aspects.

The first is morphological alterations in the NG2 cell bodies: NG2 cells in LPS administration side changed their morphology from slim shape to round ones as well as microglial cells shift from resting ramified shape to round activated amoeboid ones.

The second is that their processes shrank in pathological region contrast to their previous long processes in normal area. These two morphology changes indicated that NG2 cells are activated by LPS focal injection, just as the activations of microglia or astrocytes in response to brain injury. The NG2 cells possess the ability in response to pathological challenges in the brain. However, the mechanisms of NG2 cell responses are not understood. It is worthwhile to study the function of NG2 cells in pathological brain.

The third is the expression upregulation of NG2 positive cells in pathological region. As the expression of NG2 chondroitin-sulfate proteoglycan was also increased

after brain injury (Levine, 1994), indeed more NG2 positive cells could be observed in the brain of the saline injected side compared to that in the normal control side. The LPS administration could significantly increase the total number of NG2 cells. Two possibilities may explain the significant increment in the number of NG2 cells in the pathological brain region: proliferation or migration. The current results showed that no BrdU positive cells were positive to NG2 staining; suggesting that the increase in the NG2 cell numbers could not be attributed to NG2 cell proliferation. Therefore, NG2 cell migration might account for this cell number increase. It is possible that the NG2 cells migration from the area adjacent to the impaired brain region or from blood to brain parenchyma. In addition, it is also possible that other cells might be transformed into NG2 positive cells in particular brain pathology. However, currently, there is no direct evidence to verify these hypotheses. In the future study, more efforts can be put in to study the mechanism of NG2 cell reaction, its role in brain pathology, and especially the effect of NG2 cell reaction on drug application in treatment of brain diseases and injuries. Although the current study showed that NG2 cells are not major cells to uptake in the designed nanoparticle carrier system, NG2 cell activation may have certain impact, positive or negative, on drug delivery or drug effects.

4.2 The relationship between NG2 positive cells and microglia

It is still not clear what the relationship between NG2 cells and microglia is either in resting or activating status. Obviously, in LPS triggered pathological brain, microglia can be activated and release some cytotoxic factors (Colton and Gilbert,

1987; Lee et al., 1993; Liu et al., 2002; Moss and Bates, 2001). These factors include some cytokines such as TNF- α , IL-1 β , and IL-6 (Ajmone-Cat et al., 2003; Chao et al., 1992; Nagai et al., 2001). However, the current results showed that NG2 positive cells did not produce these cytokines when they were in pathological brain. Therefore, the role of NG2 cells was not fulfilled by releasing of these cytokines.

Interestingly, when the function of microglia complement receptor type 3, was partly blocked by their specific antibody, anti-CD11b in cortical injection site, the responses of NG2 cells in LPS treated surrounding area was down-regulated. Contrast to those increased NG2 cells in the cortex treated without microglial inhibition (LPS only); this down-regulation may suggest that microglia play an important role in the activation of NG2 positive cells. Microglia may participate in the activation of NG2 cells. In other words, NG2 cell reaction might be a downstream event of microglial activation. What this cascade reaction would be for drug delivery and drug effect in treatment of brain diseases and injuries will be further studies in the future.

One possible method to investigate NG2 cell responses to pathological stimuli or their possible relationship with microglia is to study the NG2 expressing cells *in vitro*. However, up to now, no study has been reported in which NG2-expressing cells have been directly isolated from the mature CNS and followed in culture (Dawson et al., 2000). Isolation and the primary culture of the NG2 cells may be another project for future research on impact of non-neuronal cells including NG2 cells on drug delivery or drug effects.

CHAPTER 5

CONCLUSIONS AND FUTURE STUDIES

1. Conclusions

The present studies have come to these conclusions:

1.1 PEG and *b*-cholesterol could be connected together to form PEG-*b*-Chol micelles with a diameter arrange from 150nm to 200nm in hydrophobic solvent. This amphiphilic copolymer could self assemble as a core shell-structured nanoparticle in aqueous solvent. The PEG chains formed the outer corona and the *b*-cholesterol makeup the inner core. TAT peptide (47-57), a cell penetrating peptide from HIV protein, could be conjugated to the surface of PEG-*b*-Chol to fabricate nanoparticle of TAT-PEG-*b*-Chol. The TAT-PEG-*b*-Chol particle could also form core shell structure under hydrophilic condition.

1.2 Hydrophobic molecules, such as FITC, QDs or ciprofloxacin lactate could be successfully encapsulated into the core of nanoparticles. The encapsulation has had an acceptable loading efficiency and could achieve linear drug release in PBS solution. The drug (or fluorescent marker)-loaded nanoparticles had a round morphology and an even-distributed particle size smaller than 200 nm.

1.3 The nanoparticles micelles with shorter PEG chains length and smaller particle size could be easily taken up by cultured endothelial cells and astrocytes. In the drug delivery through the BBB, FITC and QDs encapsulated TAT-PEG-*b*-Chol could penetrate the BBB around 15 minutes after they entered the blood stream. After these nanoparticles micelles crossed the BBB and reached the brain parenchyma, they

were mainly distributed in neuronal cells both in cerebral cortex and hippocampus areas. In addition, these particles did not enter the cell nuclei of neurons and were mainly in the cytoplasm around the nuclei possibly because of their relatively large size to nuclear pore. During the penetration of these nanoparticles through BBB, TAT peptide played an important role. Only TAT conjugated PEG-*b*-Chol nanoparticles could penetrate the BBB and reached the brain parenchyma.

1.4 Hydrophilic antibiotics such as Penicillin G could be directly connected to TAT peptide by EDC/NHS chemistry. This compound had no cytotoxicity to cultured brain cell lines. With the aid of TAT group, many more Penicillin G-TAT had entered cultured endothelial cells and astrocytes than pure Penicillin G. It suggests that the conjugation of TAT to Penicillin G can promote its penetration to cell membrane. In addition, TAT-Penicillin G expressed higher anti-bacterial efficacy than pure Penicillin G. In the project, feasible HPLC analytical methods for selected two antibiotics, namely, Penicillin G, Ciprofloxacin have been successfully established.

1.5 In LPS triggered pathological brain, NG2 positive cells were activated after LPS administration. Their morphological alterations with enlarge of cell bodies and shrinkage of processes were observed. Also, the number of NG2 cells in pathological region increased contrast to that of normal areas. However, unlike microglia and astrocytes, NG2 cells did not produce some cytokines when they were activated. Interestingly, a down-regulation of NG2 reaction was detected when function of

microglia complement receptor type 3 in pathological area were blocked by anti-CD11b antibody, suggesting that NG2 cells reactions may be an event downstream to microglial activation.

1.6 For drug delivery by TAT-PEG-*b*-Chol in this pathological brain, these nanoparticles micelles could quickly penetrate the BBB within 5 minutes and automatically assembled in the pathological area. The LPS triggered pathological brain model is suitable to the investigation of drug delivery using these nanoparticle carriers. In addition, this result suggests that the designed nanoparticle micelles have a promising clinical application in future drug delivery for brain disease therapies.

2. Future studies

Possible future work to continue this project includes:

2.1 The present study has revealed that nanoparticles of TAT-PEG-*b*-Chol could penetrate the BBB. However, this was just an explorative research. Further detailed research should be carried out in future studies. The following questions should be answered: How many TAT-PEG-*b*-Chol nanoparticles will finally reached brain parenchyma? Contrast to the amount of drug which been encapsulated into the core of nanoparticles, what is the penetration rate and release rate for drug molecules finally at the brain parenchyma? These quantitative researches are of great importance for

future clinical trials. As it has been known, the penetration rate of drug loaded nanoparticles will directly determines the dosage used in clinical therapy.

2.2 The current results have shown that TAT-PEG-*b*-Chol nanoparticles were mainly taken up by neurons after they reached brain parenchyma. But the reason is still unknown. It will be very interesting to investigate the biological binding between TAT peptide and receptors at cell membrane. If the mechanisms of AMT or RMT that occurred in the membranes of endothelial cells and neuronal cells are completely elucidated, more specific carrier for drug delivery can therefore be designed to targeted specific cells in the brain.

2.3 As the main components of BBB are endothelial cells and astrocytes, in future studies, *in vivo* BBB can be mimicked by coculture system using these two cells *in vitro*. Based on this system, the *in vitro* pharmacokinetics of drug-loaded TAT-PEG-*b*- Chol and TAT conjugated Penicillin G or other drug-carrier systems can be investigated.

2.4 LPS triggered pathological brain model is suitable to the investigation of drug delivery using nanoparticle carriers. In future, the nanoparticle micelles should be further studied in this brain pathological model or other models to bring specific drug molecules to cross the BBB and release drug molecules in pathological site for disease therapy. The cell responses may be compared before and after this treatment.

CONCLUSIONS AND FUTURE STUDIES

It can confirm the efficacy of therapy to brain inflammation using drug-nanoparticle carrier system. In addition, to clarify the functions of NG2 cells in pathological brain and their relationship with microglia will help us well understand their roles in the central nervous system, especially their possible roles in drug delivery and treatment.

CHAPTER 6

REFERENCES

- Abbott, N.J., Revest, P.A., 1991. Control of brain endothelial permeability. *Cerebrovasc Brain Metab Rev.* 3, 39-72.
- Abbott, N.J., Romero, I.A., 1996. Transporting therapeutics across the blood-brain barrier. *Mol Med Today.* 2, 106-13.
- Abbott, N.J., 2002. Astrocyte-endothelial interactions and blood-brain barrier permeability. *J Anat.* 200, 527.
- Abbott, N.J., 2005. Dynamics of CNS Barriers: Evolution, Differentiation, and Modulation. *Cellular and Molecular Neurobiology.* 25, 5-23.
- Abbott, N.J., Ronnback, L., Hansson, E., 2006. Astrocyte-endothelial interactions at the blood-brain barrier. *Nat Rev Neurosci.* 7, 41-53.
- Abraham, M.H., Weathersby, P.K., 1994. Hydrogen bonding. 30. Solubility of gases and vapors in biological liquids and tissues. *J Pharm Sci.* 83, 1450-6.
- Ajmone-Cat, M.A., Nicolini, A., Minghetti, L., 2003. Prolonged exposure of microglia to lipopolysaccharide modifies the intracellular signaling pathways and selectively promotes prostaglandin E2 synthesis. *J Neurochem.* 87, 1193-203.
- Aksenova, M.V., Silvers, J.M., Aksenov, M.Y., Nath, A., Ray, P.D., Mactutus, C.F., Booze, R.M., 2006. HIV-1 Tat neurotoxicity in primary cultures of rat midbrain fetal neurons: Changes in dopamine transporter binding and immunoreactivity. *Neuroscience Letters.* 395, 235-239.
- Alexis, F., Pridgen, E., Molnar, L.K., Farokhzad, O.C., 2008. Factors affecting the clearance and biodistribution of polymeric nanoparticles. *Mol Pharm.* 5, 505-15.
- Allemann, E., Leroux, J.C., Gurny, R., Doelker, E., 1993. In vitro extended-release properties of drug-loaded poly(DL-lactic acid) nanoparticles produced by a salting-out procedure. *Pharm Res.* 10, 1732-7.
- Aloisi, F., 1999. The role of microglia and astrocytes in CNS immune surveillance and immunopathology. *Adv Exp Med Biol.* 468, 123-33.
- Alyautdin, R.N., Petrov, V.E., Langer, K., Berthold, A., Kharkevich, D.A., Kreuter, J., 1997. Delivery of loperamide across the blood-brain barrier with polysorbate 80-coated polybutylcyanoacrylate nanoparticles. *Pharm Res.* 14, 325-8.

- Alyautdin, R.N., Tezikov, E.B., Range, P., Kharkevich, D.A., Begley, D.J., Kreuter, J., 1998. Significant entry of tubocurarine into the brain of rats by adsorption to polysorbate 80-coated polybutylcyanoacrylate nanoparticles: an in situ brain perfusion study. *J Microencapsul.* 15, 67-74.
- Arai, H., Furuya, T., Yasuda, T., Miura, M., Mizuno, Y., Mochizuki, H., 2004. Neurotoxic Effects of Lipopolysaccharide on Nigral Dopaminergic Neurons Are Mediated by Microglial Activation, Interleukin-1{beta}, and Expression of Caspase-11 in Mice. *J. Biol. Chem.* 279, 51647-51653.
- Arai, H., Furuya, T., Mizuno, Y., Mochizuki, H., 2006. Inflammation and infection in Parkinson's disease. *Histol Histopathol.* 21, 673-8.
- Arimoto, T., Bing, G., 2003. Up-regulation of inducible nitric oxide synthase in the substantia nigra by lipopolysaccharide causes microglial activation and neurodegeneration. *Neurobiology of Disease.* 12, 35-45.
- Astriab-Fisher, A., Sergueev, D., Fisher, M., Shaw, B.R., Juliano, R.L., 2002. Conjugates of antisense oligonucleotides with the Tat and antennapedia cell-penetrating peptides: effects on cellular uptake, binding to target sequences, and biologic actions. *Pharm Res.* 19, 744-54.
- Azmin, M.N., Stuart, J.F., Florence, A.T., 1985. The distribution and elimination of methotrexate in mouse blood and brain after concurrent administration of polysorbate 80. *Cancer Chemother Pharmacol.* 14, 238-42.
- Ball, P., 1986. Ciprofloxacin: an overview of adverse experiences. *J Antimicrob Chemother.* 18 Suppl D, 187-93.
- Bannerman, D.D., Goldblum, S.E., 2003. Mechanisms of bacterial lipopolysaccharide-induced endothelial apoptosis. *Am J Physiol Lung Cell Mol Physiol.* 284, L899-914.
- Barone, F.C., Feuerstein, G.Z., 1999. Inflammatory mediators and stroke: new opportunities for novel therapeutics. *J Cereb Blood Flow Metab.* 19, 819-34.
- Bazile, D., Prud'homme, C., Bassoullet, M.T., Marlard, M., Spenlehauer, G., Veillard, M., 1995. Stealth Me.PEG-PLA nanoparticles avoid uptake by the mononuclear phagocytes system. *J Pharm Sci.* 84, 493-8.
- Begley, D.J., Brightman, M.W., 2003. Structural and functional aspects of the blood-brain barrier. *Prog Drug Res.* 61, 39-78.

- Begley, D.J., 2004. Delivery of therapeutic agents to the central nervous system: the problems and the possibilities. *Pharmacol Ther.* 104, 29-45.
- Bickel, U., Yoshikawa, T., Landaw, E.M., Faull, K.F., Pardridge, W.M., 1993. Pharmacologic effects in vivo in brain by vector-mediated peptide drug delivery. *Proceedings of the National Academy of Sciences of the United States of America.* 90, 2618-2622.
- Bickel, U., Kang, Y.S., Yoshikawa, T., Pardridge, W.M., 1994. In vivo demonstration of subcellular localization of anti-transferrin receptor monoclonal antibody-colloidal gold conjugate in brain capillary endothelium. *J Histochem Cytochem.* 42, 1493-7.
- Bjorbaek, C., Elmquist, J.K., Michl, P., Ahima, R.S., van Bueren, A., McCall, A.L., Flier, J.S., 1998. Expression of leptin receptor isoforms in rat brain microvessels. *Endocrinology.* 139, 3485-91.
- Blanco, E., Kessinger, C.W., Sumer, B.D., Gao, J., 2008. Multifunctional Micellar Nanomedicine for Cancer Therapy. *Proc Soc Exp Biol Med.* 0808-MR-250.
- Blasi, P., Giovagnoli, S., Schoubben, A., Ricci, M., Rossi, C., 2007. Solid lipid nanoparticles for targeted brain drug delivery. *Adv Drug Deliv Rev.* 59, 454-77.
- Block, M.L., Hong, J.-S., 2005. Microglia and inflammation-mediated neurodegeneration: Multiple triggers with a common mechanism. *Progress in Neurobiology.* 76, 77-98.
- Bobo, R.H., Laske, D.W., Akbasak, A., Morrison, P.F., Dedrick, R.L., Oldfield, E.H., 1994. Convection-enhanced delivery of macromolecules in the brain. *Proc Natl Acad Sci U S A.* 91, 2076-80.
- Bodor, N., 1994. Drug targeting and retrometabolic drug design approaches Introduction. *Advanced Drug Delivery Reviews.* 14, 157-166.
- Brigati, C., Giacca, M., Noonan, D.M., Albini, A., 2003. HIV Tat, its TARgets and the control of viral gene expression. *FEMS Microbiol Lett.* 220, 57-65.
- Brigger, I., Morizet, J., Aubert, G., Chacun, H., Terrier-Lacombe, M.J., Couvreur, P., Vassal, G., 2002. Poly(ethylene glycol)-coated hexadecylcyanoacrylate nanospheres display a combined effect for brain tumor targeting. *J Pharmacol Exp Ther.* 303, 928-36.

- Brightman, M.W., Reese, T.S., 1969. Junctions between intimately apposed cell membranes in the vertebrate brain. *J Cell Biol.* 40, 648-77.
- Brightman, M.W., 1977. Morphology of blood-brain interfaces. *Exp Eye Res.* 25 Suppl, 1-25.
- Brooks, H., Lebleu, B., Vives, E., 2005. Tat peptide-mediated cellular delivery: back to basics. *Adv Drug Deliv Rev.* 57, 559-77.
- Butcher, E.C., Picker, L.J., 1996. Lymphocyte homing and homeostasis. *Science.* 272, 60-6.
- Calvo, P., Gouritin, B., Chacun, H., Desmaele, D., D'Angelo, J., Noel, J.P., Georin, D., Fattal, E., Andreux, J.P., Couvreur, P., 2001. Long-circulating PEGylated polycyanoacrylate nanoparticles as new drug carrier for brain delivery. *Pharm Res.* 18, 1157-66.
- Cao, G., Pei, W., Ge, H., Liang, Q., Luo, Y., Sharp, F.R., Lu, A., Ran, R., Graham, S.H., Chen, J., 2002. In Vivo Delivery of a Bcl-xL Fusion Protein Containing the TAT Protein Transduction Domain Protects against Ischemic Brain Injury and Neuronal Apoptosis. *J Neurosci.* 22, 5423-31.
- Chao, C.C., Hu, S., Close, K., Choi, C.S., Molitor, T.W., Novick, W.J., Peterson, P.K., 1992. Cytokine release from microglia: differential inhibition by pentoxifylline and dexamethasone. *J Infect Dis.* 166, 847-53.
- Chen, S., Zhang, X.Z., Cheng, S.X., Zhuo, R.X., Gu, Z.W., 2008. Functionalized Amphiphilic Hyperbranched Polymers for Targeted Drug Delivery. *Biomacromolecules.*
- Chognot, D., Six, J.L., Leonard, M., Bonneaux, F., Vigneron, C., Dellacherie, E., 2003. Physicochemical evaluation of PLA nanoparticles stabilized by water-soluble MPEO-PLA block copolymers. *J Colloid Interface Sci.* 268, 441-7.
- Coisne, C., Lyck, R., Engelhardt, B., 2007. Therapeutic Targeting of Leukocyte Trafficking Across the Blood-Brain Barrier. *Inflammation; Allergy-Drug Targets* 6, 210-222.
- Colton, C.A., Gilbert, D.L., 1987. Production of superoxide anions by a CNS macrophage, the microglia. *FEBS Lett.* 223, 284-8.
- Couvreur, P., Tulkens, P., Roland, M., Trouet, A., Speiser, P., 1977. Nanocapsules: a new type of lysosomotropic carrier. *FEBS Lett.* 84, 323-6.

- Curto, M., Reali, C., Palmieri, G., Scintu, F., Schivo, M.L., Sogos, V., Marcialis, M.A., Ennas, M.G., Schwarz, H., Pozzi, G., Gremo, F., 2004. Inhibition of cytokines expression in human microglia infected by virulent and non-virulent mycobacteria. *Neurochem Int.* 44, 381-92.
- Dashti, S.R., Baharvahdat, H., Spetzler, R.F., Sauvageau, E., Chang, S.W., Stiefel, M.F., Park, M.S., Bambakidis, N.C., 2008. Operative intracranial infection following craniotomy. *Neurosurg Focus.* 24, E10.
- Dawson, M.R., Levine, J.M., Reynolds, R., 2000. NG2-expressing cells in the central nervous system: are they oligodendroglial progenitors? *J Neurosci Res.* 61, 471-9.
- de Boer, A., Gaillard, P., 2007. Drug Targeting the Brain. *Annu. Rev. Pharmacol Toxicol.* 49, 1-33.
- de Lange, E.C.M., Marchand, S., van den Berg, D.-J., van der Sandt, I.C.J., de Boer, A.G., Delon, A., Bouquet, S., Couet, W., 2000. In vitro and in vivo investigations on fluoroquinolones; effects of the P-glycoprotein efflux transporter on brain distribution of sparfloxacin. *European Journal of Pharmaceutical Sciences.* 12, 85-93.
- Dehouck, B., Fenart, L., Dehouck, M.-P., Pierce, A., Torpier, G., Cecchelli, R., 1997. A New Function for the LDL Receptor: Transcytosis of LDL across the Blood-Brain Barrier. *J. Cell Biol.* 138, 877-889.
- Derossi, D., Calvet, S., Trembleau, A., Brunissen, A., Chassaing, G., Prochiantz, A., 1996. Cell internalization of the third helix of the Antennapedia homeodomain is receptor-independent. *J Biol Chem.* 271, 18188-93.
- Deshayes, S., Morris, M.C., Divita, G., Heitz, F., 2005. Cell-penetrating peptides: tools for intracellular delivery of therapeutics. *Cell Mol Life Sci.* 62, 1839-49.
- Di Bello, I.C., Dawson, M.R., Levine, J.M., Reynolds, R., 1999. Generation of oligodendroglial progenitors in acute inflammatory demyelinating lesions of the rat brain stem is associated with demyelination rather than inflammation. *J Neurocytol.* 28, 365-81.
- Dietz, G.P., Kilic, E., Bahr, M., 2002. Inhibition of neuronal apoptosis in vitro and in vivo using TAT-mediated protein transduction. *Mol Cell Neurosci.* 21, 29-37.
- Doolittle, N.D., Abrey, L.E., Bleyer, W.A., Brem, S., Davis, T.P., Dore-Duffy, P., Drewes, L.R., Hall, W.A., Hoffman, J.M., Korfel, A., Martuza, R., Muldoon, L.L., Peereboom, D., Peterson, D.R., Rabkin, S.D., Smith, Q., Stevens, G.H.,

- Neuwelt, E.A., 2005. New frontiers in translational research in neuro-oncology and the blood-brain barrier: report of the tenth annual Blood-Brain Barrier Disruption Consortium Meeting. *Clin Cancer Res.* 11, 421-8.
- Douglas, S.J., Davis, S.S., Illum, L., 1987. Biodistribution of poly(butyl 2-cyanoacrylate) nanoparticles in rabbits. *Int J Pharm.* 39, 145-152.
- Drlica, K., Zhao, X., 1997. DNA gyrase, topoisomerase IV, and the 4-quinolones. *Microbiol. Mol. Biol. Rev.* 61, 377-392.
- Duffy, K.R., Pardridge, W.M., 1987. Blood-brain barrier transcytosis of insulin in developing rabbits. *Brain Res.* 420, 32-8.
- Duffy, K.R., Pardridge, W.M., Rosenfeld, R.G., 1988. Human blood-brain barrier insulin-like growth factor receptor. *Metabolism.* 37, 136-40.
- Durand, M.L., Calderwood, S.B., Weber, D.J., Miller, S.I., Southwick, F.S., Caviness, V.S., Jr., Swartz, M.N., 1993. Acute bacterial meningitis in adults. A review of 493 episodes. *N Engl J Med.* 328, 21-8.
- Dvorak, F., Martinez-Torres, F., Sellner, J., Haas, J., Schellinger, P.D., Schwaninger, M., Meyding-Lamade, U.K., 2004. Experimental herpes simplex virus encephalitis: a long-term study of interleukin-6 expression in mouse brain tissue. *Neurosci Lett.* 367, 289-92.
- Edens, H.A., Parkos, C.A., 2000. Modulation of epithelial and endothelial paracellular permeability by leukocytes. *Adv Drug Deliv Rev.* 41, 315-28.
- Editorial, 2003. Pneumococcal Meningitis: Antibiotics essential but insufficient. *Brain.* 126, 1013-1014.
- Ehrlich, P., 1885. *Das Sauerstoff-Bedurfnis des Organismus: Eine Farbenanalytische Studie.* Berlin: Hirschwald.
- Elamanchili, P., Diwan, M., Cao, M., Samuel, J., 2004. Characterization of poly(D,L-lactic-co-glycolic acid) based nanoparticulate system for enhanced delivery of antigens to dendritic cells. *Vaccine.* 22, 2406-12.
- Emerich, D.F., Snodgrass, P., Pink, M., Bloom, F., Bartus, R.T., 1998. Central analgesic actions of loperamide following transient permeation of the blood brain barrier with Cereport (RMP-7). *Brain Res.* 801, 259-66.

- Fabio, A., Cermelli, C., Fabio, G., Nicoletti, P., Quaglio, P., 2007. Screening of the antibacterial effects of a variety of essential oils on microorganisms responsible for respiratory infections. *Phytother Res.* 21, 374-7.
- Fawell, S., Seery, J., Daikh, Y., Moore, C., Chen, L.L., Pepinsky, B., Barsoum, J., 1994. Tat-mediated delivery of heterologous proteins into cells. *Proc Natl Acad Sci U S A.* 91, 664-8.
- Fillenz, M., 2005. In vivo neurochemical monitoring and the study of behaviour. *Neurosci Biobehav Rev.* 29, 949-62.
- Fitch, M.T., van de Beek, D., 2008. Drug Insight: steroids in CNS infectious diseases (mdash) new indications for an old therapy. *Nat Clin Pract Neuro.* 4, 97-104.
- Foroumadi, A., Soltani, F., Rezaee, M.A., Moshafi, M.H., 2003. Synthesis and evaluation of in vitro antimycobacterial activity of some 5-(5-nitro-2-thienyl)-2-(piperazinyl, piperidinyl and morpholinyl)-1,3,4-thiadiazole derivatives. *Boll Chim Farm.* 142, 416-9.
- Fretz, M.M., Mastrobattista, E., Koning, G.A., Jiskoot, W., Storm, G., 2005. Strategies for cytosolic delivery of liposomal macromolecules. *Int J Pharm.* 298, 305-9.
- Friedman, W.J., Larkfors, L., Ayer-LeLievre, C., Ebendal, T., Olson, L., Persson, H., 1990. Regulation of beta-nerve growth factor expression by inflammatory mediators in hippocampal cultures. *J Neurosci Res.* 27, 374-82.
- Gaillard, P.J., van der Sandt, I.C., Voorwinden, L.H., Vu, D., Nielsen, J.L., de Boer, A.G., Breimer, D.D., 2000. Astrocytes increase the functional expression of P-glycoprotein in an in vitro model of the blood-brain barrier. *Pharm Res.* 17, 1198-205.
- Gallo, V., Zhou, J.M., McBain, C.J., Wright, P., Knutson, P.L., Armstrong, R.C., 1996. Oligodendrocyte progenitor cell proliferation and lineage progression are regulated by glutamate receptor-mediated K⁺ channel block. *J Neurosci.* 16, 2659-70.
- Gard, A.L., Pfeiffer, S.E., 1990. Two proliferative stages of the oligodendrocyte lineage (A2B5⁺O4⁻ and O4⁺GalC⁻) under different mitogenic control. *Neuron.* 5, 615-25.
- Gasper, M.M., Blanco, D., Cruz, M.E., Alonso, M.J., 1998. Formulation of L-asparaginase-loaded poly(lactide-co-glycolide) nanoparticles: influence of

- polymer properties on enzyme loading, activity and in vitro release. *J Control Release*. 52, 53-62.
- Gbadamosi, J.K., Hunter, A.C., Moghimi, S.M., 2002. PEGylation of microspheres generates a heterogeneous population of particles with differential surface characteristics and biological performance. *FEBS Lett*. 532, 338-44.
- Ghose, A.K., Viswanadhan, V.N., Wendoloski, J.J., 1999. A knowledge-based approach in designing combinatorial or medicinal chemistry libraries for drug discovery. 1. A qualitative and quantitative characterization of known drug databases. *J Comb Chem*. 1, 55-68.
- Goldman, E.E., 1913. Vitalfarbung am Zentralnervensystem. *Abh. Preuss. Akad. Wiss. Phys. Math. K11*, 1-60.
- Grabarek, Z., Gergely, J., 1990. Zero-length crosslinking procedure with the use of active esters. *Anal. Biochem*. 185, 131-135.
- Graeber, M.B., Streit, W.J., Kreutzberg, G.W., 1988. The microglial cytoskeleton: vimentin is localized within activated cells in situ. *J Neurocytol*. 17, 573-80.
- Grayo, S., Lott-Desroches, M.C., Dussurget, O., Respaud, R., Fontanet, A., Join-Lambert, O., Singlas, E., Le Monnier, A., 2008. Rapid eradication of *Listeria monocytogenes* by moxifloxacin in a murine model of central nervous system listeriosis. *Antimicrob Agents Chemother*.
- Gref, R., Minamitake, Y., Peracchia, M.T., Trubetskoy, V., Torchilin, V., Langer, R., 1994. Biodegradable long-circulating polymeric nanospheres. *Science*. 263, 1600-3.
- Gref, R., Domb, A., Quellec, P., Blunk, T., Verbavatz, J.M., Langer, R., 1995. The controlled intravenous delivery of drugs using PEG-coated sterically stabilized nanospheres. *Advanced Drug Delivery Reviews*. 16, 215-233.
- Gref, R., Couvreur, P., Barratt, G., Mysiakine, E., 2003. Surface-engineered nanoparticles for multiple ligand coupling. *Biomaterials*. 24, 4529-37.
- Gref R, Babak B, Bouillot P, Lukina I, Bodorev M, E., D., 1998. Interfacial and emulsion stabilising properties of amphiphilic water-soluble poly(ethylene glycol)-poly(lactic acid) copolymers for the fabrication of biocompatible nanoparticles. *Colloids Surfaces A*. 143, 413– 420.
- Gref R, Lućk M, Quellec P, Marchand M, Dellacherie E, S., H., 2000. 'Stealth' corona-core nanoparticles surface modified by polyethylene glycol (PEG):

- influences of the corona (PEG chain length and surface density) and of the core composition on phagocytic uptake and plasma protein adsorption. *Colloids Surfaces B:Biointerfaces*. 18, 301–313.
- Greig, N.H., 1989. Drug delivery to the brain by blood – brain barrier: circumvention and drug modification. *Implications of the Blood– Brain Barrier and its Manipulation*. Plenum, New York. 331-367.
- Grislain, L., Couvreur, P., Lenaerts, V., Roland, M., Deprez-Decampeneere, D., Speiser, P., 1983. Pharmacokinetics and distribution of a biodegradable drug-carrier. . *Int J Pharm*. 15, 335-345.
- Gulyaev, A.E., Gelperina, S.E., Skidan, I.N., Antropov, A.S., Kivman, G.Y., Kreuter, J., 1999. Significant transport of doxorubicin into the brain with polysorbate 80-coated nanoparticles. *Pharm Res*. 16, 1564-9.
- Hall, A., Giese, N.A., Richardson, W.D., 1996. Spinal cord oligodendrocytes develop from ventrally derived progenitor cells that express PDGF alpha-receptors. *Development*. 122, 4085-94.
- Hansson, E., Ronnback, L., 1995. Astrocytes in glutamate neurotransmission. *Faseb J*. 9, 343-50.
- Hawkins, B.T., Davis, T.P., 2005. The Blood-Brain Barrier/Neurovascular Unit in Health and Disease. *Pharmacol Rev*. 57, 173-185.
- Heald, C.R., Stolnik, S., De Matteis, C., Garnett, M.C., Illum, L., Davis, S.S., 2003. Characterisation of poly (lactic acid) : poly(ethyleneoxide) (PLA:PEG) nanoparticles using the self-consistent theory modelling approach. *Colloids Surfaces A*. 212, 57– 64,.
- Hellgren, I., Gorman, J., Sylven, C., 2004. Factors controlling the efficiency of Tat-mediated plasmid DNA transfer. *J Drug Target*. 12, 39-47.
- Hemmer, K., Fransen, L., Vanderstichele, H., Vanmechelen, E., Heuschling, P., 2001. An in vitro model for the study of microglia-induced neurodegeneration: involvement of nitric oxide and tumor necrosis factor-[alpha]. *Neurochemistry International*. 38, 557-565.
- Hiroaki, O., Yamamoto, M., Heya T, I.Y., Kamei S, Ogawa Y,, 1994. Drug delivery using biodegradable microspheres. . *J Control Release*. 28, 121–129.
- Hirsch, E.C., Hunot, S., Hartmann, A., 2005. Neuroinflammatory processes in Parkinson's disease. *Parkinsonism & Related Disorders*. 11, S9-S15.

- Hoshino, A., Manabe, N., Fujioka, K., Suzuki, K., Yasuhara, M., Yamamoto, K., 2007. Use of fluorescent quantum dot bioconjugates for cellular imaging of immune cells, cell organelle labeling, and nanomedicine: surface modification regulates biological function, including cytotoxicity. *J Artif Organs.* 10, 149-57.
- Hosoya, M., 2007. [Therapy and prognosis in subacute sclerosing panencephalitis]. *Nippon Rinsho.* 65, 1483-6.
- Huber, J.D., Egleton, R.D., Davis, T.P., 2001. Molecular physiology and pathophysiology of tight junctions in the blood-brain barrier. *Trends in Neurosciences.* 24, 719-725.
- Hunot, S., Dugas, N., Faucheux, B., Hartmann, A., Tardieu, M., Debre, P., Agid, Y., Dugas, B., Hirsch, E.C., 1999. FcepsilonR2/CD23 is expressed in Parkinson's disease and induces, in vitro, production of nitric oxide and tumor necrosis factor-alpha in glial cells. *J Neurosci.* 19, 3440-7.
- Huwylar, J., Wu, D., Pardridge, W.M., 1996. Brain drug delivery of small molecules using immunoliposomes. *Proc Natl Acad Sci U S A.* 93, 14164-9.
- Ikumi Tamai, A.T., 2000. Transporter-mediated permeation of drugs across the blood-brain barrier. *Journal of Pharmaceutical Sciences.* 89, 1371-1388.
- Illum, S.L., Davis, S.S., 1983. Effect of the nonionic surfactant poloxamer 338 on the fate and deposition of polystyrene microspheres following intravenous administration. *J Pharm Sci.* 72, 1086-9.
- Iravani, M.M., Kashefi, K., Mander, P., Rose, S., Jenner, P., 2002. Involvement of inducible nitric oxide synthase in inflammation-induced dopaminergic neurodegeneration. *Neuroscience.* 110, 49-58.
- Ivanov, D.V., Budanov, S.V., 2006. [Ciprofloxacin and antibacterial therapy of respiratory tract infections]. *Antibiot Khimioter.* 51, 29-37.
- Jabbari, E., 2009. Targeted Delivery with Peptidomimetic Conjugated Self-Assembled Nanoparticles. *Pharmaceutical Research.* 26, 612-630.
- Janzer, R.C., Raff, M.C., 1987. Astrocytes induce blood-brain barrier properties in endothelial cells. *Nature.* 325, 253-7.
- Jubelt, B., 2006. Dexamethasone for the treatment of tuberculous meningitis in adolescents and adults. *Curr Neurol Neurosci Rep.* 6, 451-2.

- Jung, H.J., Jeong, K.S., Lee, D.G., 2008. Effective antibacterial action of tat (47-58) by increased uptake into bacterial cells in the presence of trypsin. *J Microbiol Biotechnol.* 18, 990-6.
- Justice, J.B., Jr., 1993. Quantitative microdialysis of neurotransmitters. *J Neurosci Methods.* 48, 263-76.
- Kanellakopoulou, K., Pagoulatou, A., Stroumpoulis, K., Vafiadou, M., Kranidioti, H., Giamarellou, H., Giamarellos-Bourboulis, E.J., 2008. Pharmacokinetics of moxifloxacin in non-inflamed cerebrospinal fluid of humans: implication for a bactericidal effect. *J Antimicrob Chemother.* 61, 1328-31.
- Kang, Y.S., Boado, R.J., Pardridge, W.M., 1995. Pharmacokinetics and organ clearance of a 3'-biotinylated, internally [³²P]-labeled phosphodiester oligodeoxynucleotide coupled to a neutral avidin/monoclonal antibody conjugate. *Drug Metab Dispos.* 23, 55-9.
- Kawashima, Y., Yamamoto, H., Takeuchi, H., Hino, T., Niwa, T., 1998. Properties of a peptide containing DL-lactide/glycolide copolymer nanospheres prepared by novel emulsion solvent diffusion methods. *Eur J Pharm Biopharm.* 45, 41-8.
- Kermer, P., Klöcker, N., Bähr, M., 1999. Neuronal death after brain injury. *Cell and Tissue Research.* 298, 383-395.
- Kilic, E., Dietz, G.P., Hermann, D.M., Bahr, M., 2002. Intravenous TAT-Bcl-X1 is protective after middle cerebral artery occlusion in mice. *Ann Neurol.* 52, 617-22.
- Kim, J.A., Tran, N.D., Li, Z., Yang, F., Zhou, W., Fisher, M.J., 2006. Brain endothelial hemostasis regulation by pericytes. *J Cereb Blood Flow Metab.* 26, 209-17.
- Kleemann, E., Dailey, L.A., Abdelhady, H.G., Gessler, T., Schmehl, T., Roberts, C.J., Davies, M.C., Seeger, W., Kissel, T., 2004. Modified polyethylenimines as non-viral gene delivery systems for aerosol gene therapy: investigations of the complex structure and stability during air-jet and ultrasonic nebulization. *J Control Release.* 100, 437-50.
- Klegeris, A., McGeer, P.L., 2000. R(-)-Deprenyl inhibits monocytic THP-1 cell neurotoxicity independently of monoamine oxidase inhibition. *Exp Neurol.* 166, 458-64.

- Kohutnicka, M., Lewandowska, E., Kurkowska-Jastrzebska, I., Czlonkowski, A., Czlonkowska, A., 1998. Microglial and astrocytic involvement in a murine model of Parkinson's disease induced by 1-methyl-4-phenyl-1,2,3,6-tetrahydropyridine (MPTP). *Immunopharmacology*. 39, 167-180.
- Kramer, A.H., Bleck, T.P., 2008. Neurocritical care of patients with central nervous system infections. *Curr Treat Options Neurol*. 10, 201-11.
- Kreuter, J., 1994. Nanoparticles. *Encyclopedia of Pharmaceutical Technology*,. 10, 165-190.
- Kreuter, J., Alyautdin, R.N., Kharkevich, D.A., Ivanov, A.A., 1995. Passage of peptides through the blood-brain barrier with colloidal polymer particles (nanoparticles). *Brain Res*. 674, 171-4.
- Kreuter, J., Alyautdin, R.N., 2000. Using nanoparticles to Target drugs to the CNS. *The BBB and drug delivery to the CNS :New York Nasel*. 213.
- Kreuter, J., 2001. Nanoparticulate systems for brain delivery of drugs. *Adv Drug Deliv Rev*. 47, 65-81.
- Kreutzberg, G.W., 1996. Microglia: a sensor for pathological events in the CNS. *Trends in Neurosciences*. 19, 312-318.
- Kroll, R.A., Pagel, M.A., Muldoon, L.L., Roman-Goldstein, S., Neuwelt, E.A., 1996. Increasing volume of distribution to the brain with interstitial infusion: dose, rather than convection, might be the most important factor. *Neurosurgery*. 38, 746-52; discussion 752-4.
- Lai, C.H., Kuo, K.H., 2005. The critical component to establish in vitro BBB model: Pericyte. *Brain Res Brain Res Rev*. 50, 258-65.
- Le, W., Rowe, D., Xie, W., Ortiz, I., He, Y., Appel, S.H., 2001. Microglial Activation and Dopaminergic Cell Injury: An In Vitro Model Relevant to Parkinson's Disease. *J. Neurosci*. 21, 8447-8455.
- Lee, J., Cho, E.C., Cho, K., 2004. Incorporation and release behavior of hydrophobic drug in functionalized poly(D,L-lactide)-block-poly(ethylene oxide) micelles. *J Control Release*. 94, 323-35.
- Lee, S.C., Liu, W., Dickson, D.W., Brosnan, C.F., Berman, J.W., 1993. Cytokine production by human fetal microglia and astrocytes. Differential induction by lipopolysaccharide and IL-1 beta. *J Immunol*. 150, 2659-67.

- Leonard, J.M., Des Prez, R.M., 1990. Tuberculous meningitis. *Infect Dis Clin North Am.* 4, 769-87.
- Levine, J.M., Card, J.P., 1987. Light and electron microscopic localization of a cell surface antigen (NG2) in the rat cerebellum: association with smooth protoplasmic astrocytes. *J Neurosci.* 7, 2711-20.
- Levine, J.M., Stallcup, W.B., 1987. Plasticity of developing cerebellar cells in vitro studied with antibodies against the NG2 antigen. *J Neurosci.* 7, 2721-31.
- Levine, J.M., Stincone, F., Lee, Y.S., 1993. Development and differentiation of glial precursor cells in the rat cerebellum. *Glia.* 7, 307-21.
- Levine, J.M., 1994. Increased expression of the NG2 chondroitin-sulfate proteoglycan after brain injury. *J Neurosci.* 14, 4716-30.
- Levine, J.M., Enquist, L.W., Card, J.P., 1998. Reactions of oligodendrocyte precursor cells to alpha herpesvirus infection of the central nervous system. *Glia.* 23, 316-28.
- Levine, J.M., Reynolds, R., 1999. Activation and proliferation of endogenous oligodendrocyte precursor cells during ethidium bromide-induced demyelination. *Exp Neurol.* 160, 333-47.
- Levine, J.M., Reynolds, R., Fawcett, J.W., 2001. The oligodendrocyte precursor cell in health and disease. *Trends in Neurosciences.* 24, 39-47.
- Lewin, M., Carlesso, N., Tung, C.H., Tang, X.W., Cory, D., Scadden, D.T., Weissleder, R., 2000. Tat peptide-derivatized magnetic nanoparticles allow in vivo tracking and recovery of progenitor cells. *Nat Biotechnol.* 18, 410-4.
- Liao, H., Bu, W.Y., Wang, T.H., Ahmed, S., Xiao, Z.C., 2005. Tenascin-R plays a role in neuroprotection via its distinct domains that coordinate to modulate the microglia function. *J Biol Chem.* 280, 8316-23.
- Lindsay, R.M., 1994. Neurotrophic growth factors and neurodegenerative diseases: therapeutic potential of the neurotrophins and ciliary neurotrophic factor. *Neurobiol Aging.* 15, 249-51.
- Lipinski, C.A., 2000. Drug-like properties and the causes of poor solubility and poor permeability. *J Pharmacol Toxicol Methods.* 44, 235-49.
- Lipinski, C.A., Lombardo, F., Dominy, B.W., Feeney, P.J., 2001. Experimental and computational approaches to estimate solubility and permeability in drug

- discovery and development settings. *Advanced Drug Delivery Reviews*. 46, 3-26.
- Liu, B., Gao, H.M., Wang, J.Y., Jeohn, G.H., Cooper, C.L., Hong, J.S., 2002. Role of nitric oxide in inflammation-mediated neurodegeneration. *Ann N Y Acad Sci*. 962, 318-31.
- Liu, B., Hong, J.-S., 2003. Role of Microglia in Inflammation-Mediated Neurodegenerative Diseases: Mechanisms and Strategies for Therapeutic Intervention. *J Pharmacol Exp Ther*. 304, 1-7.
- Liu, L., Guo, K., Lu, J., Venkatraman, S.S., Luo, D., Ng, K.C., Ling, E.A., Moochhala, S., Yang, Y.Y., 2008a. Biologically active core/shell nanoparticles self-assembled from cholesterol-terminated PEG-TAT for drug delivery across the blood-brain barrier. *Biomaterials*. 29, 1509-17.
- Liu, L., Venkatraman, S.S., Yang, Y.Y., Guo, K., Lu, J., He, B., Moochhala, S., Kan, L., 2008b. Polymeric micelles anchored with TAT for delivery of antibiotics across the blood-brain barrier. *Biopolymers*. 90(5), 617-623.
- Liu, Y.Y., Yu, Y., Zhang, G.B., Tang, M.F., 2007. Preparation, characterization, and controlled release of novel nanoparticles based on MMA/beta-CD copolymers. *Macromol Biosci*. 7, 1250-7.
- Lobenberg, R., Araujo, L., von Briesen, H., Rodgers, E., Kreuter, J., 1998. Body distribution of azidothymidine bound to hexyl-cyanoacrylate nanoparticles after i.v. injection to rats. *J Control Release*. 50, 21-30.
- Loftus, L.T., Li, H.F., Gray, A.J., Hirata-Fukae, C., Stoica, B.A., Futami, J., Yamada, H., Aisen, P.S., Matsuoka, Y., 2006. In vivo protein transduction to the CNS. *Neuroscience*. 139, 1061-7.
- Lohbach, C., Neumann, D., Lehr, C.M., Lamprecht, A., 2006. Human vascular endothelial cells in primary cell culture for the evaluation of nanoparticle bioadhesion. *J Nanosci Nanotechnol*. 6, 3303-9.
- Lovric, J., Cho, S.J., Winnik, F.M., Maysinger, D., 2005. Unmodified Cadmium Telluride Quantum Dots Induce Reactive Oxygen Species Formation Leading to Multiple Organelle Damage and Cell Death. *Chemistry & Biology*. 12, 1227-1234.
- Lucke, A., Fustella, E., Tessmar, J., Gazzaniga, A., Gopferich, A., 2002. The effect of poly(ethylene glycol)-poly(D,L-lactic acid) diblock copolymers on peptide acylation. *J Control Release*. 80, 157-68.

- Lutsar, I., McCracken, G.H., Jr., Friedland, I.R., 1998. Antibiotic pharmacodynamics in cerebrospinal fluid. *Clin Infect Dis.* 27, 1117-27, quiz 1128-9.
- Mas, M., Gonzalez-Mora, J.L., Hernandez, L., 1996. In vivo monitoring of brain neurotransmitter release for the assessment of neuroendocrine interactions. *Cell Mol Neurobiol.* 16, 383-96.
- Mathisen, G.E., Johnson, J.P., 1997. Brain abscess. *Clin Infect Dis.* 25, 763-79; quiz 780-1.
- McKenzie, J.A., Watson, C.J., Rostand, R.D., German, I., Witowski, S.R., Kennedy, R.T., 2002. Automated capillary liquid chromatography for simultaneous determination of neuroactive amines and amino acids. *J Chromatogr A.* 962, 105-15.
- McPherson, C., Gal, P., Ransom, J.L., 2008. Treatment of *Citrobacter koseri* Infection with Ciprofloxacin and Cefotaxime in a Preterm Infant (July/August). *Ann Pharmacother.*
- Minghetti, L., 2005. Role of inflammation in neurodegenerative diseases. *Curr Opin Neurol.* 18, 315-21.
- Minghetti, L., Ajmone-Cat, M.A., De Berardinis, M.A., De Simone, R., 2005. Microglial activation in chronic neurodegenerative diseases: roles of apoptotic neurons and chronic stimulation. *Brain Res Brain Res Rev.* 48, 251-6.
- Moellering, R.C., Jr., 1996. The place of quinolones in everyday clinical practice. *Chemotherapy.* 42 Suppl 1, 54-61.
- Moghimi, S.M., Szebeni, J., 2003. Stealth liposomes and long circulating nanoparticles: critical issues in pharmacokinetics, opsonization and protein-binding properties. *Prog Lipid Res.* 42, 463-78.
- Mogi, M., Harada, M., Riederer, P., Narabayashi, H., Fujita, K., Nagatsu, T., 1994. Tumor necrosis factor-alpha (TNF-alpha) increases both in the brain and in the cerebrospinal fluid from parkinsonian patients. *Neurosci Lett.* 165, 208-10.
- Mogi, M., Harada, M., Narabayashi, H., Inagaki, H., Minami, M., Nagatsu, T., 1996. Interleukin (IL)-1 beta, IL-2, IL-4, IL-6 and transforming growth factor-alpha levels are elevated in ventricular cerebrospinal fluid in juvenile parkinsonism and Parkinson's disease. *Neurosci Lett.* 211, 13-6.

- Moos, T., Morgan, E., 2000. Transferrin and Transferrin Receptor Function in Brain Barrier Systems. *Cellular and Molecular Neurobiology*. 20, 77-95.
- Morgan, S.C., Taylor, D.L., Pocock, J.M., 2004. Microglia release activators of neuronal proliferation mediated by activation of mitogen-activated protein kinase, phosphatidylinositol-3-kinase/Akt and delta-Notch signalling cascades. *J Neurochem*. 90, 89-101.
- Mosqueira, V.C., Legrand, P., Gulik, A., Bourdon, O., Gref, R., Labarre, D., Barratt, G., 2001a. Relationship between complement activation, cellular uptake and surface physicochemical aspects of novel PEG-modified nanocapsules. *Biomaterials*. 22, 2967-79.
- Mosqueira, V.C.F., Legrand, P., Morgat, J.-L., Vert, M., Mysiakine, E., Gref, R., Devissaguet, J.-P., Barratt, G., 2001b. Biodistribution of Long-Circulating PEG-Grafted Nanocapsules in Mice: Effects of PEG Chain Length and Density. *Pharmaceutical Research*. 18, 1411-1419.
- Moss, D.W., Bates, T.E., 2001. Activation of murine microglial cell lines by lipopolysaccharide and interferon-gamma causes NO-mediated decreases in mitochondrial and cellular function. *Eur J Neurosci*. 13, 529-38.
- Mrak, R.E., Griffin, W.S.T., 2005. Glia and their cytokines in progression of neurodegeneration. *Neurobiology of Aging*. 26, 349-354.
- Mun-Bryce, S., Lukes, A., Wallace, J., Lukes-Marx, M., Rosenberg, G.A., 2002. Stromelysin-1 and gelatinase A are upregulated before TNF-alpha in LPS-stimulated neuroinflammation. *Brain Res*. 933, 42-9.
- Nagai, A., Nakagawa, E., Hatori, K., Choi, H.B., McLarnon, J.G., Lee, M.A., Kim, S.U., 2001. Generation and characterization of immortalized human microglial cell lines: expression of cytokines and chemokines. *Neurobiol Dis*. 8, 1057-68.
- Neuwelt, E.A., Rapoport, S.I., 1984. Modification of the blood-brain barrier in the chemotherapy of malignant brain tumors. *Fed Proc*. 43, 214-9.
- Nishiyama, A., Lin, X.H., Giese, N., Heldin, C.H., Stallcup, W.B., 1996. Co-localization of NG2 proteoglycan and PDGF alpha-receptor on O2A progenitor cells in the developing rat brain. *J Neurosci Res*. 43, 299-314.
- Ogata, A., Tashiro, K., Nukuzuma, S., Nagashima, K., Hall, W.W., 1997. A rat model of Parkinson's disease induced by Japanese encephalitis virus. *J Neurovirol*. 3, 141-7.

- Oldendorf, W.H., Cornford, M.E., Brown, W.J., 1977. The large apparent work capability of the blood-brain barrier: a study of the mitochondrial content of capillary endothelial cells in brain and other tissues of the rat. *Ann Neurol.* 1, 409-17.
- Olivier, J.C., Vauthier, C., Taverna, M., Puisieux, F., Ferrier, D., Couvreur, P., 1996. Stability of orosomucoid-coated polyisobutylcyanoacrylate nanoparticles in the presence of serum. *J Control Release.* 40, 157-168.
- Olivier, J.C., Fenart, L., Chauvet, R., Pariat, C., Cecchelli, R., Couet, W., 1999. Indirect evidence that drug brain targeting using polysorbate 80-coated polybutylcyanoacrylate nanoparticles is related to toxicity. *Pharm Res.* 16, 1836-42.
- Olivier, J.C., Huertas, R., Lee, H.J., Calon, F., Pardridge, W.M., 2002. Synthesis of pegylated immunonanoparticles. *Pharm Res.* 19, 1137-43.
- Olivier, J.C., 2005. Drug transport to brain with targeted nanoparticles. *NeuroRx.* 2, 108-19.
- Olson, R.J., Justice, J.B., Jr., 1993. Quantitative microdialysis under transient conditions. *Anal Chem.* 65, 1017-22.
- Ong, W.Y., Garey, L.J., 1996. A light and electron microscopic study of GluR4-positive cells in human cerebral cortex. *Neurosci Lett.* 210, 107-10.
- Ong, W.Y., Levine, J.M., 1999. A light and electron microscopic study of NG2 chondroitin sulfate proteoglycan-positive oligodendrocyte precursor cells in the normal and kainate-lesioned rat hippocampus. *Neuroscience.* 92, 83-95.
- Onishi, H., Machida, Y., Machida, Y., 2003. Antitumor properties of irinotecan-containing nanoparticles prepared using poly(DL-lactic acid) and poly(ethylene glycol)-block-poly(propylene glycol)-block-poly(ethylene glycol). *Biol Pharm Bull.* 26, 116-9.
- Ooie, T., Suzuki, H., Terasaki, T., Sugiyama, Y., 1996a. Comparative distribution of quinolone antibiotics in cerebrospinal fluid and brain in rats and dogs. *J Pharmacol Exp Ther.* 278, 590-6.
- Ooie, T., Suzuki, H., Terasaki, T., Sugiyama, Y., 1996b. Kinetics of quinolone antibiotics in rats: efflux from cerebrospinal fluid to the circulation. *Pharm Res.* 13, 1065-8.

- Ooie, T., Suzuki, H., Terasaki, T., Sugiyama, Y., 1996c. Characterization of the transport properties of a quinolone antibiotic, fleroxacin, in rat choroid plexus. *Pharm Res.* 13, 523-7.
- Paemeleire, K., 2002. The cellular basis of neurovascular metabolic coupling. *Acta Neurol Belg.* 102, 153-7.
- Pantarotto, D., Singh, R., McCarthy, D., Erhardt, M., Briand, J.P., Prato, M., Kostarelos, K., Bianco, A., 2004. Functionalized carbon nanotubes for plasmid DNA gene delivery. *Angew Chem Int Ed Engl.* 43, 5242-6.
- Pardridge, W.M., Eisenberg, J., Yang, J., 1987. Human blood-brain barrier transferrin receptor. *Metabolism.* 36, 892-5.
- Pardridge, W.M., 1995. Transport of small molecules through the blood brain barrier: biology and methodology. *Adv. Drug Deliv. Rev.* 15, 5-36.
- Pardridge, W.M., Kang, Y.-S., Buciak, J.L., Yang, J., 1995. Human Insulin Receptor Monoclonal Antibody Undergoes High Affinity Binding to Human Brain Capillaries in Vitro and Rapid Transcytosis Through the Blood-Brain Barrier in Vivo in the Primate. *Pharmaceutical Research.* 12, 807-816.
- Pardridge, W.M., 1997. Drug delivery to the brain. *J Cereb Blood Flow Metab.* 17, 713-31.
- Pardridge, W.M., 1999. Non-invasive drug delivery to the human brain using endogenous blood-brain barrier transport systems. *Pharm Sci Technolo Today.* 2, 49-59.
- Pardridge, W.M., 2002. Drug and gene targeting to the brain with molecular Trojan horses. *Nat Rev Drug Discov.* 1, 131-9.
- Pardridge, W.M., 2007. Blood-brain barrier delivery. *Drug Discovery Today.* 12, 54-61.
- Peracchia, M.T., Vauthier, C., Puisieux, F., Couvreur, P., 1997. Development of sterically stabilized poly(isobutyl 2-cyanoacrylate) nanoparticles by chemical coupling of poly(ethylene glycol). *J Biomed Mater Res.* 34, 317-26.
- Peracchia, M.T., Fattal, E., Desmaele, D., Besnard, M., Noel, J.P., Gomis, J.M., Appel, M., d'Angelo, J., Couvreur, P., 1999. Stealth PEGylated polycyanoacrylate nanoparticles for intravenous administration and splenic targeting. *J Control Release.* 60, 121-8.

- Perez, C., Sanchez, A., Putnam, D., Ting, D., Langer, R., Alonso, M.J., 2001. Poly(lactic acid)-poly(ethylene glycol) nanoparticles as new carriers for the delivery of plasmid DNA. *J Control Release*. 75, 211-24.
- Persidsky, Y., Ramirez, S., Haorah, J., Kanmogne, G., 2006. Blood–brain Barrier: Structural Components and Function Under Physiologic and Pathologic Conditions. *Journal of Neuroimmune Pharmacology*. 1, 223-236.
- Pfister, H.W., Feiden, W., Einhaupl, K.M., 1993. Spectrum of complications during bacterial meningitis in adults. Results of a prospective clinical study. *Arch Neurol*. 50, 575-81.
- Plard, J.P., Didier, B., 1999. Comparison of the safety profiles of PLA50 and Me.PEG-PLA50 nanoparticles after single dose intravenous administration to rat. *Colloids Surfaces B*. 16, 173–183.
- Polito, A., Reynolds, R., 2005. NG2-expressing cells as oligodendrocyte progenitors in the normal and demyelinated adult central nervous system. *J Anat*. 207, 707-16.
- Prabha, S., Zhou, W.Z., Panyam, J., Labhasetwar, V., 2002. Size-dependency of nanoparticle-mediated gene transfection: studies with fractionated nanoparticles. *Int J Pharm*. 244, 105-15.
- Pringle, N.P., Mudhar, H.S., Collarini, E.J., Richardson, W.D., 1992. PDGF receptors in the rat CNS: during late neurogenesis, PDGF alpha-receptor expression appears to be restricted to glial cells of the oligodendrocyte lineage. *Development*. 115, 535-51.
- Raff, M.C., Miller, R.H., Noble, M., 1983. A glial progenitor cell that develops in vitro into an astrocyte or an oligodendrocyte depending on culture medium. *Nature*. 303, 390-6.
- Ramge, P., Unger, R.E., Oltrogge, J.B., Zenker, D., Begley, D., Kreuter, J., Von Briesen, H., 2000. Polysorbate-80 coating enhances uptake of polybutylcyanoacrylate (PBCA)-nanoparticles by human and bovine primary brain capillary endothelial cells. *Eur J Neurosci*. 12, 1931-40.
- Rao, K.S., Reddy, M.K., Horning, J.L., Labhasetwar, V., 2008. TAT-conjugated nanoparticles for the CNS delivery of anti-HIV drugs. *Biomaterials*. 29, 4429-4438.
- Raphael, R., Roland, S., David, S., Fred, G., 2004. Rubin's Pathology: Clinicopathologic foundations of Medicine. Lippincott Williams Wilkins. p42.

- Redwine, J.M., Armstrong, R.C., 1998. In vivo proliferation of oligodendrocyte progenitors expressing PDGF α R during early remyelination. *J Neurobiol.* 37, 413-28.
- Reed, M.D., 1986. Current concepts in clinical therapeutics: bacterial meningitis in infants and children. *Clin Pharm.* 5, 798-809.
- Reese, T.S., Karnovsky, M.J., 1967. Fine structural localization of a blood-brain barrier to exogenous peroxidase. *J Cell Biol.* 34, 207-17.
- Regoes, R.R., Wiuff, C., Zappala, R.M., Garner, K.N., Baquero, F., Levin, B.R., 2004. Pharmacodynamic functions: a multiparameter approach to the design of antibiotic treatment regimens. *Antimicrob Agents Chemother.* 48, 3670-6.
- Reichmann, H., 2008. Initiation of Parkinson's disease treatment. *J Neurol.* 255 Suppl 5, 57-9.
- Reimold, I., Domke, D., Bender, J., Seyfried, C.A., Radunz, H.-E., Fricker, G., 2008. Delivery of nanoparticles to the brain detected by fluorescence microscopy. *European Journal of Pharmaceutics and Biopharmaceutics.* 70, 627-632.
- Reynolds, R., Hardy, R., 1997. Oligodendroglial progenitors labeled with the O4 antibody persist in the adult rat cerebral cortex in vivo. *J Neurosci Res.* 47, 455-70.
- Rhodes, K.E., Raivich, G., Fawcett, J.W., 2006. The injury response of oligodendrocyte precursor cells is induced by platelets, macrophages and inflammation-associated cytokines. *Neuroscience.* 140, 87-100.
- Ribe, E.M., Serrano-Saiz, E., Akpan, N., Troy, C.M., 2008. Mechanisms of neuronal death in disease: defining the models and the players. *Biochem J.* 415, 165-82.
- Richards, M.L., Prince, R.A., Kenaley, K.A., Johnson, J.A., LeFrock, J.L., 1981. Antimicrobial penetration into cerebrospinal fluid. *Drug Intell Clin Pharm.* 15, 341-68.
- Rietschel, E.T., Brade, H., 1992. Bacterial endotoxins. *Sci Am.* 267, 54-61.
- Rietschel, E.T., Brade, H., Holst, O., Brade, L., Muller-Loennies, S., Mamat, U., Zahringer, U., Beckmann, F., Seydel, U., Brandenburg, K., Ulmer, A.J., Mattern, T., Heine, H., Schletter, J., Loppnow, H., Schonbeck, U., Flad, H.D., Hauschildt, S., Schade, U.F., Di Padova, F., Kusumoto, S., Schumann, R.R., 1996. Bacterial endotoxin: Chemical constitution, biological recognition, host

- response, and immunological detoxification. *Curr Top Microbiol Immunol.* 216, 39-81.
- Riley T, Govender T, Stolnik S, Xiong CD, Garnett MC, L, I., 1999. Colloidal stability and drug incorporation aspects of micellar-like PLA-PEG nanoparticles. *Colloids Surfaces B: Biointerfaces.* 16, 147–159.
- Riley T, Govender T, Stolnik S, Xiong CD, Garnett MC, L, I., 2001. Physicochemical evaluation of nanoparticles assembled from poly(lactic acid)-poly(ethylene glycol) (PLA-PEG) block copolymers as drug delivery vehicles. *Langmuir.* 17, 3168 –3174.
- Rock, R.B., Gekker, G., Hu, S., Sheng, W.S., Cheeran, M., Lokensgard, J.R., Peterson, P.K., 2004. Role of Microglia in Central Nervous System Infections. *Clin. Microbiol. Rev.* 17, 942-964.
- Rousselle, C., Clair, P., Lefauconnier, J.M., Kaczorek, M., Scherrmann, J.M., Temsamani, J., 2000. New advances in the transport of doxorubicin through the blood-brain barrier by a peptide vector-mediated strategy. *Mol Pharmacol.* 57, 679-86.
- Rowland, L.P., Fink, M.E., Rubin, L.L., 1992. Cerebrospinal fluid: blood-brain barrier, brain oedema and hydrocephalus. In *Principles of Neural Science*, New York: Elsevier. 1050-1060.
- Rubenstein, H.S., Fine, J., Coons, A.H., 1962. Localization of endotoxin in the walls of the peripheral vascular system during lethal endotoxemia. *Proc Soc Exp Biol Med.* 111, 458-67.
- Rubin, L.L., Staddon, J.M., 1999. The cell biology of the blood-brain barrier. *Annu Rev Neurosci.* 22, 11-28.
- Sader, H.S., Fedler, K.A., Rennie, R.P., Stevens, S., Jones, R.N., 2004. Omiganan pentahydrochloride (MBI 226), a topical 12-amino-acid cationic peptide: spectrum of antimicrobial activity and measurements of bactericidal activity. *Antimicrob Agents Chemother.* 48, 3112-8.
- Salem, A.K., Cannizzaro, S.M., Davies, M.C., Tendler, S.J., Roberts, C.J., Williams, P.M., Shakesheff, K.M., 2001. Synthesis and characterisation of a degradable poly(lactic acid)-poly(ethylene glycol) copolymer with biotinylated end groups. *Biomacromolecules.* 2, 575-80.

- Santra, S., Yang, H., Dutta, D., Stanley, J.T., Holloway, P.H., Tan, W., Moudgil, B.M., Mericle, R.A., 2004. TAT conjugated, FITC doped silica nanoparticles for bioimaging applications. *Chem Commun (Camb)*. 2810-1.
- Santra, S., Yang, H., Holloway, P.H., Stanley, J.T., Mericle, R.A., 2005a. Synthesis of water-dispersible fluorescent, radio-opaque, and paramagnetic CdS:Mn/ZnS quantum dots: a multifunctional probe for bioimaging. *J Am Chem Soc*. 127, 1656-7.
- Santra, S., Yang, H., Stanley, J.T., Holloway, P.H., Moudgil, B.M., Walter, G., Mericle, R.A., 2005b. Rapid and effective labeling of brain tissue using TAT-conjugated CdS:Mn/ZnS quantum dots. *Chem Commun (Camb)*. 3144-6.
- Schenkel, A.R., Mamdouh, Z., Muller, W.A., 2004. Locomotion of monocytes on endothelium is a critical step during extravasation. *Nat Immunol*. 5, 393-400.
- Schroder, U., Sabel, B.A., 1996. Nanoparticles, a drug carrier system to pass the blood-brain barrier, permit central analgesic effects of i.v. dalargin injections. *Brain Res*. 710, 121-4.
- Schwarze, S.R., Ho, A., Vocero-Akbani, A., Dowdy, S.F., 1999. In vivo protein transduction: delivery of a biologically active protein into the mouse. *Science*. 285, 1569-72.
- Seow, W.Y., Yang, Y.Y., George, A.J., 2009. Oligopeptide-mediated gene transfer into mouse corneal endothelial cells: expression, design optimization, uptake mechanism and nuclear localization. *Nucleic Acids Res*.
- Shashoua, V.E., Hesse, G.W., 1996. N-docosahexaenoyl, 3 hydroxytyramine: a dopaminergic compound that penetrates the blood-brain barrier and suppresses appetite. *Life Sci*. 58, 1347-57.
- Singh, R., Pantarotto, D., McCarthy, D., Chaloin, O., Hoebeke, J., Partidos, C.D., Briand, J.P., Prato, M., Bianco, A., Kostarelos, K., 2005. Binding and condensation of plasmid DNA onto functionalized carbon nanotubes: toward the construction of nanotube-based gene delivery vectors. *J Am Chem Soc*. 127, 4388-96.
- Shi, N., Pardridge, W.M., 2000. Noninvasive gene targeting to the brain. *Proc Natl Acad Sci U S A*. 97, 7567-72.

- Shi, N., Zhang, Y., Zhu, C., Boado, R.J., Pardridge, W.M., 2001. Brain-specific expression of an exogenous gene after i.v. administration. *Proc Natl Acad Sci U S A.* 98, 12754-9.
- Shoji, H., Watanabe, M., Itoh, S., Kuwahara, H., Hattori, F., 1993. Japanese encephalitis and parkinsonism. *J Neurol.* 240, 59-60.
- Shumei Man, E.E.U.R.M.R., 2007. Inflammatory Cell Migration into the Central Nervous System: A Few New Twists on an Old Tale. *Brain Pathology.* 17, 243-250.
- Silvers, J.M., Aksenova, M.V., Aksenov, M.Y., Mactutus, C.F., Booze, R.M., 2007. Neurotoxicity of HIV-1 Tat protein: Involvement of D1 dopamine receptor. *NeuroToxicology.* 28, 1184-1190.
- Simeonova, M., Ivanova, T., Raikova, E., Georgieva, M., Raikov, Z., 1988. Tissue distribution of polybutylcyanoacrylate nanoparticles carrying spin-labelled nitrosourea. *Int J Pharm.* 43, 267-271.
- Smith, Q.R., 1993. Drug delivery to brain and the role of carrier-mediated transport. *Adv Exp Med Biol.* 331, 83-93.
- Soppimath, K.S., Aminabhavi, T.M., Kulkarni, A.R., Rudzinski, W.E., 2001. Biodegradable polymeric nanoparticles as drug delivery devices. *J Control Release.* 70, 1-20.
- Sorgel, F., Jaehde, U., Naber, K., Stephan, U., 1989. Pharmacokinetic disposition of quinolones in human body fluids and tissues. *Clin Pharmacokinet.* 16 Suppl 1, 5-24.
- Spector, R., Johanson, C.E., 1989. The mammalian choroid plexus. *Sci Am.* 261, 68-74.
- Springer, T.A., 1994. Traffic signals for lymphocyte recirculation and leukocyte emigration: the multistep paradigm. *Cell.* 76, 301-14.
- Staddon, J.M., Rubin, L.L., 1996. Cell adhesion, cell junctions and the blood--brain barrier. *Current Opinion in Neurobiology.* 6, 622-627.
- Stallcup, W.B., Beasley, L., 1987. Bipotential glial precursor cells of the optic nerve express the NG2 proteoglycan. *J Neurosci.* 7, 2737-44.
- Steiniger, S.C., Kreuter, J., Khalansky, A.S., Skidan, I.N., Bobruskin, A.I., Smirnova, Z.S., Severin, S.E., Uhl, R., Kock, M., Geiger, K.D., Gelperina, S.E., 2004.

- Chemotherapy of glioblastoma in rats using doxorubicin-loaded nanoparticles. *Int J Cancer*. 109, 759-67.
- Stolnik, S., Heald, C.R., Neal, J., Garnett, M.C., Davis, S.S., Illum, L., Purkis, S.C., Barlow, R.J., Gellert, P.R., 2001. Polylactide-poly(ethylene glycol) micellar-like particles as potential drug carriers: production, colloidal properties and biological performance. *J Drug Target*. 9, 361-78.
- Streit, W.J., Walter, S.A., Pennell, N.A., 1999. Reactive microgliosis. *Prog Neurobiol*. 57, 563-81.
- Streit, W.J., 2000. Microglial Response to Brain Injury: A Brief Synopsis. *Toxicol Pathol*. 28, 28-30.
- Strijbos, P.J., Zamani, M.R., Rothwell, N.J., Arbuthnott, G., Harkiss, G., 1995. Neurotoxic mechanisms of transactivating protein Tat of Maedi-Visna virus. *Neurosci Lett*. 197, 215-8.
- Suk, J.S., Suh, J., Choy, K., Lai, S.K., Fu, J., Hanes, J., 2006. Gene delivery to differentiated neurotypic cells with RGD and HIV Tat peptide functionalized polymeric nanoparticles. *Biomaterials*. 27, 5143-50.
- Tacconi, M.T., 1998. Neuronal death: is there a role for astrocytes? *Neurochem Res*. 23, 759-65.
- Tamai, I., Sai, Y., Kobayashi, H., Kamata, M., Wakamiya, T., Tsuji, A., 1997. Structure-Internalization Relationship for Adsorptive-Mediated Endocytosis of Basic Peptides at the Blood-Brain Barrier. *J Pharmacol Exp Ther*. 280, 410-415.
- Tao-Cheng, J.H., Nagy, Z., Brightman, M.W., 1987. Tight junctions of brain endothelium in vitro are enhanced by astroglia. *J Neurosci*. 7, 3293-9.
- Tao-Cheng, J.H., Brightman, M.W., 1988. Development of membrane interactions between brain endothelial cells and astrocytes in vitro. *Int J Dev Neurosci*. 6, 25-37.
- Tessmar, J., Mikos, A., Gopferich, A., 2003. The use of poly(ethylene glycol)-block-poly(lactic acid) derived copolymers for the rapid creation of biomimetic surfaces. *Biomaterials*. 24, 4475-86.
- Tessmar, J.K., Mikos, A.G., Gopferich, A., 2002. Amine-reactive biodegradable diblock copolymers. *Biomacromolecules*. 3, 194-200.

- Tobio, M., Gref, R., Sanchez, A., Langer, R., Alonso, M.J., 1998. Stealth PLA-PEG nanoparticles as protein carriers for nasal administration. *Pharm Res.* 15, 270-5.
- Tontsch, U., Bauer, H.-C., 1991. Glial cells and neurons induce blood-brain barrier related enzymes in cultured cerebral endothelial cells. *Brain Research.* 539, 247-253.
- Torchilin, V.P., Rammohan, R., Weissig, V., Levchenko, T.S., 2001. TAT peptide on the surface of liposomes affords their efficient intracellular delivery even at low temperature and in the presence of metabolic inhibitors. *Proc Natl Acad Sci U S A.* 98, 8786-91.
- Torriero, A.A., Salinas, E., Marchevsky, E.J., Raba, J., Silber, J.J., 2006a. Penicillamine determination using a tyrosinase micro-rotating biosensor. *Anal Chim Acta.* 580, 136-42.
- Torriero, A.A., Salinas, E., Raba, J., Silber, J.J., 2006b. Sensitive determination of ciprofloxacin and norfloxacin in biological fluids using an enzymatic rotating biosensor. *Biosens Bioelectron.* 22, 109-15.
- Townsend, G.C., Scheld, W.M., 1998. Infections of the central nervous system. *Adv Intern Med.* 43, 403-47.
- Trehin, R., Merkle, H.P., 2004. Chances and pitfalls of cell penetrating peptides for cellular drug delivery. *Eur J Pharm Biopharm.* 58, 209-23.
- Tsuji, A., Tamai, I.I., 1999. Carrier-mediated or specialized transport of drugs across the blood-brain barrier. *Adv Drug Deliv Rev.* 36, 277-290.
- Tsuzuki, N., Hama, T., Kawada, M., Hasui, A., Konishi, R., Shiwa, S., Ochi, Y., Futaki, S., Kitagawa, K., 1994. Adamantane as a brain-directed drug carrier for poorly absorbed drug. 2. AZT derivatives conjugated with the 1-adamantane moiety. *J Pharm Sci.* 83, 481-4.
- Tunkel, A.R., Wispelwey, B., Scheld, W.M., 1990. Bacterial meningitis: recent advances in pathophysiology and treatment. *Ann Intern Med.* 112, 610-23.
- Tzankaki, G., Markou, F., Kesanopoulos, K., Levidiotou, S., Pangalis, A., Tsolia, M., Liakou, V., Papapavasiliou, E., Voyiatzi, A., Kansouzidou, A., Foustoukou, M., Blackwell, C., Kremastinou, J., 2006. Phenotypic assessment of *Neisseria meningitidis* isolates obtained from patients with invasive meningococcal disease in Greece, 1993-2003: implications for serogroup B vaccines based on PorA serosubtype antigens. *Vaccine.* 24, 819-25.

- Unger, E.C., MacDougall, P., Cullis, P., Tilcock, C., 1989. Liposomal Gd-DTPA: effect of encapsulation on enhancement of hepatoma model by MRI. *Magn Reson Imaging*. 7, 417-23.
- van de Beek, D., de Gans, J., 2006. Dexamethasone in adults with community-acquired bacterial meningitis. *Drugs*. 66, 415-27.
- van de Beek, D., 2007. Brain teasing effect of dexamethasone. *Lancet Neurol*. 6, 203-4.
- Verdun, C., Brasseur, F., Vranckx, H., Couvreur, P., Roland, M., 1990. Tissue distribution of doxorubicin associated with polyisohexylcyanoacrylate nanoparticles. *Cancer Chemother Pharmacol*. 26, 13-8.
- Vick, R.S., Neuberger, T.J., DeVries, G.H., 1992. Role of adult oligodendrocytes in remyelination after neural injury. *J Neurotrauma*. 9 Suppl 1, S93-103.
- Vital Durand, D., Gerard, A., Rousset, H., 2002. [Neurological manifestations of Whipple disease]. *Rev Neurol (Paris)*. 158, 988-92.
- Vittaz, M., Bazile, D., Spenlehauer, G., Verrecchia, T., Veillard, M., Puisieux, F., Labarre, D., 1996. Effect of PEO surface density on long-circulating PLA-PEO nanoparticles which are very low complement activators. *Biomaterials*. 17, 1575-81.
- Vives, E., Brodin, P., Lebleu, B., 1997. A truncated HIV-1 Tat protein basic domain rapidly translocates through the plasma membrane and accumulates in the cell nucleus. *J Biol Chem*. 272, 16010-7.
- Vorbrodt, A.W., 1989. Ultracytochemical characterization of anionic sites in the wall of brain capillaries. *J Neurocytol*. 18, 359-68.
- Wade, L.A., Katzman, R., 1975. Rat brain regional uptake and decarboxylation of L-DOPA following carotid injection. *Am J Physiol*. 228, 352-9.
- Wadia, J.S., Dowdy, S.F., 2002. Protein transduction technology. *Curr Opin Biotechnol*. 13, 52-6.
- Wadia, J.S., Stan, R.V., Dowdy, S.F., 2004. Transducible TAT-HA fusogenic peptide enhances escape of TAT-fusion proteins after lipid raft macropinocytosis. *Nat Med*. 10, 310-5.

- Wang, Y., Ke, C.Y., Weijie Beh, C., Liu, S.Q., Goh, S.H., Yang, Y.Y., 2007a. The self-assembly of biodegradable cationic polymer micelles as vectors for gene transfection. *Biomaterials*. 28, 5358-68.
- Wang, Y., Wang, L.S., Goh, S.H., Yang, Y.Y., 2007b. Synthesis and characterization of cationic micelles self-assembled from a biodegradable copolymer for gene delivery. *Biomacromolecules*. 8, 1028-37.
- Waser, P.G., Müller, U., Kreuter, J., Berger, S., Munz, K., Kaiser, E., 1987. Localization of colloidal particles (liposomes, hexylcyanoacrylate nanoparticles and albumin nanoparticles) by histology and autoradiography in mice. *Int J Pharm* 39, 213-227.
- Watson, C.J., Venton, B.J., Kennedy, R.T., 2006. In vivo measurements of neurotransmitters by microdialysis sampling. *Anal Chem*. 78, 1391-9.
- Weerasuriya, A., 1987. Permeability of endoneurial capillaries to K, Na and Cl and its relation to peripheral nerve excitability. *Brain Res*. 419, 188-96.
- Weisfelt, M., de Gans, J., van de Beek, D., 2007. Bacterial meningitis: a review of effective pharmacotherapy. *Expert Opin Pharmacother*. 8, 1493-504.
- Weninger, W., von Andrian, U.H., 2003. Chemokine regulation of naive T cell traffic in health and disease. *Semin Immunol*. 15, 257-70.
- Wersinger, C., Sidhu, A., 2002. Inflammation and Parkinson's disease. *Curr Drug Targets Inflamm Allergy*. 1, 221-42.
- Wikipedia, 2008. <http://en.wikipedia.org/wiki/Neuron>.
- Williams, K.C., Corey, S., Westmoreland, S.V., Pauley, D., Knight, H., deBakker, C., Alvarez, X., Lackner, A.A., 2001. Perivascular macrophages are the primary cell type productively infected by simian immunodeficiency virus in the brains of macaques: implications for the neuropathogenesis of AIDS. *J Exp Med*. 193, 905-15.
- Wiradharma, N., Tong, Y.W., Yang, Y.Y., 2009. Self-assembled oligopeptide nanostructures for co-delivery of drug and gene with synergistic therapeutic effect. *Biomaterials*. 30, 3100-9.
- Wissing, S.A., Kayser, O., Muller, R.H., 2004. Solid lipid nanoparticles for parenteral drug delivery. *Adv Drug Deliv Rev*. 56, 1257-72.

- Yi-Yan, Y., Yong, W., Ross, P., Peggy, C., 2006. Polymeric core-shell nanoparticles for therapeutics. *Clinical and Experimental Pharmacology and Physiology*. 33, 557-562.
- Yoo, H.S., Park, T.G., 2001. Biodegradable polymeric micelles composed of doxorubicin conjugated PLGA-PEG block copolymer. *J Control Release*. 70, 63-70.
- Zambaux, M.F., Bonneaux, F., Gref, R., Dellacherie, E., Vigneron, C., 1999. Preparation and characterization of protein C-loaded PLA nanoparticles. *J Control Release*. 60, 179-88.
- Zhang, Y., Schlachetzki, F., Pardridge, W.M., 2003. Global non-viral gene transfer to the primate brain following intravenous administration. *Mol Ther*. 7, 11-8.
- Zhao, M., Kircher, M.F., Josephson, L., Weissleder, R., 2002. Differential conjugation of tat peptide to superparamagnetic nanoparticles and its effect on cellular uptake. *Bioconjug Chem*. 13, 840-4.
- Zhao, M., Weissleder, R., 2004. Intracellular cargo delivery using tat peptide and derivatives. *Med Res Rev*. 24, 1-12.
- Zhou, S.Y., Zuo, H., Stobaugh, J.F., Lunte, C.E., Lunte, S.M., 1995. Continuous in vivo monitoring of amino acid neurotransmitters by microdialysis sampling with on-line derivatization and capillary electrophoresis separation. *Anal Chem*. 67, 594-9.